The evolution of metallic luster in plumage

Klara Katarina Nordén

a dissertation
presented to the faculty
of princeton university
in candidacy for the degree
of Doctor of Philosophy

recommended for acceptance
by the Department of
Ecology and Evolutionary Biology

Adviser: Mary Caswell Stoddard

September 2023

Abstract

Plumage with metallic luster gives rise to some of the most mesmerizing colors in the natural world—including that of the peacock's tail, the vibrant blue of a superb bird-of-paradise and the throat coloration of many hummingbirds. These colors arise from a nanostructure in the feather barbules consisting of arrays of melanosomes (melanin-filled organelles). Apart from their beauty, structural barbule coloration offer a rich set of questions at the intersection of evolutionary biology, optics and visual ecology. In this dissertation, I tackle three key questions. First, I explore the diversity of feather nanostructures that give rise to metallic luster, and try to understand this diversity using optics and evolutionary biology. I find that to produce bright and saturated metallic luster, two key nanostructural features are necessary: a multilayer structure and optimal size of the melanin layers. Birds have achieved this in multiple ways, explaining the diversity in structures. Second, I clarify the terminology surrounding structural barbule coloration by separating two properties that are often confounded: iridescence and metallic luster. I develop a quantitative measure of metallic luster using cross-polarization photography and demonstrate that it is metallic luster, and not iridescence, that set structural barbule colors apart from other types of color mechanisms. Third, I explore the role of historical contingency on the evolution of metallic luster in plumage. Evolving metallic luster requires the modification of melanosome shape and organization, which likely takes time to evolve. Yet, some clades, like the Cuculidae, exhibit frequent gains and losses of the trait. By describing the feather nanostructures of 21 species in the Cuculidae, I show that species that have lost metallic luster still retain modified melanosome shapes. This provides a mechanism for the frequent gain and loss of this trait in this clade, since only melanosome organization has to re-evolve. These results emphasize the role of historical contingency on the evolution of plumage colors.

Contents

Abstract iii

1 Introduction 1

2 Evolution of brilliant iridescent feather nanostructures 5
- 2.1 Introduction . . . 6
- 2.2 Results . . . 11
- 2.3 Discussion . . . 30
- 2.4 Materials and methods . . . 38
- 2.5 Data availability . . . 45

3 On metallic luster and iridescence 47
- 3.1 Changeable colors . . . 48
- 3.2 Definitions . . . 52
- 3.3 Birds of an iridescent feather . . . 55
- 3.4 All that glitters is not gold . . . 60
- 3.5 Measuring metallic luster . . . 63
- 3.6 Discussion . . . 71
- 3.7 Conclusion . . . 77

4 The role of historical contingency on feather barbule nanostructures in cuckoos 79
- 4.1 Introduction . . . 80
- 4.2 Results . . . 85
- 4.3 Discussion . . . 96
- 4.4 Methods . . . 99

Appendix A Appendix for Chapter 2 105
- A.1 Additional figures . . . 106
- A.2 Additional tables . . . 108

Appendix B Appendix for Chapter 3 113
- B.1 Significance of defining iridescence as a change in hue versus peak spectral wavelength with viewing/illumination angle . . . 114
- B.2 Validation of image color calibration . . . 115
- B.3 Specimens imaged with cross-polarization photography . . . 115

Appendix C Appendix for Chapter 4 123

C.1 Ancestral state reconstructions 124
C.2 Specimens sampled and imaged with cross-polarization photography 127
C.3 Validation of image analysis method to estimate melanosome diameters . . 129

References 145

To curious minds, wherever they may be.

Acknowledgments

Life is a series of improbable events, and it was certainly never a given that I would end up writing a thesis on shimmering plumage in Princeton. The path here has been long and winding and I am immensely grateful to everyone who has traveled with me, guided me, and inspired me during the journey.

Thanks to all my mentors, who have inspired me and encouraged me from the very beginning. To Elisabeth Einarsson, who let me help her at the fossil site in Åstorp, all the way back when I was just a very keen high schooler who liked dinosaurs. To Michael Benton, who encouraged me to write my very first, first-authored scientific paper as an undergraduate, and whose lectures first awoke my interest in macroevolutionary questions. To Jakob Vinther, who introduced me to the study of melanosomes—which I am still stuck with five years later—and who gave me the confidence to apply to the Princeton graduate school.

For the work presented in this thesis I am especially indebted to my PhD advisor Cassie Stoddard, who allowed me to follow my own research ideas wherever they took me—from photonics to philosophy. Not only did she support me in these pursuits, but she engaged with every one of the topics and showed unwavering enthusiasm for each project—even when mine was at a low-point. Her ability to see clarity in my sometimes convoluted trains of thought has elevated the quality of every one of the chapters in this thesis. Thanks also to the members of my committee: Christie Riehl, David Wilcove and Andy Dobson. Their different perspectives and sharp scientific minds made discussing my projects during committee meeting a very fun and intellectually stimulating experience, and always made me see my projects in a new light.

I am grateful to the community of The Department of Ecology and Evolutionary Biology at Princeton, and in particular the Stoddard lab, for providing me with a supportive and inspiring environment to do my research. Thanks to everyone who made me feel welcome in the department and who I've discussed science with over the years—more people than I can mention. In particular, I'd like to thank Audrey, Jarome, Monica, Meghan, Rosalyn, Ben, Ciara, Merlijn, Alec, Aiyu, Freda and Jessica—who not only helped me develop my research but are also my good friends. I've also been fortunate enough to live with the most amazing housemates during these last few years—thank you. Doing a PhD can sometimes be a challenging and quite lonely experience, and I don't know how I would have made it through without this truly wonderful circle of friends.

Thanks to my friends beyond Princeton—in Sweden and from Bristol—for providing me with perspective on my life in the strange world that is academia. In particular, thanks to Frane Babarović, who provided much interesting discussion and inspiration for the research in this thesis (beginning all the way back in Bristol). I hope to discuss melanosomes (and life) with Frane soon again over a coffee in Zagreb (or Ghent).

My family has provided me with a solid mountain of support without which nothing of what I've accomplished would be possible. Thanks to my dad, who encouraged me to explore

nature, and to my mum, from whom I have inherited an incurable curiosity about the world. Thanks to my sisters—Anna, Tove and Elsa—who generously shared their life wisdom with the youngest one from day one. I don't know how anyone goes through life without having three sisters to consult with on all of life's intricacies and complications.

I am incredibly lucky to have the support and love from Raphael Steiner, who have not only directly contributed to parts of this thesis, but engaged with me in many long discussions about color, vision and melanosomes. Thanks for being there for me always.

1

Introduction

Scientists and artists alike have been fascinated for centuries by the metallic, shimmering hues shown by some natural objects—peacock feathers were among the first objects to be studied under a microscope (Hooke, 1665) and the elytra of jewel beetles (family Buprestidae) were used to make elaborate ornaments by the ancient Egyptians (Kritsky, 1991). These colors owe their captivating appearance to the fact that they arise from the interaction of light with a nanostructure rather than from the absorbance of a pigment—this is called a structural color. As light is reflected from a regularly spaced nanostructure, specific wavelengths are reinforced while all others are canceled out (light interference). This give many structural colors unusual properties: they can shift in hue with viewing/observation angle (iridescence) and they reflect colored specular light, which can make them appear metallic.

The focus of this thesis is a particular set of structural colors, namely those produced by nanostructures in the feather barbules of birds. Examples of structural barbule colors in birds are the plumage of peafowl (*Pavo pavo*), hummingbirds (family Trochilidae) and many starlings (family Sturnidae)—but the trait is widespread in birds (Durrer, 1977). They are often called "iridescent structural colors", however, as I will explore in Chapter 3, they are more appropriately characterized by their metallic sheen (metallic luster) than their iridescence. Structural barbule coloration is typically both iridescent and metallic, but the metallic luster is their only unique quality. Many structural colors—and even some pigmentary colors (Reed et al., 2020)—exhibit iridescence. The usage of "iridescence" in the literature, including by myself in Chapter 2 of this thesis, often confound metallic luster with iridescence. While it is not wrong to call structural barbule colors iridescent, describing them as "weakly iridescent" or "brilliant iridescent" (Chapter 3, Auber, 1957) is confusing, since the adjectives here really refers to the intensity of the metallic luster, not the degree of iridescence (in fact, what it means to differ in degree of iridescence is another unresolved matter!).

I think the confusion surrounding even the definition of these colors speaks to how little we still know about metallic luster in nature—despite centuries of fascination with such colors (Finet, 2023). Moreover, what makes metallic luster a particularly fascinating object of study is its interdiciplinary nature. While the heart of the questions in this dissertation are motivated

by evolutionary biology, through the chapters I make connections to areas as widespread as photonics, material science, psychology and visual ecology. This also means that the insights we can gain from studying metallic luster are not limited to plumage color evolution, but extend to general topics such as: what role does historical contingency play in evolution?; how are complex traits gained?; how is a nanostructure optimized for color production? and, why are we attracted to shiny objects?

A brief outline of the topics explored in each chapter is presented below.

Chapter 2: Evolution of brilliant iridescent feather nanostructures. In this chapter, I present an overview of the diversity of feather nanostructures that produce metallic luster in birds (referred to in this chapter as iridescent structural colors, in line with the published text, see Nordén et al., 2021), and use optical modeling and color measurements of plumage to answer whether this diversity evolved to produce more vibrant colors. I evaluate how different melanosome shapes (melanin-filled organelles that act as building blocks in the nanostructures) affect the saturation and brightness of the produced color. I find that there is one key aspect of melanosome shape that is needed to produce bright and saturated colors—thickness of melanin layers. However, since this optimal layer thickness can be achieved through various melanosome modifications (hollowing out the interior, flattening or shrinking of the melanosome), this explains some of the diversity of nanostructures we see in birds.

Chapter 3: On iridescence and metallic luster. To ask the right questions, it is important to have the right definitions. In this chapter, I argue that two properties of structural barbule color—iridescence and metallic luster—are often confounded. I show using optical models and color measurements of plumage that structural barbule colors are not unique in producing iridescent colors—other types of plumage colors also have this property. Rather, the unique property of structural barbule coloration is the metallic luster. I explore why structural barbule colors look metallic, and develop a measure of this quality using cross-polarization photography. Separating metallic luster from iridescence opens the door to many

new interesting questions: is metallic luster important as a signal in animal communication? Are other animals than humans attracted to "shiny things"?

Chapter 4: The role of historical contingency on feather barbule nanostructures in cuckoos. Feather nanostructures that give rise to metallic luster are complex, requiring modification to melanosome shape and organization to evolve. It is therefore surprising that some clades, such as the Cuculidae, appear to frequently lose and gain the trait. By exploring the nanostructures of 21 cuckoo species, I investigated whether historical contingency, i.e. the path-dependency of evolution, could explain this pattern. I show that modified melanosome shapes are retained in species that have lost metallic luster in the plumage. This could provide a mechanism for the frequent gain and loss of metallic luster in cuckoos, since only melanosome organization has to re-evolve. I speculate that such retention of modified melanosomes could explain the uneven distribution of metallic luster across the bird phylogeny—once metallic luster has evolved in a lineage, it is more likely to reappear.

Probably no subject in modern biological optics is described with more mysticism and less clarity than photonic crystals.

Sönke Johnsen, The Optics of Life

2

Evolution of brilliant iridescent feather nanostructures

Notes

This chapter (with minor adjustments) has previously been published in the journal *elife*: Klara Katarina Nordén, Chad M Eliason, Mary Caswell Stoddard (2021) Evolution of brilliant iridescent feather nanostructures, *eLife* 10:e71179.

Abstract

The brilliant iridescent plumage of birds creates some of the most stunning color displays known in the natural world. Iridescent plumage colors are produced by nanostructures in feathers and have evolved in diverse birds. The building blocks of these structures—melanosomes (melanin-filled organelles)—come in a variety of forms, yet how these different forms contribute to color production across birds remains unclear. Here, we leverage evolutionary analyses, optical simulations, and reflectance spectrophotometry to uncover general principles that govern the production of brilliant iridescence. We find that a key feature that unites all melanosome forms in brilliant iridescent structures is thin melanin layers. Birds have achieved this in multiple ways: by decreasing the size of the melanosome directly, by hollowing out the interior, or by flattening the melanosome into a platelet. The evolution of thin melanin layers unlocks color-producing possibilities, more than doubling the range of colors that can be produced with a thick melanin layer and simultaneously increasing brightness. We discuss the implications of these findings for the evolution of iridescent structures in birds and propose two evolutionary paths to brilliant iridescence.

2.1 Introduction

Many animal colors—and indeed some plant, algae, and possibly fungus colors (Brodie et al., 2021)—are structural, produced by the interaction of light with micro- and nano-scale structures (reviewed in Kinoshita et al., 2008). In birds, structural colors greatly expand—relative to pigment-based mechanisms—the range of colors birds can produce with their feathers (Stoddard & Prum, 2011, Maia et al., 2013b). Some structural colors are iridescent: the perceived

hue changes with viewing or lighting angle. Iridescent coloration features prominently in the dynamic courtship displays of many bird species, including birds-of-paradise (Paradisaeidae), hummingbirds (Trochilidae), and pheasants (Phasianidae) (Greenewalt et al., 1960, Stavenga et al., 2015, Zi et al., 2003). These dazzling displays showcase the kind of bright and saturated iridescent colors that have previously been qualitatively categorized as "luxurious" (Auber, 1957) or "brilliant" (Durrer, 1977), in contrast to the more muted "faint" (Auber, 1957) or "weak" (Durrer, 1977) iridescent colors of, for example, a brown-headed cowbird (*Molothrus ater*). Following these authors, we use the terms "brilliant" and "weak" to describe this difference in color appearance, where brilliant iridescence describes colors of high saturation and brightness and weak iridescence describes colors of low saturation and brightness.

Typically, brilliant iridescence is associated with more complex feather nanostructures, relative to weak iridescence. All iridescent feather coloration is produced by nanostructures in the feather barbules consisting of melanin-filled organelles (melanosomes) and keratin (Figure 2.1), but brilliant iridescent coloration arises from light interference by photonic crystal-like structures (henceforth photonic crystals), while weak iridescent coloration is produced by structures with a single layer of melanosomes (Durrer, 1977). A photonic crystal is defined by having periodic changes in refractive index (Joannopoulos et al., 2008); in feather barbules, this is created by periodic arrangements of melanosomes in keratin. By adding more reflection interfaces, a photonic crystal greatly amplifies color saturation and brightness compared to a single-layered structure, the latter of which typically functions as a simple thin film (Kinoshita et al., 2008). Thus, brilliant iridescence describes bright, highly saturated colors arising from melanosomes arranged in a photonic crystal.

In iridescent feathers, it is not just the arrangement of melanosomes that can vary: the melanosomes also come in a variety of different shapes. Durrer (1977) classified melanosomes into five main types: (1) thick solid rods (S-type, Figure 2.2A); (2) thin solid rods (St-type, Figure 2.2B); (3) hollow rods (with an air-filled interior, R-type, Figure 2.2C); (4) platelets (P-type, Figure 2.2D); and (5) hollow platelets (K-type, Figure 2.2E). All five melanosome types occur in single-layered structures producing weak iridescence. Four of these types—all but

thick solid rods—occur in photonic crystals producing brilliant iridescence. This diversity is extraordinary given that the shape of melanosomes in other melanized vertebrate tissues, including black and gray feathers, is typically a solid rod (D'Alba & Shawkey, 2019). The thick solid rods found in weakly iridescent feathers resemble the melanosomes found in plain black feathers (Durrer, 1977) and are likely ancestral to the four more modified, derived melanosome shapes (Shawkey et al., 2006, Maia et al., 2012). Because the derived melanosome shapes (but not the ancestral thick solid rods) are arranged as photonic crystals, these two innovations together—novel shapes and photonic crystal structure—may have been critical for the evolution of brilliant iridescence. Supporting this idea, Maia et al. (2013b) showed that the evolution of hollow and/or platelet-shaped melanosomes in African starlings (Sturnidae) was associated with great expansions in color diversity and increases in brilliance. Moreover, Eliason et al. (2013) used optical modeling and plumage color measurements of the violet-backed starling (*Cinnyricinclus leucogaster*) and wild turkey (*Meleagris gallopavo*) to show that hollow rods increase the brightness of iridescent colors compared to structures with solid rods.

While previous studies focusing on nanostructural evolution and color-producing mechanisms in a variety of avian groups (Eliason et al., 2020, 2015, 2013, Eliason & Shawkey, 2012, Gammie, 2013, Gruson et al., 2019b, Maia et al., 2013b, Quintero & Espinosa de los Monteros, 2011) have given us valuable insights into the evolution and optics of iridescent structures, they have focused on specific species, small clades, or a particular melanosome type. Thus, they have not uncovered the broader, general principles governing the evolution of brilliant iridescent plumage, and several key questions remain unanswered.

Why have bird species with brilliant iridescence evolved not one but four different melanosome types? How are these melanosome types phylogenetically distributed? Are particular melanosome types associated with different plumage colors? Since Durrer's initial work (Durrer, 1977), there has been no broad-scale evolutionary analysis of the melanosomes in iridescent feathers, and no study has compared the optical effects of all five of Durrer's melanosome types. To find general principles underlying differences in color production, we identify key modifications that, based on optical theory, are likely to be important. This enables us to com-

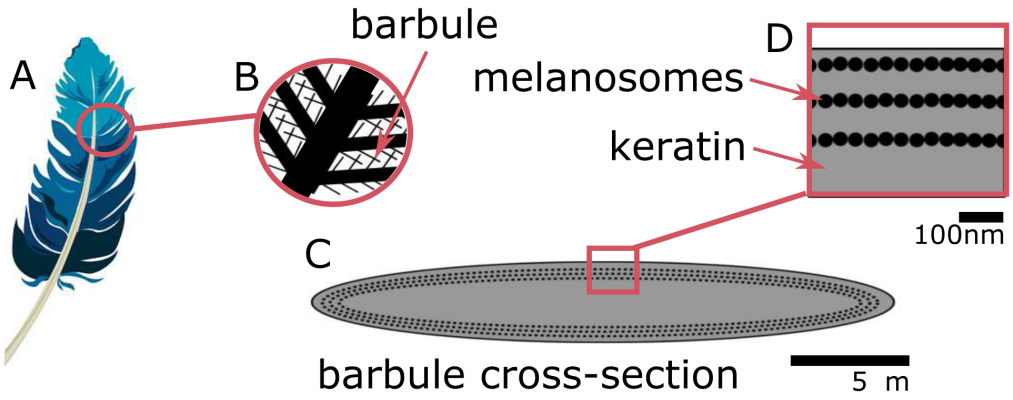

Figure 2.1: Iridescent plumage is produced by nanostructures in the feather barbules. A vaned feather (A) consists of branching structures where the barbules (B) are the interlocking filaments. A cross-section of a barbule from an iridescent feather (C) reveals the intricate nanostructure responsible for the color, consisting of layers of melanosomes in keratin (D). Blue feather in (A) from Pixabay, licensed under the Pixabay License.

pare the five melanosome types rigorously, since each type can have several modifications. For example, a hollow platelet (Figure 2.2E) has both an air-filled interior and a flattened shape, both of which might influence feather color—perhaps in different ways. Therefore, a simple comparison of the melanosome types cannot reveal which modifications affect color production or pinpoint their precise optical effects.

In this study, we search for general design principles underlying the production of brilliant iridescent coloration. First, we identify three key modifications of melanosomes in brilliant iridescent structures: thin melanin layers, hollowness, and platelet shape (Figure 2.2). Second, we create a feather iridescence database using published descriptions of iridescent feather structures. Using the database, we explore the evolutionary history of the three key modifications of brilliant iridescent structures. Third, we use optical modeling to simulate colors that could be produced with each melanosome type; we estimate light reflectance from 4500 different structures using parameter ranges derived from the database. Finally, we analyze spectral data from 111 plumage regions across 80 diverse bird species with known nanostructures to test the predictions of our optical model.

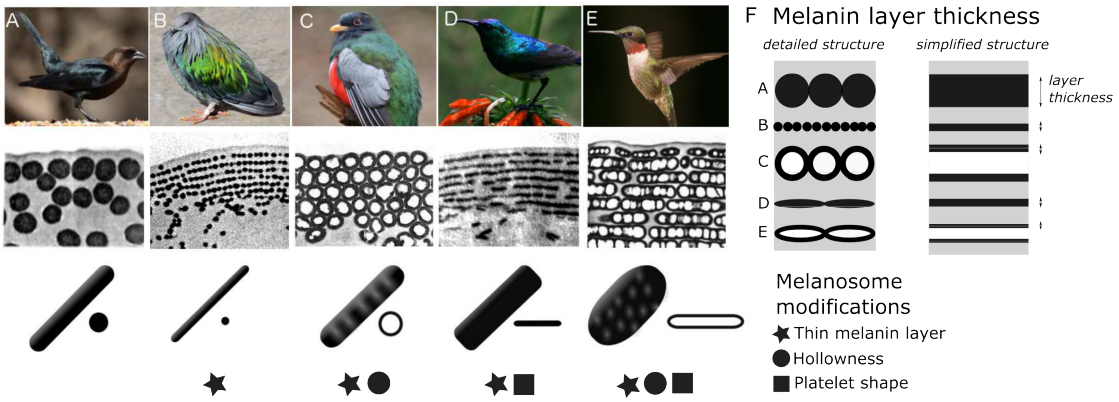

Figure 2.2: Iridescent feather nanostructures are diverse. Structures can vary both in melanosome type and melanosome organization. There are five main types of melanosomes (shown as schematics in bottom row, each viewed from the side and in cross-section (A–E)) and two main types of structural organization (shown by microscope images of barbule cross-sections, middle row: single-layered (A) and photonic crystal (B–E)). A single-layered structure with thick solid rods (A) gives rise to the dark, black-blue iridescence of a brown-headed cowbird (*Molothrus ater*). This type of structure generally gives rise to "weak" iridescent colors, with low color saturation and brightness. Photonic crystals (B–E) with multiple layers of melanosomes generally give rise to "brilliant" iridescent colors, with high saturation and brightness. Thin solid rods (B) in a multilayer configuration (also called a one-dimensional photonic crystal) produce the iridescent colors of the Nicobar pigeon (*Caloenas nicobarica*). In the elegant trogon (*Trogon elegans*), the iridescent green color is produced by hexagonally packed hollow rods (C). Sunbird (here the variable sunbird, *Cinnyris venustus*) barbules contain melanosomes stacked in multilayers, with solid platelet-shaped melanosomes serving as the building blocks (D). The fifth melanosome type is a hollow platelet (E), which forms multilayer configurations in many hummingbird species (here a ruby-throated hummingbird, *Archilochus colubris*). The five types of melanosomes are characterized by different combinations of three key modifications: thin melanin layers, hollowness, and platelet shape, which are indicated as symbols under each melanosome type. Thin melanin layers are present in four melanosome types, but they are achieved in different ways, as is shown by the schematic in (F). A simplified diagram of each melanosome type (F, right) shows how solid forms translate to a single melanin layer, while hollow forms create two thinner melanin layers intersected by an air layer. All photographs (top row) are under a Public Domain License. Transmission Electron Microscope images from Durrer (1977), reproduced with permission.

2.2 Results

2.2.1 Identifying key melanosome modifications

The size, composition, and shape of materials that form the periodic layers in a photonic crystal can all contribute to its reflectance properties (Joannopoulos et al., 2008). In iridescent structural feather colors, the layers are formed by melanosomes, and we can identify three melanosome modifications that likely have important optical effects. We define these modifications relative to the thick solid rods found in weakly iridescent feathers, since we presume these to be unmodified or minimally modified from melanosomes found in other non-iridescent melanized tissues, which they closely resemble (Durrer, 1977). For a more detailed analysis of thick solid rods in weakly iridescent versus black feathers, see the next section (§2.2.2, *Evolution of modified melanosomes in iridescent structures*). The three modifications are: thin melanin layers (size of layers), an air-filled interior (layer material composition), and platelet shape (shape of layers). "Thin" here refers to something thinner than the ancestral thick solid rods. A "melanin layer" refers to a single layer in the optical structure. For solid rods and platelets, a layer's thickness is simply the rod or platelet diameter, but for hollow rods and platelets, it is the thickness of a single melanin wall (Figure 2.2F). Each of Durrer's five melanosome types can be described in terms of the absence/presence of one or several modifications (Figure 2.2).

What are the potential optical advantages of melanosomes with these features? First let us consider thin melanin layers. Thin melanin layers may tune the structure so that it reflects optimally in the bird-visible spectrum. This possibility was raised by Durrer (1977), who noted that structures producing brilliant iridescent colors tended to have thin (melanin) layers. However, Durrer's work is only available in German, and this idea has remained largely overlooked. We refine and extend Durrer's idea here using established optical theory, specifically multilayer optics (reviewed in Kinoshita et al., 2008, Kinoshita, 2008). To produce first-order interference peaks, which will result in brighter colors than higher-order interference peaks, the optical thickness (thickness times refractive index) of each repeating unit in a one-

dimensional photonic crystal (also often termed multilayer, Figure 2.2B, D–E) should approximate half a wavelength ($\lambda/2$) (Durrer, 1977, Kinoshita et al., 2008, Land, 1972). The repeating unit in an iridescent feather nanostructure consists of one layer of melanosomes and one layer of keratin, and we can therefore express this as $(t_{\mathrm{mel}} \cdot n_{\mathrm{mel}}) + (t_{\mathrm{k}} \cdot n_{\mathrm{k}}) = \lambda/2$, where t_{mel} is the thickness of the melanin layer, t_{k} is the thickness of the keratin layer, n_{mel} is the refractive index of the melanin layer, and n_k is the refractive index of the keratin layer. Among the configurations that satisfy this condition, maximum reflection is achieved when both layers have equal optical thickness, which can be expressed as $(t_{\mathrm{mel}} \cdot n_{\mathrm{mel}}) = (t_{\mathrm{k}} \cdot n_{\mathrm{k}}) = \lambda/4$ (Kinoshita et al., 2008, Land, 1972). From this, we can express the range within which we would expect melanin optical layer thickness to fall as $(t_{\mathrm{mel}} \cdot n_{\mathrm{mel}}) < \lambda/2$, with maximum reflectance at $(t_{\mathrm{mel}} \cdot n_{\mathrm{mel}}) = \lambda/4$. If we assume that the structure should reinforce wavelengths within the bird-visible spectrum (300–700nm), we can calculate the range we should expect for melanin layer thickness, using 300nm and 700nm as endpoints. Here, we use the refractive indices $n_{\mathrm{mel}} = 2$ for 300nm and $n_{\mathrm{mel}} = 1.7$ for 700nm, following Stavenga et al. (2015). This gives us a maximum melanin layer thickness ranging from $<$ 75nm (maximum thickness for reinforcing ultraviolet wavelengths) to $<$ 206nm (maximum thickness for reinforcing red wavelengths), with maximum reflectance (where $(t_{\mathrm{mel}} \cdot n_{\mathrm{mel}}) = \lambda/4$) at layer thicknesses of 37.5nm and 103nm, respectively. Note that the maximum values of 206nm and 75nm represent situations where the optical thicknesses of melanin layers alone equal $\lambda/2$, and thus keratin layers must be zero. Such a structure would not function as a photonic crystal, since it consists of a single thick layer of melanin. Thus, for iridescent structures producing first-order interference peaks, we expect melanin layer thickness to be below 206nm. Moreover, we expect a lower limit at 37.5nm, since melanin layer thickness is unlikely to have evolved below the thickness required for maximum reflectance at ultraviolet wavelengths. This gives us an expected range of 37.5–206nm. The typical diameter of melanosomes found in vertebrates is $\sim$300nm (Li et al., 2014), exceeding this range.

Now let us consider why melanosomes with hollow interiors might be advantageous. A hollow interior could increase reflectance by creating a sharper contrast in refractive index in

the structure (Durrer, 1977, Eliason et al., 2013, Kinoshita et al., 2008, Land, 1972, Stavenga et al., 2018), making a color brighter. This is because the refractive index of air ($n = 1$) is lower than that of keratin ($n = 1.56$).

To estimate the expected thickness of hollow interiors (air pockets), we can extend the argument for expected thickness of the melanin layer. If air pockets conform to the expected size range, this would suggest that they are tuned together with melanin layers to produce brilliant iridescence. Analogous to describing melanin rods as a melanin layer (Figure 2.2F), we can think of air pockets as an air layer. Since the equations above define reflection for a structure with only two materials (of high and low refractive index, respectively), we must assume that air layers have the same optical thickness as the keratin layers. Thus, both the keratin and air layers can be described by a single term, since $(t_{\mathrm{k}} \cdot n_{\mathrm{k}}) = (t_{\mathrm{a}} \cdot n_{\mathrm{a}})$, where a denotes air and $n_{\mathrm{a}} = 1$. In this situation, the air layer should have a thickness < 350nm to produce first-order interference in the bird-visible spectrum—and a thickness of 75–175nm to meet the condition for maximal reflectance. Thus, the expected range is 75–350nm. However, we note that a one-dimensional photonic crystal with three materials could have varying optical thickness for all three types of layers (where $(t_{\mathrm{k}} \cdot n_{\mathrm{k}}) \neq (t_{\mathrm{a}} \cdot n_{\mathrm{a}})$). The optimal configuration of such a system is much harder to derive, making it difficult to generate specific predictions for this case.

Finally, let us explore why platelet-shaped melanosomes might be beneficial. Platelet-shaped melanosomes have been hypothesized to increase reflection by creating smooth, mirror-like reflection surfaces (Durrer, 1977, Land, 1972). Moreover, the thin platelet shape might allow for more layers to be packed within a photonic crystal, which would increase total reflection (Maia et al., 2013b).

Which of the four derived melanosome types in brilliant iridescent feathers possess these modifications? Hollowness and platelet shape are each present in two types, but thin melanin layers are likely shared by all four derived melanosome types (Figure 2.2). Durrer (1977) noted the prevalence of thin melanin layers but never analyzed them formally. Nonetheless, this potential convergence on thin melanin layers hints at the intriguing possibility that the four derived melanosome types present diverse paths to the same end: achieving optimal melanin

layer thickness. A hollow interior or a platelet shape may simply be different mechanisms for reducing melanin layer thickness. This would also explain why thick solid rods are typically only found in single-layered structures. Single-layered structures typically function as thin films, where the thickness of the overlying keratin cortex determines the interference colors (Doucet, 2006, Lee et al., 2012, Maia et al., 2009, Yin et al., 2006). The layer of melanosomes only functions to delimit the keratin layer, so the thickness of the melanin layer itself is largely irrelevant. Thus, there would be no selection pressure to decrease melanin layer thickness in single-layered structures, and we would expect the ancestral condition (thick solid rods) to remain.

We suggest that the diverse melanosome types found in brilliant iridescent structures evolved to generate thin melanin layers in different ways. This possibility has not been investigated previously, probably because melanosome types are generally analyzed on the basis of their overall morphology rather than—as we have proposed here—on the basis of specific optical modifications.

2.2.2 Evolution of modified melanosomes in iridescent structures

We surveyed the literature for all published descriptions of iridescent feather structures—including weak and brilliant iridescent colors—in order to build a species-level database (henceforth the feather iridescence database) of key structural parameters (Figure 2.8). These parameters included melanosome type (solid rod, hollow rod, solid platelet, and hollow platelet), melanin layer thickness, details about the structure (single-layered or photonic crystal), and size of the internal air pockets. We found that iridescent feather nanostructures have been described in 306 bird species representing 15 different orders and 35 families. The feather iridescence database, which includes a complete list of the references we consulted, is available to download from the Dryad Digital Repository.

Descriptions of iridescent feather structures are taxonomically biased, with some groups well represented (>20 species represented in the database: Sturnidae, Trochilidae, Phasianidae, Trogonidae, and Anatidae) but most groups sparsely sampled (< 5 species represented

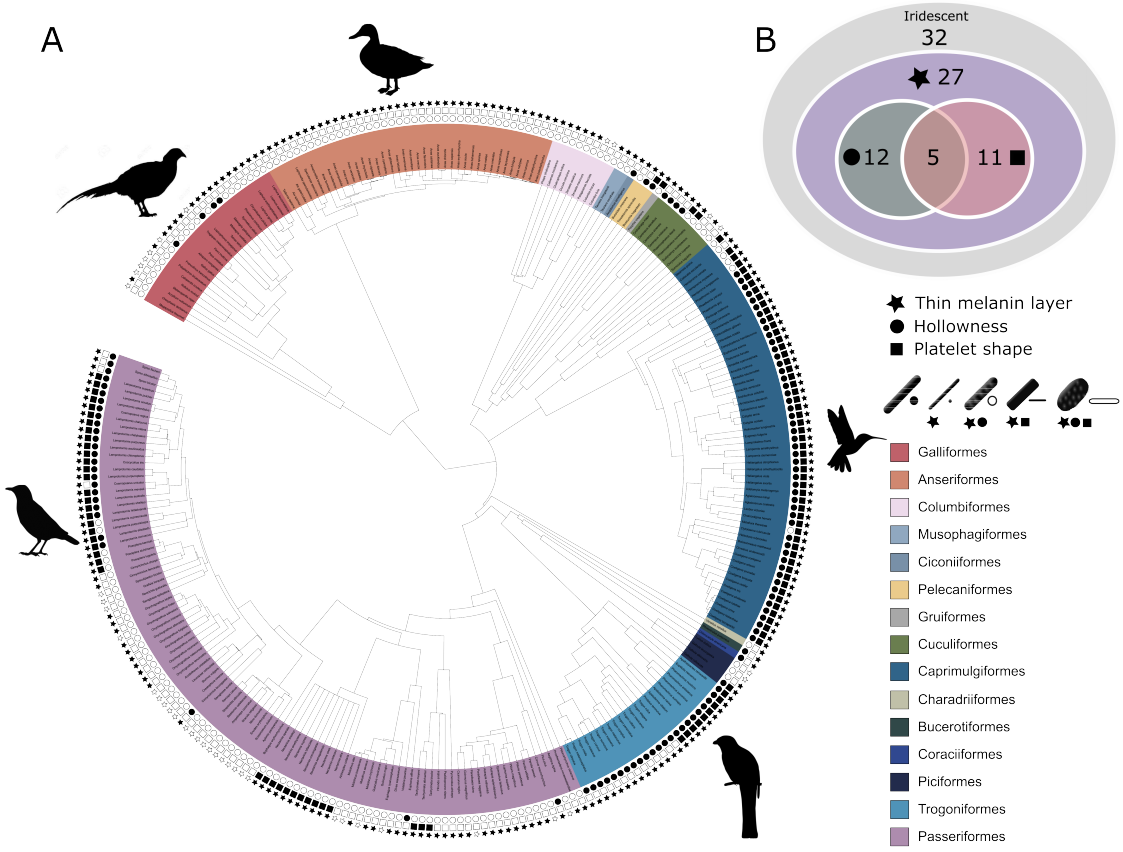

Figure 2.3: Evolutionary distribution of three key melanosome modifications in iridescent structures: thin melanin layers (star), hollowness (circle), and platelet shape (square). Schematics of melanosomes in the key show how combinations of modifications correspond to each melanosome type. (A) Melanosome modifications mapped onto a phylogeny including all species in the feather iridescence database (280 species, after excluding 26 species lacking data on melanosome type). Note that where data on melanin layer thickness was not available for a species with hollow and/or platelet-shaped melanosomes, they were assumed to have thin melanin layers, since all known hollow and platelet structures do. Silhouettes shown for the five families that are best represented in the feather iridescence database ($>$ 20 species represented in the database): Sturnidae, Phasianidae, Anatidae, Trogonidae, and Trochilidae. (B) Venn diagram showing the number of bird families in the feather iridescence database for which each modification was present. The majority of bird families with iridescent plumage studied have evolved thin melanin layers, and there are no hollow or platelet-shaped melanosomes that have not also evolved this modification. A similar number of families have hollow or platelet-shaped melanosomes, but only five families have evolved both modifications together. Note that this plot depicts the number of occurrences of each modification, not independent evolutionary origins. Silhouettes from Phylopic.org, licensed under a Public Domain License.

in the database) or absent despite some species possessing iridescent plumage (e.g. Picidae). Even in well-sampled groups (e.g. Trochilidae), the feather structures of only about 15% of all the species in the family have been described. Some published descriptions included measurements of every structural parameter, while others only included partial information on melanosome modifications. For example, descriptions for only 61% of species included details about melanin layer thickness, while descriptions for almost all species had complete information on the presence/absence of melanosome hollowness and/or platelet shape (92%). Most species records (83%) described the type of structure (single-layered or photonic crystal). These data, though taxonomically biased, allowed us to describe the properties of the three melanosome modifications we defined (thin melanin layers, hollowness, and platelet shape). Using an avian phylogeny (Jetz et al., 2012), we mapped these modifications for all 280 species for which complete information on melanosome type was present in our database (Figure 2.3A). Although these species represent only a fraction of those with iridescent feathers, the major iridescent orders are represented. Our analysis thus provides a broad snapshot of iridescent feather structure diversity and evolution across birds. In the sections below, we use this data set to test functional hypotheses for each modification and to discuss evolutionary patterns in more detail.

2.2.3 Thin melanin layers

We have suggested that all four melanosome types found in brilliant iridescent structures (Figure 2.2B–E) share a common trait: a reduction in melanin layer thickness. This is plausible based on the measurements and description of melanosome types given by Durrer (1977), who proposed a division of solid rods into a thinner (diameter of ~100nm) and thicker variety (diameter of ~200nm), but has not been formally quantified. In the current literature, solid rods are often treated as a single melanosome type with a continuous size distribution (Eliason et al., 2013, Maia et al., 2013b, Nordén et al., 2019). Thus, to study the evolution of thin melanin layers, we first needed to explore the distribution of solid rod diameters using the feather iridescence database. Specifically, we used the feather iridescence database to show

that: (1) solid rods can be divided into two distinct distributions (a thinner and thicker variety); and (2) hollow and/or platelet-shaped melanosomes have equally thin or thinner melanin layers than thin solid rods, demonstrating that they share this modification.

Analyzing the distribution of melanosome diameter in all solid rods, we found a significant bimodal distribution (Figure 2.4, unimodality rejected, $p < 0.001$, bimodality not rejected, $p = 0.888$). Based on the bimodal distribution of melanosome diameters in solid rods, we define "thick solid rods" as those with a diameter $\geq$ 190nm and "thin solid rods" as those with a diameter $<$ 190nm. It should be noted that this definition differs slightly from Durrer's categorization, which specifies a range of 70–140nm for the thin solid rods he measured (Durrer, 1977). Thick solid rods are similar in size to melanosomes in black feathers (Figure 2.4; data from Li et al., 2012), supporting the hypothesis that thick solid rods represent minimally modified or unmodified melanosomes. Iridescent structures most likely evolved from black plumage (Maia et al., 2012, Shawkey et al., 2006); therefore, we can use the size of melanosomes in black feathers to represent an "unmodified" melanosome. In contrast, the melanosomes in black feathers are considerably thicker than the thin solid rods in iridescent feathers (Figure 2.4), suggesting that thin solid rods are considerably modified from the ancestral state.

We can now define "thin melanin layers" as any melanosome with melanin layers $<$ 190nm. This value is just below the upper limit in our expected range for melanin layer thickness (206nm), in line with our prediction (see §2.2.1, *Identifying key melanosome modifications*). Using this new definition, we found that all hollow and/or platelet-shaped melanosomes can indeed be classified as having thin melanin layers (range 24–139nm, Figure 2.5). Whether a single melanin wall in hollow melanosomes always represents one melanin layer is debatable: some photonic crystals with hollow melanosomes have little or no keratin interspersed between melanosome layers (e.g. Figure 2.2C–E). In these cases, it may be more appropriate to think of a single melanin layer as the sum of two melanin walls. However, all hollow forms in photonic crystals have a single melanin wall thickness of $<$ 95nm (Figure 2.5), so they would still qualify as "thin" even if this value were doubled. All four derived melanosomes with thin melanin layers have significantly thinner melanin layers than melanosomes in black feathers

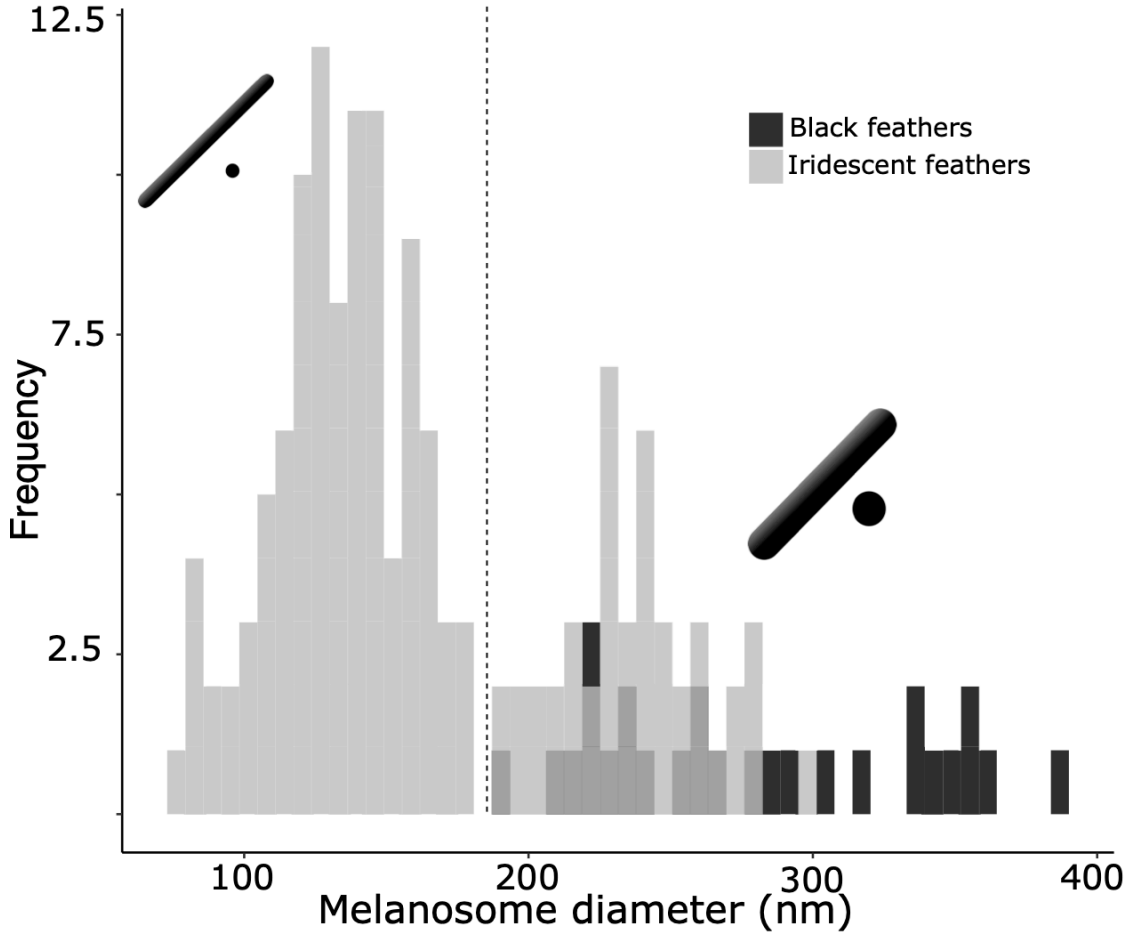

Figure 2.4: There are two distinct types of solid rods in iridescent structures: thick solid rods and thin solid rods. This is evident from the clear bimodal distribution shown by the histogram of melanosome diameters found among all solid rods in the feather iridescence database (gray). Based on this distribution, we define "thin solid rods" as any solid rod with a diameter $<$ 190nm (marked with dashed line). Plotted in black is the distribution of diameters from melanosomes in black feathers (data from Li et al., 2012), which overlaps with the distribution of thick solid rods in iridescent structures.

and thick solid rods (phylogenetic pairwise t-test, all $p < 0.01$, see details in Table A.1).

Next, we tested our hypothesis that thin melanin layers evolved for a specific optical benefit—to allow photonic crystals to produce bright and saturated colors. We have already shown that the four derived melanosomes share the modification of thin melanin layers, but it is possible that this evolved for reasons unrelated to color production, such as to minimize the cost of melanin production. We predicted that if thin melanin layers did evolve for an optical benefit, they should have converged on the expected range for producing bright interference peaks in the bird-visible spectrum (i.e. a layer thickness between 37.5–206nm). In addition, we predicted that melanosomes with a thickness outside this favorable range should be rare or absent in photonic crystals. We found that all derived melanosomes indeed have converged on thicknesses well within this expected range (Figure 2.5). Moreover, all derived melanosome types achieve optical thicknesses of $\lambda/4$ (37.5–103nm). Such structures could in theory produce ideal multilayers, which produce the greatest reflectance for a two-material reflector (Land, 1972). We also found that the vast majority of photonic crystals contain melanosomes with thin melanin layers (99% of all species with photonic crystals). Overall, these findings are compatible with the hypothesis that the primary benefit of thin melanin layers in photonic crystals is to produce bright and saturated colors. The importance of this key modification—thin melanin layers—for iridescent color production can also be inferred from its phylogenetic distribution. Over 80% of all families represented in the feather iridescence database have evolved thin melanin layers (27 out of 32 families, Figure 2.3B). The families that lack the thin modification also lack species with brilliant iridescent plumage (Numididae, Aegithinidae, Irenidae, Buphagidae, Megapodiidae, and Lybiidae).

However, it is also true that many single-layered structures are formed with melanosomes with thin melanin layers (present in 59% of all species with single-layered structures). If derived melanosome types evolved to provide brilliant iridescent color via thin melanin layers, why do they exist in single-layered structures, too? We propose two likely explanations. The first possibility is that thin melanin layers are advantageous also in single-layered structures, by forming a two-layered structure when the cortex is of a similar thickness to the melanin layer.

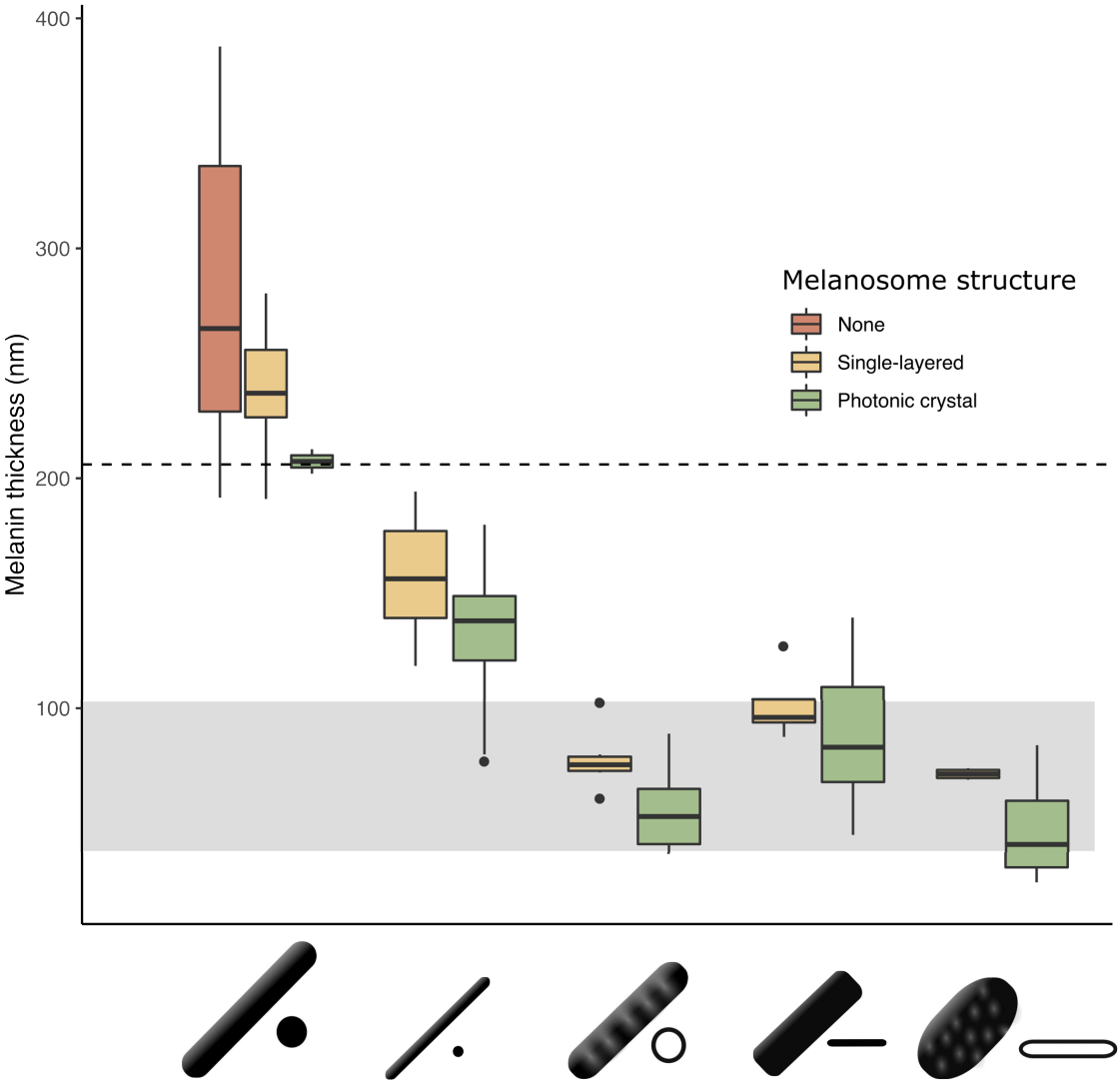

Figure 2.5: The thickness of melanin layers in derived melanosomes has converged toward the theoretical expected range, where optical thickness $< \lambda/2$ (below dashed line, for bird-visible spectrum). Boxplot shows the distribution of melanin layer thicknesses for each melanosome type in single-layered structures (yellow) and photonic crystals (green) in the feather iridescence database. 'None" corresponds to melanosomes in a black feather without organization (data from Li et al., 2012). All melanosome types except thick solid rods, which are predominantly found only in single-layered structures with weak iridescence, have converged toward an optical thickness of $< \lambda/2$. Hollow and platelet forms often reach thicknesses closer to $< \lambda/4$, which can in theory form ideal multilayers (gray box, for bird-visible spectrum). Note that three species are recorded to have thick solid rods in a photonic crystal: *Paradisaea rubra* (Red bird-of-paradise), *Parotia lawesii* (Lawes' parotia), and *Eudynamys scolopaceus* (Asian koel). *Paradisaea rubra* and *Parotia lawesii* have melanosomes with porous interiors (see §2.3, *Discussion*), so they are not "true" thick solid rods and will have an optical thickness closer to that of a derived melanosome. The structure in *Eudynamys scolopaceus* consists of tightly, hexagonally packed rods and appears to produce relatively weak iridescent color. It may be an example of a structure evolving toward brilliant iridescence (Path 2, Figure 2.7C).

This would increase the saturation and brightness of interference colors, though the effect would not be as strong as in a photonic crystal with many layers. The second possibility is that derived melanosomes evolve in single-layered structures due to another advantage, not because of their thin melanin layers. For example, a hollow interior or platelet may be beneficial to increase the brightness of the color. In either scenario, thin melanin layers are potentially co-opted in photonic crystals to produce brilliant iridescence, a possibility we explore in the Discussion.

2.2.4 Hollowness

Hollowness occurs in both rod-shaped and platelet-shaped melanosomes. However, whether the size of internal air pockets (d_{air}, Figure 2.8C) differs in hollow rods compared to hollow platelets has never been tested. If air pockets function primarily to produce strong interference colors in bird-visible wavelengths, we predict that there should be no difference between the air pocket diameters in hollow rods and hollow platelets and that diameters should be constrained between 75 and 350nm (see §2.2.1, *Identifying key melanosome modifications*). On the other hand, if hollowness evolved for different reasons in rods and platelets, and/or for non-optical functions, their air pocket diameters may differ. Air pocket diameter ranged from 50 to 251nm and did not differ significantly between rods and platelets (phylogenetic ANOVA, $F(1, 55) = 16.80$, $p = 0.176$, $df = 1$). This range does indeed include the thickness (75–350nm) that would produce interference colors of the first order in the bird-visible range. Taken together with our results on melanin layer thickness (see previous section), both air pockets in hollow melanosomes and thin melanin layers appear to be tuned to produce bright and saturated colors.

Our phylogenetic analysis shows that a hollow interior has evolved in at least 12 bird families, or 34% of all families in the feather iridescence database (Figure 2.3B). Many families with brilliant iridescence are included, such as Phasianidae, Trochilidae, and Sturnidae. However, hollow melanosomes do not appear to be a requirement for brilliant iridescence. Unlike thin melanin layers, which are present in all families exhibiting brilliant iridescence, hollow melano-

somes are absent in many families containing brilliant iridescent species, such as Nectariniidae, Paradisaeidae, and Columbidae. Still, the occurrence of a hollow modification is phylogenetically widespread. The 12 families with a hollow modification belong to 10 different orders (Galliformes, Coraciiformes, Passeriformes, Bucerotiformes, Trogoniformes, Cuculiformes, Pelecaniformes, Caprimulgiformes, Piciformes, and Ciconiiformes), which suggests that the genetic changes associated with producing a hollow melanosome are either likely to occur or are highly conserved in birds. A more comprehensive phylogenetic analysis will be required to determine how many times hollow melanosomes have evolved independently in birds, but our study indicates that this modification evolved many times independently.

2.2.5 Platelet shape

We classified structures as "platelet-shaped" if they diverged from a circular cross-section. The degree of divergence varies, resulting in platelets with a range of eccentricities. Unfortunately, with few exceptions, the studies surveyed did not include measurements of the width of platelets, preventing us from quantifying and exploring the eccentricity of platelets. We did not find support for the hypothesis that platelets allow birds to incorporate a greater number of layers in the iridescent structure. There was no significant difference between number of layers in structures with platelets compared to rods (phylogenetic ANOVA, $F(1, 220) = 21.88$, $p = 0.321$).

Platelets are present in 11 bird families, or 31% of all families represented in the feather iridescence database (Figure 2.3B). This is very similar to the frequency of the hollow modification (34% of families). In fact, many of the families that have evolved a hollow modification have also evolved platelets. In some cases, the modifications have evolved in combination, producing hollow platelets—but in other cases solid platelets and hollow rods have evolved separately within a family. Only Nectariniidae, Hirundinidae, Hemiprocnidae, Apodidae, and Psophiidae have evolved platelet shapes but never hollow forms (Figure 2.3A, with the caveat that this may change with increased sampling). As with hollowness, platelets are present in many but not all families with brilliant iridescence. For example, platelets are absent in Paradisaei-

dae, Phasianidae, and Columbidae. Nevertheless, platelets are widely distributed across birds; they are present in seven different orders (Passeriformes, Pelecaniformes, Caprimulgiformes, Trogoniformes, Gruiformes, Piciformes, and Cuculiformes).

2.2.6 Evolution of multiple modifications

We hypothesized that hollow and platelet shape modifications are in fact different mechanisms for achieving thin melanin layers. This is supported by the fact that hollow and platelet-shaped melanosomes always have thin melanin layers—there are no platelets or hollow forms with melanin layers $\geq$ 190nm. However, five bird families have evolved all three modifications: thin melanin layers, hollowness, and platelet shape (Trochilidae, Trogonidae, Sturnidae, Galbulidae, and Threskiornithidae, Figure 2.3B). If hollowness and platelet shape are alternative ways to achieve thin melanin layers, then why have some birds evolved both? The repeated evolution of hollow platelets suggests that at least one modification carries some additional functional value. For example, hollowness may in itself also increase the brightness of colors. Though it is possible that both modifications evolved together due to a shared mechanistic path, rather than due to some adaptive benefit, this is unlikely because species in each order with hollow platelets have close relatives with solid platelets, solid rods and/or hollow rods (Figure 2.3A). Moreover, as noted above, some species within a family have evolved solid platelets while others have hollow rods. Thus, there does not appear to be a strong constraint on evolving these particular modifications together, since each modification exists in isolation.

2.2.7 Optical consequences of modified melanosomes

To understand how each melanosome modification affects color production in brilliant iridescent structures, we simulated light reflection from different structures using optical modeling. We generated 4500 unique structures (900 for each of the five melanosome types) that varied systematically in structural parameters (including diameter of melanosomes, lattice spacing, hollowness, and platelet shape; see full model description in Materials and methods). All the structures were of photonic crystal type, since we were interested in the evolution of bril-

liant iridescence. The parameter ranges used to generate the structures were derived from the known ranges reported in the feather iridescence database for each melanosome type (Table 2.1). Thus, although the simulated structures are hypothetical, they represent a realistic approximation of the structural variation that could exist, while allowing us to standardize parameters that could bias comparisons in real structures. For example, we modeled all simulated structures with four layers (the median number of layers for photonic crystals in the feather iridescence database), while real structures have varying numbers of layers, which would affect the brightness and saturation of colors independent of melanosome type.

We modeled the simulated reflectance spectra in avian color space to estimate color saturation and diversity in a manner that is relevant to bird color perception. The avian tetrahedral color space represents all the colors a bird can theoretically perceive (Endler & Mielke, 2005, Goldsmith, 1990, Stoddard & Prum, 2008). Reflectance spectra can be represented in tetrahedral avian color space as a function of how they would stimulate a bird's four color cone types. Once reflectance spectra are mapped in avian color space, we can extract values of saturation (distance to the achromatic center of the tetrahedron) and color diversity (mean Euclidean distance between all points—color span, and number of voxels occupied, see Materials and methods for details). To quantify the brightness of a spectrum, we used two measures: (1) peak reflectance (% reflectance at the wavelength of maximum reflectance); and (2) estimated stimulation of the avian double cones, which may play a role in achromatic perception (Hart, 2001, Jones & Osorio, 2004). We refer to both metrics as "brightness" for convenience; the term luminance is often used to describe the perception of signal intensity (here modeled using the avian double cones). Taken together, these metrics give a good representation of the saturation, color diversity, and brightness of simulated reflectance spectra, where saturation and brightness together describe the brilliance.

Optical modeling revealed that thick solid rods are severely constrained in color diversity (Figure 2.6A). The simulated spectra are clustered toward the center of the tetrahedron, which means that they are producing colors of low saturation. In known feather nanostructures, thick solid rods are almost exclusively found in single-layered structures, which produce colors

of low saturation and brightness. In theory, low color saturation and brightness could be due to the single-layered structure, as opposed to the melanosome type. However, we modeled all structures with four layers, suggesting that it is the thick solid rods themselves—and not the number of layers—that limits color production. In other words, producing saturated colors is not possible with thick solid melanosomes, irrespective of whether the structure is single-layered or a photonic crystal.

In contrast, all four derived melanosome types with thin melanin layers are capable of producing a large range of saturated colors (Figure 2.6B–E). Color diversity (color span and voxel occupancy) is very similar for the four derived types, suggesting that melanin thinness—the only modification they all share—is the most important modification for achieving saturated and varied colors (Figure 2.6K–L). We note that the four derived melanosome types can also produce unsaturated colors, near the origin of the colorspace (Figure 2.6B–E). This is not surprising, since our simulated structures were generated across the full range of possible combinations of melanosome size and spacing. The reflectance from a photonic crystal will depend on both melanosome size and spacing. Thus, even if the melanin layer thickness is within the expected range, it needs to be paired with the appropriate keratin thickness to produce bright interference colors (see §2.2.1, *Identifying key melanosome modifications*). Saturation will also vary for structures with thin melanin layers depending on how closely they approximate the ideal condition (where optical thickness of melanin layers $= \lambda/4$). This pattern can be seen by plotting mean saturation for simulated structures with solid rods of increasing diameters (Figure A.2). There is no instantaneous leap to high saturation at 190nm—rather, at 190nm saturation starts to increase and reaches a peak at around 100nm. This fits well with our theoretical expectation—saturation should start to increase below 206nm (where optical melanin layer thickness $< \lambda/2$) and then peak around 103nm (upper value where the condition of optical melanin layer thickness $= \lambda/4$ is satisfied).

To explore the effects of thin melanin layers, hollowness, and platelet shape on color properties in detail, we constructed linear models with melanosome modifications as binary predictors (present and absent) and saturation and brightness (described by two measures: double

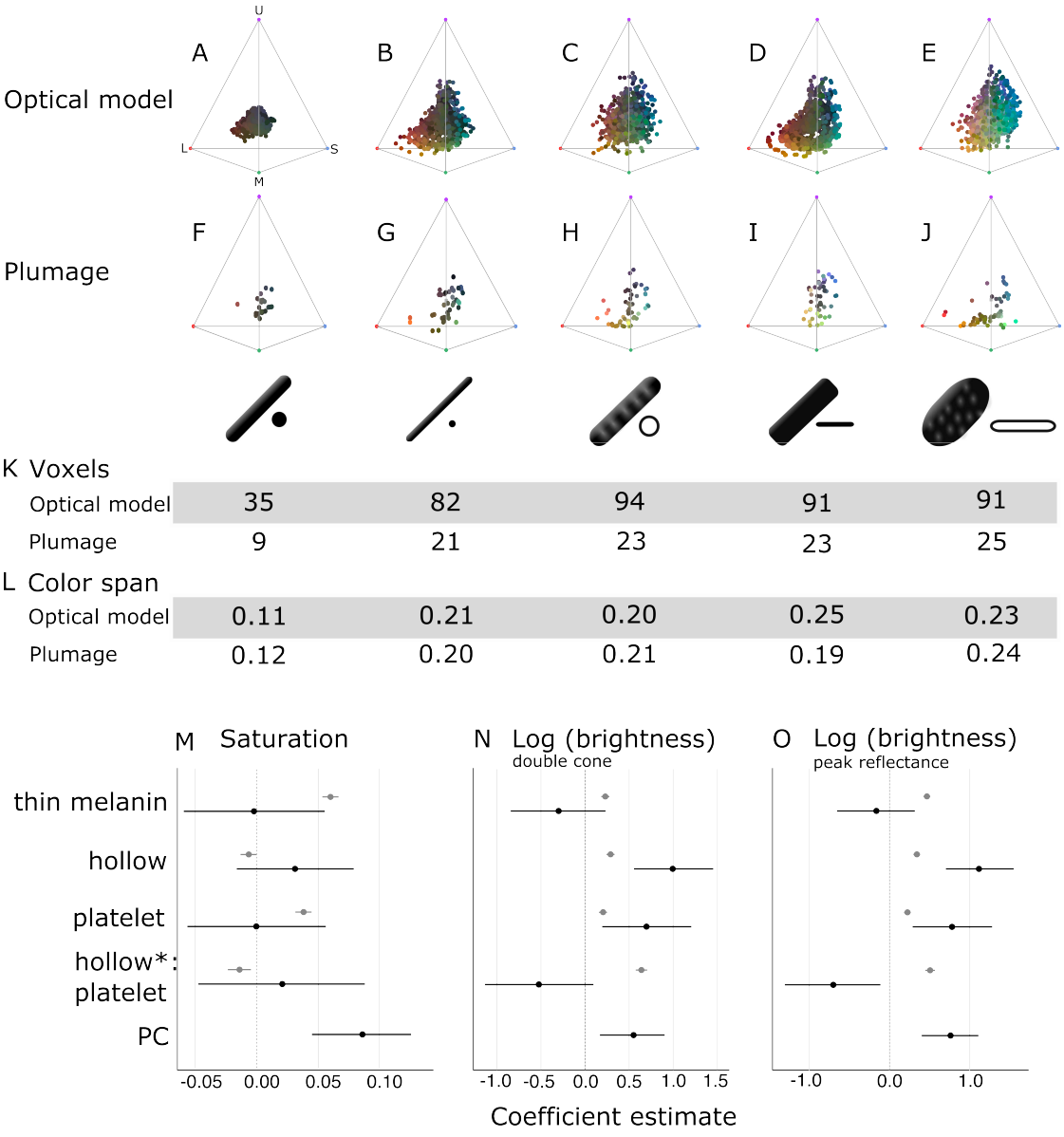

Figure 2.6: Optical effects of different melanosome modifications, as predicted by an optical model and found in empirical plumage analysis. (A–J) show the color diversity for structures with each type of melanosome represented in an avian tetrahedral color space (optical model (A–E); plumage data (F–J)). Statistics for color diversity are presented in terms of the number of occupied voxels (K) and mean color span (L) for both data sets. Thick solid rods produce colors of substantially lower diversity and saturation (A, F) than all melanosome types with thin melanin layers (B–E, G–J). In contrast, hollowness and platelet shape do not affect color diversity notably (C–E, H–J). (M–O) depict the estimates for the effects of each melanosome modification on saturation (M), log (brightness, double-cone) (N), and log (brightness, peak reflectance) (O), as predicted by linear models. The parameter PC describes variation explained by having a photonic crystal, which was used to control for variation in plumage data (see §2.2, *Results*). Gray points show coefficient estimates for a model based on optical model simulations, and black dots show the posterior coefficient estimates for a model based on the plumage data. Horizontal lines show 95% confidence intervals for estimates.

cone stimulation and peak reflectance) as responses. This allowed us to separate the effects of the different modifications, which are combined in many melanosome types (e.g. hollow rods are both hollow and have thin melanin layers). In agreement with the results for color space occupancy (Figure 2.6A–E), melanin layer thickness explained the greatest amount of variation in saturation in our linear model (Figure 2.6M; gray points). A positive effect was also seen for a platelet shape, which suggests that of the four derived melanosome types, solid platelets produce colors of the highest saturation. Small losses in saturation are incurred from incorporating hollowness, as can be seen from the negative coefficients of the variable hollowness and the interaction term hollowness×platelet shape (describing hollow platelets).

The linear model yielded similar results for both of our brightness measures (Figure 2.6N–O; gray points). All modifications increase brightness, but this effect is strongest for the interaction of hollowness and platelet shape (Figure 2.6N–O; gray points). Thus, the optical model predicts that hollow platelets produce the brightest colors. This effect likely arises from a lowered overall refractive index of melanosome layers with hollow platelets, which have a lower melanin-to-air ratio than layers built with hollow rods. However, this effect may be considerably weaker in real structures, where hollow platelets often have an internal honeycomb-like structure of melanin (Figure 2.2E), which would make the effective refractive index closer to that of hollow rods. Thick solid rods, hollow rods, and solid platelets produce colors that are less bright than those of hollow platelets but similarly bright to one another (Figure 2.6N; gray points).

Taken together, these results indicate that evolving thin melanin layers is the single most important factor for dramatically increasing color diversity and saturation (Figure 2.6A–E and M; gray points) while simultaneously increasing brightness (Figure 2.6N–O; gray points). When the effect of thin melanin layers is accounted for, a platelet shape has a similar but weaker effect on saturation and brightness (Figure 2.6M–O; gray points). Hollowness only increases brightness further (Figure 2.6M–O; gray points).

2.2.8 Testing predictions with plumage data

Next, we investigated whether we could recover the same patterns in the iridescent plumage of birds with different nanostructures. We collected spectral data from 111 patches on 80 species that were represented in the feather iridescence database and possessed known melanosome types. Plumage patches included weak and brilliant iridescent colors, with melanosomes arranged in single layers and photonic crystals, respectively. We included single-layered structures in our plumage data set since thick solid rods do not occur in photonic crystals. Including single-layered structures allowed us to compare all five melanosome types.

In agreement with the optical model results, the color diversity of structures with thick solid rods is low, almost half of that found in structures with thin melanin layers (Figure 2.6F). Moreover—mirroring the results in our optical model simulations—thin solid rods, hollow rods, solid platelets, and hollow platelets are all nearly equal in color diversity (Figure 2.6K–L). While the four derived melanosome types also produce unsaturated colors, these colors are mainly produced by single-layered structures (Figure 2.6, Figure A.1). However, some differences between the optical model simulations and plumage data are noteworthy. In contrast to other melanosome types, solid platelets do not produce any saturated red colors. This is unlikely to be due to any inherent developmental or physical constraint, since our optical model simulations—based on realistic melanosome properties, including size—indicate that solid platelets can clearly produce colors in this area of color space (Figure 2.6D). Rather, this effect may be a consequence of phylogenetic bias, as the majority of species with solid platelets in our data set are sunbirds (Family Nectariniidae), a group that uses carotenoid pigments—rather than structural colors—for red plumage coloration.

To explore further how thin melanin layers, hollowness, and a platelet shape affect saturation and brightness, we fitted generalized linear mixed models using Bayesian methods that allowed us to account for multiple measurements within a species (i.e. we obtained two reflectance measurements per plumage patch per species). In contrast to our optical model simulations, melanosomes in the real plumage patches we measured were arrayed in a variable number of layers. Since having many layers is known to increase the brightness and satura-

tion of colors, we added a parameter to control for this effect. The binary parameter "PC" (photonic crystal) described whether a structure contained a single layer of melanosomes (not a photonic crystal), or several repeating layers of melanosomes (photonic crystal). In our data set, 38 species had a single layer and 42 species had a photonic crystal structure.

In this linear model, there were no significant effects of either platelet shape or hollowness on saturation (Figure 2.6M; black points). Thus, we did not find support for the optical model prediction that solid platelets produce more saturated colors. We also did not find a significant positive effect of thin melanin layers (Figure 2.6M; black points), in contrast to our findings with the optical model. However, since our plumage data did not include any photonic crystals with thick melanin layers, the effect of thick versus thin melanin layers could only be compared for single-layered structures. Thus, our model suggests that thin melanin layers do not increase saturation for single-layered structures. This is supported by the low and similar color diversity seen across single-layered structures, irrespective of melanosome type (Figure A.1). The model also confirms that photonic crystals produce colors of significantly higher saturation than single-layered structures (Figure 2.6M; black points). While the plumage data cannot directly tell us the effect of thin melanin layers in a photonic crystal, the simulations from our optical model show that thick solid rods in a photonic crystal would not produce more saturated colors than a typical single-layered structure (Figure 2.6A). Thus, the plumage data and optical model together suggest that both a photonic crystal and thin melanin layers are required to produce saturated and diverse colors.

In terms of brightness, the plumage data compare to the optical model simulations in interesting ways. In agreement with the optical model, the linear model revealed a significant positive effect of hollowness and platelet shape on the brightness of colors (Figure 2.6N–O; black points). However, we did not see a large positive effect of hollow platelets in the empirical data. In fact, this parameter has a negative effect, which is significant for peak reflectance (Figure 2.6O; black points). This discrepancy may be due to the fact that—in the real plumage structures measured—hollow platelets tended to be arranged in relatively few layers. Our sample of structures with solid platelets consisted almost entirely of different species of sunbirds

(Family Nectariniidae), which exhibit 5–8 layers (Durrer, 1962), while the sample for hollow platelets contained several groups with fewer layers (e.g. Durrer, 1977). We could not control for this because the number of layers is not known in many of the structures we sampled; instead, we only included a parameter to indicate if a structure was a photonic crystal or not. We can, however, compare the brightness of single-layered structures with hollow platelets versus solid platelets. This comparison shows that the hollow platelets produce brighter colors (phylogenetic ANOVA, $F(1, 34) = 12.10$, $p = 0.034$, $df = 1$). Thus, the general conclusion that hollowness increases brightness is well supported, although this advantage is likely to diminish with increasing number of layers in the structure. Reflection from a multilayer with melanin and keratin becomes saturated at > 9 layers (Land, 1972), so it is likely that the greatest advantage of hollowness is gained for structures with ≤ 9 layers.

When interpreted alongside the optical modeling, the plumage data support the general conclusions that thin melanin layers, in combination with a photonic crystal structure, are critically important for producing diverse and brilliant colors, while hollowness and platelet shape are less crucial. We observe a near doubling of color diversity for real plumage structures with thin melanin layers compared to structures with thick solid rods, consistent with the results of the optical model. While the plumage data alone cannot prove that this difference is driven by the combination of thin melanin layers and photonic crystal structure, as opposed to the PC parameter by itself, our optical models exclude this possibility (see Figure 2.6). A for a simulation of photonic crystals with thick solid rods). Hollowness and a platelet shape increase the brightness of colors further, in agreement with the optical model.

2.3 Discussion

Brilliant iridescence has been linked to the evolution of different melanosome modifications, most notably hollowness and a platelet shape (Eliason et al., 2013, Maia et al., 2013b), but how these modifications affect color production has not been evaluated in a unified framework. Here, we have taken a broad approach, comparing all five melanosome types found in iridescent feathers, to uncover general design principles governing the production of bril-

liant iridescence. We find that the most important modification for increasing brilliance is not hollowness or a platelet shape per se, but rather a third modification that unites all melanosomes found in brilliant iridescent structures: thin melanin layers. Specifically, we show that melanosomes in brilliant structures have converged on a melanin layer thickness of approximately 40–200nm (Figure 2.5), which is the theoretical expected thickness to produce first-order interference peaks in the bird-visible spectrum. Our optical simulations and empirical data demonstrate that this modification alone nearly doubles color diversity (Figure 2.6A–L) and simultaneously increases saturation and brightness (Figure 2.6M–O). In contrast, hollowness and platelet shape on their own only contribute to increased brightness, in line with earlier work on hollow rods (Eliason et al., 2013).

Our results have interesting implications for the evolution of brilliant iridescent structures in birds. For the production of weakly iridescent colors, it is sufficient to organize a single layer of melanosomes of any size, since it is typically the thickness of the overlying keratin cortex that controls the interference color (Doucet, 2006, Maia et al., 2009). In contrast, to produce brilliant iridescence, we show that two key optical innovations are required: a photonic crystal (multiple periodic layers of melanosomes) and melanin layers with an optical thickness $< \lambda/2$. Indeed, Durrer (1977) observed that these two features were common to the brilliant structures he studied and here we validate the importance of his observation with optical modeling and plumage color measurements. Specifically, we find that saturation increases for structures with melanin layer thickness $<$ 190nm (Figure 2.6A–E, Figure A.2), which we define as "thin melanin layers." Above this value, iridescent structures produce colors that have low saturation and brightness, irrespective of the number of melanosome layers (Figure 2.6A). This insight could be used to place a lower bound on when brilliant iridescence first evolved in feathers, using the fossil record. For example, the preserved melanosomes from the plumage of *Microraptor*, a feathered theropod that is predicted to have exhibited iridescent plumage, have an average diameter of 196nm (Li et al., 2012). This suggests that *Microraptor* exhibited weak iridescence, as opposed to brilliant iridescence. However, we caution that preserved melanosomes with melanin layers $<$ 190nm do not necessarily prove that the feathers originally

produced brilliant iridescence. Both a photonic crystal and thin melanin layers are required to produce brilliant iridescence—and the three-dimensional structure is usually lost in fossil feathers.

Our results show that photonic crystals with all four melanosome types found in brilliant iridescent structures have similar optical qualities. This suggests that variability in melanosome type may be strongly influenced by historical factors, as opposed to particular types being associated with specific optical functions. In other words, birds have a seemingly flexible "nanostructure toolkit" with which to produce diverse and brilliant iridescent colors. Thus, the reason that sunbirds (Nectariniidae) produce brilliant iridescence with solid platelets while hummingbirds (Trochilidae) mainly use hollow platelets (Figure 2.3A) is likely related to variation in evolutionary history rather than to variation in selection for different optical properties. Supporting this interpretation is the fact that diverse photonic crystals in birds often have independent evolutionary origins. In Galliformes, some families have photonic crystals with thin solid rods and others have photonic crystals with hollow rods (Figure 2.3A), but these different structures have almost certainly evolved from an ancestor with a non-iridescent or single-layered structure rather than a photonic crystal (Gammie, 2013). Similarly, in Sturnidae, photonic crystals with hollow rods in the genus *Cinnyricinclus* and photonic crystals with hollow platelets in the genus *Lamprotornis* likely evolved independently from non-iridescent structures (see Figure 2.3A, cf. Durrer & Villiger, 1970a, Maia et al., 2013b).

Yet in some groups, melanosome type is highly variable within the same genus, or even within the same species (interpatch variability). In the birds-of-paradise (Paradisaeidae), which typically display photonic crystals with thin solid rods, two species (*Paradisaea rubra* and *Parotia lawesii*) are known to have evolved large rods with a porous interior (see Figure 2.5, cf. Durrer, 1977, Stavenga et al., 2015). In Lawes' parotia (*Parotia lawesii*), other iridescent patches contain structures with thin solid rods, proving interpatch variability in melanosome type. Hummingbirds, whose iridescent structures are typically built with hollow platelets, can also exhibit interpatch variability in melanosome type. Some patches may contain a structure with solid platelets, or even mixed structures with both hollow and solid platelets (Gruson

et al., 2019b). It is notable that the only known examples of interpatch variability in melanosome type come from the birds-of-paradise and hummingbirds—groups that are known to have exceptionally high rates of color evolution (Beltrán et al., 2021, Eliason et al., 2020, Ligon et al., 2018, Parra, 2010). One hypothesis to explain this variation could be that modifications in hollowness/platelet shape tune the brightness of some patches (Figure 2.6N–O). However, this seems unlikely. Both birds-of-paradise and hummingbirds typically have > 9 melanosome layers in their iridescent structures, which already achieves nearly 100% reflectance irrespective of melanosome type. Moreover, our results suggest that there would be little or no difference in brightness between structures with solid platelets and hollow platelets (Figure 2.6N–O)—only between thick solid rods and hollow and/or platelet-shaped melanosomes. Indeed, Gruson et al. (2019b) found color production to be similar among patches with different melanosome types in hummingbirds. We speculate that high interpatch variability in melanosome type in hummingbirds and birds-of-paradise is not related to general optical benefits of specific melanosome types or modifications, but rather to general high rates of color change in these groups (Eliason et al., 2020, Parra, 2010). Our optical modeling results (Figure 2.6B–E) show that there are multiple ways to reach the same areas of color space—using different melanosome types. It is possible that a change in melanosome type may be the fastest route to a new area of color space, even though the same color shift could in theory be produced by adjusting the size of the original melanosome type. This idea is hard to test with our current very limited understanding of the genetics of iridescent structures, but we predict that groups with high variation in melanosome type will have a greater standing variation in genetic traits associated with different melanosome types. We also predict that plumage patches with higher rates of color evolution will have greater variability in melanosome type.

We have proposed that evolutionary history can explain the diversity of derived melanosome types in iridescent feather nanostructures, as opposed to particular types being associated with specific optical functions. However, we cannot fully exclude hypotheses based on general adaptive explanations tied to melanosome type. Our plumage color data set, though phylogenetically broad, is relatively small, and it is possible that increased sampling could re-

veal some differences in color production between derived melanosome types. It would be important to pair a larger data set with detailed information on the number of layers in the iridescent structures, since this is a parameter for which we could not fully control (number of layers is rarely reported in the literature). Future studies should also investigate potential interactions with the feather micro- or macrostructure. Iridescent feathers are known to have highly modified barbules (Durrer, 1977), which has been shown to affect coloration in Lawes' parotia (Stavenga et al., 2011) and the African emerald cuckoo (*Chrysococcyx cupreus*), (Harvey et al., 2013). The interaction of feather microstructure and coloration is an active field of study (McCoy et al., 2021), but how nanostructures and microstructures may interact is a largely unexplored topic. Such an investigation would likely explain some of the discrepancies between the plumage data (which is measured from many feathers with micro- and macro-shape) and the optical model simulations (which consider only the nanostructure). In addition, it is important to stress that we still lack a full understanding of how modified melanosomes function in single-layered structures. We found that hollow melanosomes and platelets only increase brightness, while saturation remained low irrespective of melanosome modifications in single-layered structures. However, our analysis did not investigate potential interactions between cortex thickness and melanosome type. Such interactions are of less importance in photonic crystals but could be significant for single-layered structures. Cortex thickness and melanosomes could be tuned together to produce in effect a multilayered structure, which would result in a stronger interference peak. Such "cortex tuning" may explain why some African starlings with a single layer of hollow platelets produce unusually bright and saturated colors (Figure A.1). A more detailed investigation is key to understanding why the derived melanosome types are found not only in photonic crystals—where they produce brilliant iridescence—but also in weakly iridescent single-layered structures.

Another open question involves the potential non-signaling functions of different melanosome types. Melanin has been shown to influence a feather's mechanical properties (Burtt Jr., 1979) and ability to resist bacterial degradation (Goldstein et al., 2004). An interesting question is therefore whether different types of iridescent structures contain different amounts

of melanin. Our results show that structures with derived melanosomes have converged on a shared range of melanin layer thicknesses (Figure 2.5), which suggests that differences in melanin content may not be large. However, melanin content has never been compared across different iridescent structures. This would be an exciting avenue for future research, especially since differences in melanin production may induce pleiotropic effects on other traits, such as immune function or behavior (Ducrest et al., 2008).

Beyond elucidating the many functions of iridescent colors in birds, we need to understand how brilliant structures evolve to resolve fully the mystery of their structural diversity. To our knowledge, no general models have been proposed to explain how photonic crystals with modified melanosomes evolve from more simple, single-layered structures (but see discussion by Durrer, 1977, Durrer & Villiger, 1970a). We can use the insights derived from our study to propose two hypothetical routes to brilliant iridescence.

Brilliant iridescent structures likely originated from single-layered structures with thick solid rods (Maia et al., 2012, Shawkey et al., 2006). To achieve brilliant iridescent colors, such a structure must evolve to incorporate a photonic crystal-like organization of melanosomes—and the melanosomes must have thin melanin layers. However, our results showed that either of these changes on their own does not increase color saturation or brightness. This leads to an interesting problem, where only the two adaptations together produce a great advantage in brilliance. How could such a structure evolve? We propose two evolutionary paths through which this may have occurred—either via elaboration of melanosome shape first and photonic crystals second (Path 1) or via elaboration of photonic crystals first and melanosome shape second (Path 2). Both paths lead to feather structures with thin melanin layers, fully capable of making a broad range of brilliant iridescent colors (Figure 2.7).

In the first route, modified melanosomes with thin melanin layers evolve for reasons unrelated to color saturation (Figure 2.7B), perhaps to enhance brightness. Hollow and platelet-shaped modifications may evolve initially to produce brighter colors, while thin solid rods have been hypothesized to facilitate the formation of thin film structures through their elongate shape (Maia et al., 2012). Once evolved, melanosomes with thin melanin layers allow for

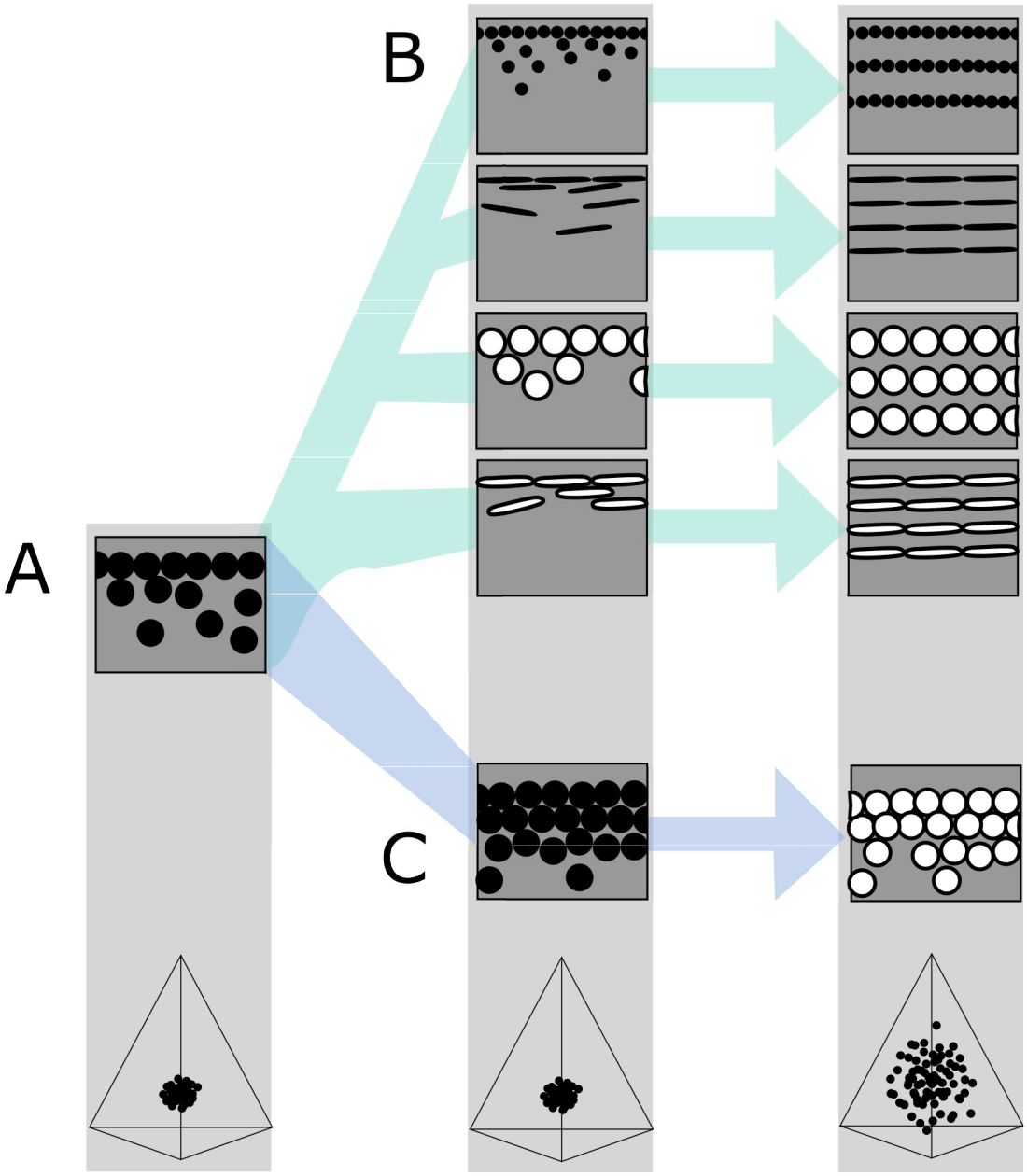

Figure 2.7: Hypothetical evolutionary paths to brilliant iridescence. Gray squares depict schematics of barbule cross-sections, showing the iridescent nanostructures within, while the tetrahedra below show hypothetical color diversity for each evolutionary 'step" represented in avian color space. (A) Assumed ancestral state for iridescent structures—a single-layered structure with thick solid rods. Note that a layer refers to a continuous layer of melanosomes; scattered or disorganized melanosomes often seen below a continuous single layer do not constitute additional layers. From this state, structures may either first evolve modified melanosomes in a single-layered structure (B, Path 1) or first evolve multilayered, hexagonal structuring of thick solid rods (C, Path 2). Both of these states are expected to give a negligible advantage in terms of color saturation and diversity, as seen in the hypothetical color spaces corresponding to each stage (bottom). We argue that Path 1 might initially be driven by selection for brighter colors, while Path 2 could form spontaneously from higher concentrations of melanosomes in the barbule. Both paths can then evolve toward more brilliant forms (multilayers in (B), modified melanosomes with thin melanin layers in (C)), which will drastically expand the possible color diversity.

the evolution of photonic crystals, since such structures would produce brighter and more saturated colors. The second route to brilliant iridescence involves the spontaneous formation of a photonic crystal from a single-layered structure, which then selects for modified melanosomes with thin melanin layers (Figure 2.7C). In many single-layered structures, a discontinuous second layer can be seen beneath the top layer, where melanosomes are packed hexagonally (e.g. Figure 2.2A). This likely provides a more mechanically stable configuration during barbule development (as suggested by Eliason et al., 2013). It is easy to see how the evolution of hollowness in such a structure would lead to the production of brilliant iridescence.

The feather iridescence database gives some support to both of these hypothetical paths. Single-layered structures with modified melanosomes are relatively common (Figure 2.5), suggesting that Path 1—where melanosome shape diversifies first—may be a common route to more complex structures. In support of Path 2, hexagonally arranged photonic crystals with hollow rods are common in many groups (Galliformes and Trogoniformes) that also contain taxa with single-layered structures of thick solid rods. However, very few clades are sampled in sufficient detail to draw inferences about the transitions between different structures. To test our hypotheses, careful characterization of nanostructures in a group with repeated transitions to brilliant iridescence is needed. Such a study could also lay the groundwork for exploring the genetic regulation of iridescent structures, an area of research in its infancy (Saranathan & Finet, 2021, Rubenstein et al., 2021, Price-Waldman & Stoddard, 2021).

By investigating the evolution and optical properties of brilliant iridescent feather nanostructures spanning 15 avian orders, we have identified some features common to iridescent nanostructure design and some features that are likely to result from differences in evolutionary history. The key feature uniting melanosomes in brilliant iridescent structures is the presence of thin (<190 nm) melanin layers, which tunes a photonic crystal to produce bright and saturated colors in the bird-visible spectrum. We suggest that much of the diversity in melanosome type in brilliant iridescent structures—such as the prevalence of solid platelets in sunbirds but hollow platelets in hummingbirds—could be explained by differences in evolutionary history, since different melanosome types offer alternative routes to producing thin

melanin layers. We propose two likely evolutionary routes, which could be explored further in a careful study of a clade with repeated transitions to brilliant iridescence. This would clarify the steps associated with the evolution of brilliant iridescence—and potentially link these steps to genetic changes.

The large-scale patterns uncovered in this study are only a first step toward gaining a deeper understanding of how brilliant iridescence has evolved in birds. By focusing on large-scale patterns and general themes, our study may obscure or overlook some unique or unusual nanostructural strategies evolved by particular species or genera. However, our broad study should provide a powerful springboard for more focused studies.

2.4 Materials and methods

2.4.1 Building the feather iridescence database

We surveyed the literature for microscopy studies of iridescent feathers using two complementary approaches. For studies published earlier than 2006, we used the references in Prum (2006) and Durrer (1977) as a starting point. For later publications, we used Google Scholar to search for articles containing the terms "iridescence" and "feather." We then extracted the following information from each study (where available, or possible to infer from redundant measurements): melanosome arrangement (single-layered, photonic crystal), melanosome type (i.e. solid rod, hollow rod, solid platelet, or hollow platelet), melanosome diameter (d_{melsom}), lattice spacing (a), the number of melanosome layers (n), diameter of hollow interior (if present, d_{air}), thickness of keratin layers (ks), thickness of melanin layers (mt; for solid forms $mt = d_{\mathrm{melsom}}$, for hollow forms $mt = (d_{\mathrm{melsom}} d_{\mathrm{air}})/2$), cortex thickness ($c$), the patch from which the studied feather originated, and the color of the feather. A schematic of all measurements is shown in Figure 2.8. With few exceptions, most studies sampled only a single iridescent patch from each species. This is based on the assumption that iridescent nanostructures are similar in all iridescent patches in a species, which seems to be true in most species but not all; hummingbirds and birds-of-paradise are the only known exceptions (Durrer, 1977, Gruson et al., 2019b).

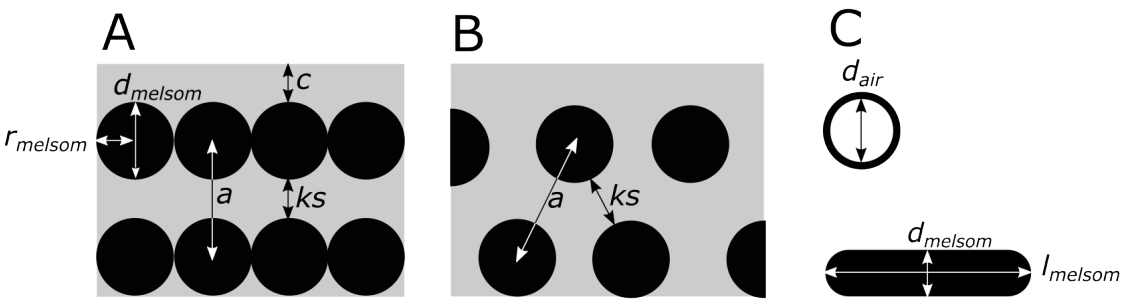

Figure 2.8: Definitions of parameters used in the study, shown in schematics of cross-sections of iridescent structures. (A) Laminar photonic crystal (multilayer); (B) hexagonal photonic crystal; and (C) isolated hollow and flat melanosomes. In (A), d_{melsom}: diameter of melanosome (shortest axis in flat melanosomes), r_{melsom}: radius of melanosome ($d_{\mathrm{melsom}}/2$), c: thickness of keratin cortex, a: lattice spacing (center-center distance between melanosomes), ks: keratin spacing (thickness of keratin layer between melanosomes at the thinnest point). In (B), keratin spacing (ks) and lattice spacing (a) are shown for a hexagonal photonic crystal. In (C), d_{air}: diameter of internal air pockets (shortest axis of air pockets in hollow platelets), l_{melsom}: width of platelets. Melanin layer thickness is defined as (d_{melsom} for solid forms, and ($d_{\mathrm{melsom}} - d_{\mathrm{air}})/2$) for hollow forms.

For a small number of records ($n = 17$), we produced new measurements of iridescent structures using transmission electron microscope images previously collected by Nordén et al. (2019). Images were measured using the program ImageJ (Abràmoff et al., 2004). All images used for new measurements are available to download from the Dryad Digital Repository.

In total, our database covers 47 studies from 1952 to 2020 and 306 unique species, across 35 families and 15 orders (37% of total orders and 14% of total families in Aves, after taxonomy in Billerman et al. (2022). Out of these, 280 species had enough data to be included in our phylogenetic analyses.

2.4.2 Phylogeny

We used the phylogenies of Jetz et al. (2012), which are based on a Hackett et al. (2008) backbone, to construct a tree including all the species in the feather iridescence database and the species from the Li et al. (2012) data set. The data set from Li et al. (2012) of melanosome diameters in black feathers was included to compare with the data on melanosomes in iridescent structures. We sampled 1000 pruned trees from the tree distribution available at birdtree.org and then constructed a 50% consensus tree from this distribution. Branch lengths were calculated using the "consensus.edge" function in the R package *phytools* (Revell, 2012). This tree was then pruned as necessary for different analyses.

2.4.3 Optical modeling

We modeled the reflectance from iridescent feather structures using the software package MIT Electromagnetic Equation Propagation (MEEP) (Oskooi et al., 2010). Simulations were performed in one unit cell, with an absorbing perfectly matched layer in the x-direction, and periodic boundaries in the y-direction. Resolution was set to 80 pixels/μm, which gives 12 sampling points for one 300nm wave in the material with the highest refraction index (melanin). We set the extinction coefficient (k) of melanin to 0.1, the refractive index (n) of keratin to 1.56, and the refractive index of melanin to 2. These values are an approximation based on published values (Brink & van der Berg, 2004, Stavenga et al., 2015). In reality, these values vary over the light spectrum for most materials. Both n and k decrease from short wavelengths to longer wavelengths for melanin. A higher refractive index is expected to broaden and increase reflection peaks, while a high extinction coefficient will tend to decrease the amplitude of the reflectance peak. Thus, peaks in the short wavelengths will tend to be slightly broader (but not taller), resulting in a brighter but less saturated color, compared to long-wavelength colors. However, we did not observe any large differences between modeled and plumage data in this direction, and thus we expect the effects of a varying refractive index to be insignificant for the larger patterns we describe. The extinction coefficient for keratin is likely to be low ($k = 0.03$, Brink & van der Berg, 2004) and was omitted (set to 0).

Table 2.1: Model parameter ranges for each melanosome type. The values reported in parentheses are the number of evenly spaced steps with which the parameter was varied. For each melanosome type, we simulated 900 unique structural configurations.

Melanosome type	Melanosome diameter	Hollowness	Flatness	Relative lattice spacing	Cortex	Hexagonal
Thick solid rods	190–300 (30)	0	1	0.15–0.5 (5)	5–1000 (3)	Yes
Thin solid rods	65–180 (30)	0	1	0.15–0.5 (5)	5–1000 (3)	Yes
Hollow rods	135–440 (10)	0.26–0.69 (3)	1	0.15–0.5 (5)	5–1000 (3)	Yes
Solid platelets	45–140 (30)	0	2.4	0.15–0.5 (5)	5–1000 (3)	No
Hollow platelets	135–280 (10)	0.26–0.69 (3)	2.4	0.15–0.5 (5)	5–1000 (3)	No

The structural parameters varied in the model were melanosome diameter (d_{melsom}), relative hollowness ($d_{\mathrm{air}}/d_{\mathrm{melsom}}$), flatness ($l_{\mathrm{melsom}}/d_{\mathrm{melsom}}$), relative lattice spacing (r_{melsom}/a),

and cortex thickness (c, Figure 2.8). We set the ranges for parameters related to melanosome shape to match the known ranges for each melanosome type, extracted from the feather iridescence database. For lattice spacing and cortex thickness, we modeled values over the total range reported in the feather iridescence database, and number of layers was fixed to 4 (the median in the feather iridescence database). For structures with rods, we modeled structures with a hexagonal packing in addition to the standard laminar configuration (Figure 2.8B and A, respectively) to represent the diversity present in real structures. Although a square configuration also exists, we did not model this since it has only been recorded in a single genus, the peafowls (*Pavo*). Table 2.1 gives a detailed overview of the model settings for each melanosome type. Notice that the melanosome diameter of solid forms is varied in 30 steps, while the diameter of hollow forms is only varied in 10 steps. The thickness of melanin layers is important for determining hue, and hollow forms have two parameters that adjust this value (diameter and hollowness), while solid forms have only one (diameter). To avoid a bias toward greater hue variability in hollow forms due to this effect, we allowed the diameter of solid forms to vary in an equal number of steps as the combined effect of diameter and hollowness in hollow forms ($10 \cdot 3 = 30$).

In total, we ran 4500 simulations, with 900 simulations for each melanosome type.

2.4.4 Plumage measurements and spectral analysis

We collected spectral measurements of 80 bird species (across 13 orders) for which nanostructures were already known (see references in the feather iridescence database), housed in the American Natural History Museum, New York. Two individuals were used for each species, and all iridescent patches with different color (as perceived by human vision) were measured. In total, 111 unique patches were measured. Spectral measurements were taken directly on the specimen following standard procedures (Andersson & Prager, 2006). Briefly, we used a USB4000 spectrophotometer and a PX-2 xenon light source (Ocean Optics, Dunedin, FL). We measured color over a range of angles (15–135°) using a goniometer, keeping the light source fixed at 75°.

Spectra were analyzed in R v.3.6.1 (R Core team, 2019) using the package *pavo* (Maia et al., 2013a). All spectral data were first smoothed to remove noise, using locally weighted smoothing (LOESS) and a smoothing parameter of 0.2. We removed negative values by adding the minimal reflectance to the spectrum, and then rescaling this range back to 0–100% reflectance. We then extracted the spectra with maximum total brightness (area under the curve) for each patch. The variability between individuals of each species was assessed using pairwise distances in tetrahedral color space. If the patch measurements for the two individuals were very different in terms of color (separated by > 0.1 Euclidean distance in color space), we inspected the spectral measurements to identify possible inaccurate readings. Nine spectra were removed from the data set after this process, leaving a total of 213 spectra used for analysis.

2.4.5 Calculation of color variables used in analysis

To compare color diversity and color properties of different structures, we focused on five variables: (1) the number of voxels occupied in avian color space, (2) mean color distance in avian color space, (3) color saturation, (4) stimulation of the avian double cones, and (5) peak reflectance. These variables describe color diversity (1–2), color purity (3), perceptual brightness (4), and objective brightness (5), respectively. Peak reflectance is simply the maximum reflectance from each spectrum. Perceptual brightness was modeled as the photon catch from a chicken double cone (*Gallus gallus*, built-in data in the *pavo* package; see details above), since current evidence suggests that the double cones mediate achromatic/brightness perception in birds (Hart, 2001, Jones & Osorio, 2004). Saturation and color diversity were based on modeling spectra in avian color space (Stoddard & Prum, 2008). This space represents all the colors a bird can theoretically perceive. Relative cone stimulation was calculated from photon cone catches using cone sensitivity functions in *pavo*. Bird species vary in their ultraviolet spectral sensitivity; some species have a VS (violet-sensitive) cone type that is maximally sensitive in the violet range while others have a UVS (ultraviolet-sensitive) cone type that is maximally sensitive in the ultraviolet range (Hart, 2001). Because we modeled plumage colors across many phylogenetic groups, we used the sensitivity curves in *pavo* for an "average UVS"

(λ_{max} = 372nm) and "average VS" (λ_{max} = 416nm) type system. Since results in general were similar for a UVS- and VS-type system, we only include analyses based on a VS-type visual model (summary statistics for a UVS-type cone can be found in Table A.5-A.6), which is the ancestral condition in birds (Ödeen & Håstad, 2003).

Saturation in tetrahedral color space is simply the distance from the center of the tetrahedron (r vector, as defined by Stoddard & Prum (2008). For number of voxels occupied, we followed the approach of Delhey (2015). The tetrahedral color space is divided into 3D pixels (voxels), and then the number of voxels that have at least one data point are counted. The resolution of raster cells was set to 0.1, which gives a total of 236 voxels in tetrahedral color space. Mean color span is a measure of the spread of samples in color space and is calculated as the mean of pairwise Euclidean distances between all samples. This measure is more robust to sample size differences than voxel occupancy, which makes it better suited for comparing the plumage colors in our data set.

2.4.6 Statistical analysis

To compare iridescent structures recorded in the feather iridescence database (thickness of melanin layers, diameter of interior hollowness, and number of layers), we applied simulation-based phylogenetic analyses of variance (ANOVA), as described by Garland et al. (1993) using the R package *phytools* (Revell, 2012). Since this function assumes Brownian evolution of traits, we measured phylogenetic signal (Pagel's lambda) in the traits tested to confirm that this assumption was not violated. All traits tested recorded a high and significant lambda (Table A.2). To clarify relationships between groups, we also performed phylogenetic pairwise t-tests where necessary (using the R package *phytools* (Revell, 2012), Table A.1). Species that had more than one entry in the database (e.g. from multiple studies or multiple patches) were averaged before analysis. For comparison, we also included melanosome diameters from black feathers in some analyses. These data were taken from Li et al. (2012).

We performed a test for multimodality to assess whether solid rods show a binary distribution, following the method described by Fisher & Marron (2001), which is implemented in

the R package *modetest* (Ameijeiras-Alonso et al., 2018).

To explore how melanosome modifications affect color production, we fitted separate linear models with response variables saturation, avian double cone stimulation, and peak reflectance. Avian double cone stimulation and peak reflectance were log-transformed before inclusion into the models to achieve normally distributed residuals. We used binary predictors to describe the absence/presence of the three melanosome modifications: thin melanin layers ($<$ 190nm), hollowness and platelet shape. We also added the interaction term hollowness×platelet, since the optical effect of hollow platelets is not expected to be simply the addition of hollowness and platelet shape. This is because hollow platelets lower the refractive index of melanosome layers by having relatively less melanin in each layer. This property only applies to melanosomes that have both modifications (hollow and platelet) simultaneously. Note that since we have included an interaction term, the variables hollow and platelet are only describing a situation where the interaction is zero (i.e. for hollow rods and solid platelets, respectively).

Spectral data derived from optical simulations were analyzed using multiple linear regressions with the variables described above (summary of results can be found in Table A.7-A.9). For plumage data, we also needed to account for phylogenetic relatedness, as well as individual variability in patch color (for each species we had measurements from two individuals). We did this using Bayesian linear mixed models, adding phylogenetic structure and patch as random factors in the model. The phylogeny used was the same as for earlier analyses but pruned to contain only the 80 species in our plumage measurements. We also added a fourth predictor: presence/absence of a photonic crystal (PC). This variable accounts for expected variation in color brightness and saturation that is explained by whether the structure has a single layer of melanosomes or several (in the optical model simulations, all structures had four layers). We used the R package *MCMCglmm* (Hadfield, 2010) to run our Bayesian model with Markov Chain Monte Carlo methods. We ran chains for each model for 50 million generations, with a sampling frequency of 500. The first 50,000 generations were discarded as burnin. We used the default priors for the fixed effects and set an inverse gamma distribution prior for the vari-

ance of residuals and random factors. We checked that the analysis had reached a stable phase by visually examining trace plots and checked that autocorrelation values between parameters was low (all < 0.1). We also formally tested convergence of the chain using Heidelberg's and Welch's convergence diagnostics (all variables passed both tests). Summary of results for each model can be found in Table A.10-A.12.

2.5 Data availability

All data generated or analyzed during this study are included in the manuscript and supporting files. All datasets, supporting code and raw data to reproduce analyzes have been deposited with Dryad.

"Tell me one last thing," said Harry. "Is this real? Or has this been happening inside my head?" Dumbledore beamed at him, and his voice sounded loud and strong in Harry's ears even though the bright mist was descending again, obscuring his figure. "Of course it is happening inside your head, Harry, but why on earth should that mean that it is not real?"

J. K. Rowling, Harry Potter and the Deathly Hallows

3

On metallic luster and iridescence

Notes

This work was developed with co-authors Raphael S. Steiner, Anna B. Stephenson and Mary Caswell Stoddard.

Abstract

Some structural colors in nature are frequently described as metallic—for example hummingbird plumage, jewel beetles and *Morpho* butterflies. While much attention has been paid to describing the often-shifting hues of these structural colors, there has been little interest in explaining why they appear metallic. In this paper, we argue that the metallic luster of some structural colors arises in part from a combination of two factors: a very low diffuse reflection and a colored specular reflection. This type of reflection is found in metals and is distinct from other material reflections in nature. We propose that metallic luster can be classified based on these reflectance properties and suggest that some of the ambiguity surrounding the term "iridescent structural color" can be traced to the frequent confounding of metallic luster with a common definition of iridescence: a shift of peak spectral wavelength (often referred to as hue) with viewing angle. We show using optical models and cross-polarization imaging of bird plumage that two types of structural colors that are often classified as "iridescent" and "non-iridescent" both display iridescence—but only one has metallic luster. By considering metallic luster and iridescence separately, we simultaneously clarify terminology in structural colors and open up many new interesting questions regarding the perception of metallic luster in animals.

3.1 Changeable colors

In many cultures, "iridescence" has been used to symbolize a mysterious or unpredictable power that is difficult to grasp (Sutton & Snow, 2015). In a curious parallel, the term "iridescence" in natural sciences is difficult to define and is used to describe a range of visual effects. "Iridescence" has been used to describe rainbow-like colors in beetles and flowers (Seago et al.,

2009), the pearlescent colors of nacre (Ozaki et al., 2021) and the metallic colors found in, for example, bird plumage and insect cuticles (Doucet & Meadows, 2009, Seago et al., 2009). In The Oxford English Dictionary, the entry for "iridescent" reads: "displaying colours like those of the rainbow, or those reflected from soap bubbles and the like; glittering or flashing with colours which change according to the position from which they are viewed" (Simpson et al., 1989). This definition thus involves rainbow-like colors, colors that change with viewing angle, and glittering or flashing of colors (similar to metallic luster). However, all three of these effects do not necessarily occur together (for example, the rainbow is not glittering or flashing, but displays rainbow colors which change with viewing angle), and therefore a more precise definition of "iridescence" is needed in the sciences. This has indeed been pointed out in previous reviews of "iridescence" in nature, which restrict the term to a change in hue with viewing or illumination angle (Stuart-Fox et al., 2020, Ospina-Rozo et al., 2022). Hue is typically chosen as opposed to the broader term color (which includes hue, saturation and brightness), since almost all objects will change in brightness and saturation with viewing or illumination angle due to the effects of specular reflection. To get an intuition for this, imagine turning a shiny, red apple. As you do so, specular highlights will move across the surface of the apple. Thus, the brightness and saturation of the apple change with viewing and illumination angle. To exclude such effects, recent reviews of "iridescence" in nature have therefore argued that the term "iridescence" should be restricted to changes in hue (Stuart-Fox et al., 2020, Ospina-Rozo et al., 2022), while gloss is an already well-established term for angle-dependent changes in brightness and saturation (Chadwick & Kentridge, 2015). Following these reviews, we use the term iridescence to mean a shift in peak spectral wavelength with a change in observation or viewing geometry, while "iridescence" (in quotation marks) refers to the concept in a broader sense (see §3.2, *Definitions*). With a narrower definition, it might appear that the confusion surrounding the term "iridescence" has been resolved. In this paper, we argue that this is not the case, since many authors still use the term "iridescence" for a feature currently without a rigorous definition: metallic luster.

Metallic luster is a term originating from geology, where it is defined as "having the sheen

characteristic of metal" (Allaby, 2013). Minerals with metallic luster include pure metals such as gold, copper and silver, as well as metal-containing compounds such as pyrite. Many minerals combine iridescence with metallic luster, such as bornite (often called "peacock ore")—yet it is clear that these two aspects of minerals are distinct (Figure 3.1). It is possible to exhibit iridescence without metallic luster (such as in nacre, Figure 3.1B) and metallic luster without iridescence (such as in gold, Figure 3.1E). The key argument of our paper is that this dichotomy has remained unappreciated in the animal coloration literature. "Iridescence" is often used for objects that exhibit metallic luster or metallic luster in combination with iridescence (e.g. by some of us previously in Nordén et al., 2021)—but not always for iridescent objects that lack metallic luster. This has two unfortunate consequences. First, the iridescence of objects that lack metallic luster have been explored little and is generally disregarded. Second, for objects that exhibit both iridescence and metallic luster, only the iridescent qualities are emphasized, with little attention to metallic luster. To rectify these problems, we will show that many structural colors in nature that are referred to as "non-iridescent" are in fact iridescent, just like structural colors often referred to as "iridescent". We will also introduce a method for approximating a material's metallic luster, offering researchers a way of describing the distinct contribution of metallic luster to structural colors.

We hope that this will inspire new questions in the study of these remarkable colors.

The paper is structured as follows: In §3.2, *Definitions*, we define various terms we will use throughout the paper.

In §3.3, *Birds of an iridescent feather*, we use examples from the bird coloration literature to illustrate that two types of structurally colored plumage, commonly called "iridescent" and "non-iridescent", do not in fact differ in iridescence when measured over changing angles between illumination and observation. We support our argument with a theoretical analysis of peak spectral wavelength shifts for both structures, as well as with data from the literature of measured peak spectral wavelength shifts in both types of plumage.

In §3.4, *All that glitters is not gold*, we outline what a metallic reflection is and give a verbal argument based on the known optics of feather nanostructures that can explain why they—

despite not containing any metals—appear metallic. We argue that it is in fact this metallic-like reflection (metallic luster) that clearly sets "iridescent" structural colors apart from other types of color mechanisms, and we propose a classification based on two reflection properties that are characteristic of objects with metallic luster.

In §3.5, *Measuring metallic luster*, we develop a simple quantitative measure of metallic luster based on these reflectance properties using cross-polarization photography. We demonstrate this method using a sample of plumage patches with different color mechanisms.

Lastly, in the *Discussion*, §3.6, we discuss the merits of incorporating metallic luster into discussions of animal structural color. In particular, we argue that doing so is more than an exercise in building precise definitions: it in fact opens the door to intriguing research questions and new directions.

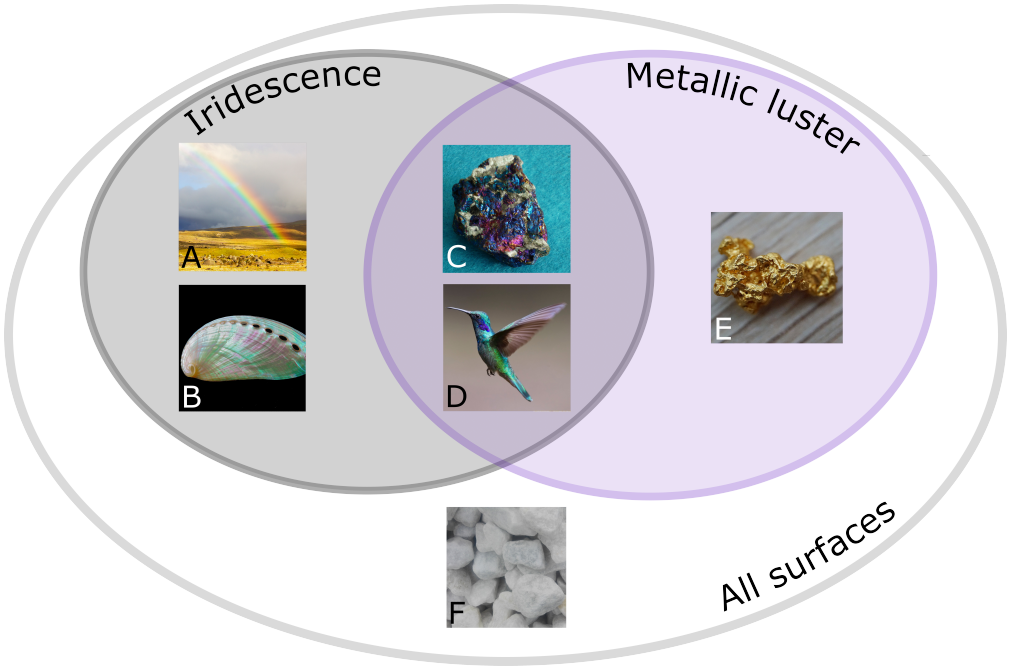

Figure 3.1: Iridescence and metallic luster are two separate properties that are often confused. Even though some objects are both iridescent and exhibit metallic luster, such as bornite (C) and the plumage of a hummingbird (D), these two properties need not be linked. Objects can be iridescent and lack metallic luster, as is the case for the rainbow (A) and nacre (B), or exhibit metallic luster but lack iridescence, as is the case for gold (E). Many objects, of course, lack both features—for example calcium carbonate (F). Images sourced from pixabay.com under a Pixabay license

3.2 Definitions

Due to the aforementioned ambiguity surrounding the term "iridescence", we will give precise definitions of *iridescence*, *metallic luster*, and related terms, of which we shall henceforth make use. When relevant, we have added remarks to give some background and motivation for our usage of the term.

Hue. The tint of a color, which is dependent on the spectral distribution of the reflectance, the illumination and the viewer's visual system.

Remarks: This term is interchangeably used in the animal coloration literature to describe a perceptual quality (as in our definition), or a proxy for this, usually the peak spectral wavelength (Montgomerie, 2006). The measures are related—but differ fundamentally since perceptual hue depends on the viewer's visual system, while peak spectral wavelength is an objective measure from the physical reflectance spectrum.

Peak spectral wavelength. The wavelength of maximum reflectance in a reflectance spectrum.

Remarks: There are many variations of this measure suited to different types of spectra. For example, spectral location (Ospina-Rozo et al., 2022) may better capture variations of broad spectral peaks. However, all such measures aim to specify the position of the spectral peak and are thus conceptually the same. Since the spectra we are analyzing in this paper generally have well defined peaks, we used peak spectral wavelength.

Iridescence. A shift in peak spectral wavelength with change in observation or viewing geometry.

Remarks: More commonly, this is defined as a shift in hue with viewing or observation angle, but with the dual meaning of hue implied (perceptual or objective) it can thus be interpreted as either a perceptual or an objective property. Since iridescence is almost always measured as a shift in peak spectral wavelength (or some version of this) and this measure does

not require choosing a specific visual system, we use this measure to develop our argument in this paper.

"Iridescence". Indicates general uses of the term (including rainbow colors, pearlescence (appearance similar to a pearl), glossiness and metallic luster), and/or where the precise meaning was not defined in the source referenced.

Metallic luster. Metallic sheen of an object, the reflection of which can be characterized as having 1) a colored specular reflectance; and 2) very low diffuse reflectance.

Remarks: Metallic luster is a perceptual concept, which is difficult to measure directly. However, it can be measured by a proxy: in this paper, we use aspects of the specular reflection.

Specular reflectance. A reflection seen at the mirror angle of light incidence with respect to the tangent of the surface (i.e. angles of light incidence and reflection are equal).

Remarks: On rough surfaces, the specular reflection will appear blurry due to the influence of the varied surface geometry (Figure 3.5B). On smooth surfaces, the specular reflection will appear sharp (Gloss, Figure 3.5A). Note that we have adapted here definitions of specular reflectance and gloss that are typically used in reflection models for computer graphics—see Ginneken et al. (1998).

Diffuse reflectance. A reflection that is seen at equal intensity from all viewing angles.

Remarks: Diffuse reflectance arises from sub-surface scattering in a material. This causes the light to be scattered multiple times, and it will therefore exit the material at a random angle.

Single-scattered light. Light that has only been scattered a single time.

Remarks: Specular reflections originate from single-scattered light. Note that while a specular reflection is defined by its direction (reflected at the mirror angle), the term single-scattered is only defined by the type of scatter, not its direction.

Multiple-scattered light. Light that has been scattered multiple times.

Remarks: Diffuse reflections of objects arise from multiple-scattered light. Note that while a diffuse reflection is defined by the uniform distribution of the reflectance direction, the term multiple-scattered light is only defined by the type of scatter, not its direction.

Gloss. The specular reflection of a smooth object.

Remarks: For most objects, the gloss will have the same spectral distribution as the illumination (typically white). The exceptions are metals and some structurally colored objects, which can reflect colored gloss.

Structural color. Colors arising from the interaction of light with a structure (i.e. a material with spatial inhomonogeneity). Optical processes such as reflection, refraction, scattering, interference and diffraction are the mechanisms behind color production.

Remarks: Structural colors can be contrasted with pigmentary colors, where the color arises from the interaction of light with an absorbing pigment. Note however, that many colors in nature involve both mechanisms, but to different degrees.

Barbule structural color. Type of structural colors in feather barbules, consisting of ordered arrays of melanin granules (melanosomes, Figure 3.2A). In an optical sense, these structures can be approximated well by a multilayer structure. In the context of bird feather colors, often used interchangeably in the literature with *"iridescent" structural colors*.

Barb structural colors. Type of structural colors in feather barbs, consisting of air and keratin (spongy keratin, Figure 3.2B). In an optical sense, these structures can be approximated well by a photonic glass. In the context of bird feather colors, often used interchangeably with *"non-iridescent" structural colors*.

3.3 Birds of an iridescent feather

To illustrate our argument that the term "iridescent" is often confounded with metallic luster, we will use bird plumage coloration, since there is a long history of classifying structural coloration of feathers as "iridescent" and "non-iridescent" (Gadow, 1882, Auber, 1957, Michelson, 1911, Haecker, 1890). In birds, one type of structural color is located in the feather barbules, gives a metallic shine and tends to shimmer when viewing angle is varied (Figure 3.2A). This type of coloration is found in, for example, the European starling (*Sturnus vulgaris*), Indian peafowl (*Pavo cristatus*), and many hummingbirds (family Trochilidae). A second type of structural color is located in the feather barbs and appears diffuse—not unlike pigmentary colors (Figure 3.2B). This type of coloration gives rise to, for example, the blue of the European kingfisher (*Alcedo atthis*), Blue jay (*Cyanocitta cristata*), and Indigo bunting (*Passerina cyanea*). Thus, there is clearly a distinct difference in the visual appearance of these two types of colors (at least to humans). Though they are commonly called "iridescent" and "non-iridescent", what we aim to show is that iridescence is in fact not the main visual property in which they differ. We stated in the previous section that previous authors have suggested that angle-dependent change in reflectance can be divided into two terms: gloss (or a change in intensity/spectral purity with viewing angle) and iridescence (a change in peak spectral wavelength with viewing angle) (Stuart-Fox et al., 2020, Seago et al., 2009, Ospina-Rozo et al., 2022). However, neither of these properties–gloss and iridescence–separates structural barbule coloration ("iridescent" structural colors) from barb coloration ("non-iridescent" structural colors). We unpack this in the sections below.

3.3.1 Gloss

The first aspect of angle-dependent change is gloss, which involves a change in light intensity with angle. All structural barbule coloration is glossy—but not all glossy plumage is produced by structural barbule coloration. Gloss is frequently found in pigmentary plumage (Iskandar et al., 2016) as well as plumage with structural barb coloration (Fig. 3.3). One might imagine

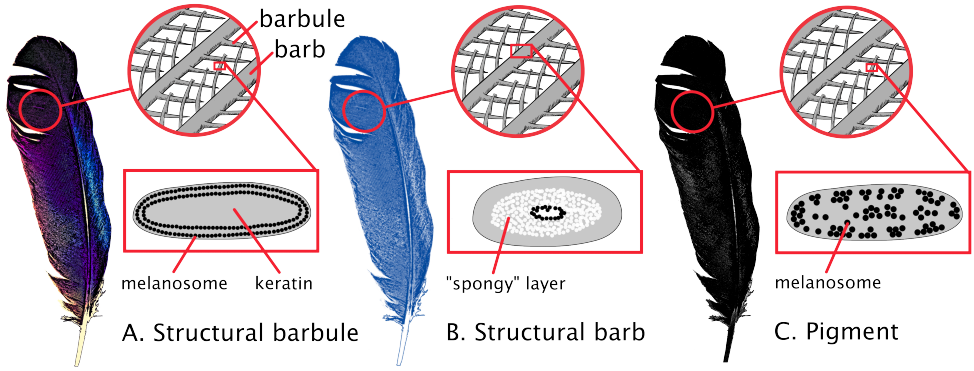

Figure 3.2: The color mechanisms of feathers can be divided into three main categories: structural barbule (A), structural barb (B), and pigmentary (C). Cross-sections of barbs/barbules shown in boxes. Structural barbules (A) give rise to shimmering and metallic colors and are produced from ordered arrays of melanin-containing organelles (melanosomes) in the barbules. Structural barbs (B) give rise to diffuse blue and green colors and are produced from a sponge-like structure in the barbs made of keratin and air underlain by melanin. Pigmentary colors (C) give rise to a range of different hues depending on the absorbance of the pigment. The pigment is usually distributed in both barb and barbules. Here, a black melanin-colored feather is pictured with disordered melanosomes in the barbules (compare to (A)).

that glossiness (measured as a change in reflected intensity with angle) is greater in structural barbule colors than in pigmented or structural barb colors, but this is not true. While some structural barbule coloration can achieve a reflectance ranging from almost zero to 100% when viewing/illumination angle is varied, it is easy to see that the same is also true for glossy dark pigmentary plumage (a dark surface will reflect almost no light if illuminated perpendicularly, but nearly 100% at grazing angles, as described by the Fresnel equations). Thus, neither the presence nor magnitude of gloss uniquely captures structural barbule coloration—despite being a feature of this type of coloration.

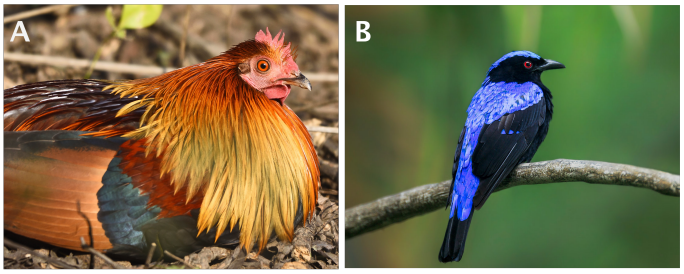

Figure 3.3: Gloss is a common property of many types of plumage, including pigmentary and structural barb colors. A) Glossy pigmentary feathers on the back of the Junglefowl (*Gallus gallus*). B) Glossy structural barb coloration in the Asian fairy blue-bird (*Irena puella*). Image credits: A) all rights reserved by copyright holder Praveen Pandian, reproduced here with permission; B) all rights reserved by copyright holder Akhanhk, reproduced here with permission.

3.3.2 Iridescence

Now, let us turn to the second aspect of angle-dependent change—iridescence. It turns out that iridescence, like gloss, is neither unique nor greater in "iridescent" than "non-iridescent" structural colors. This statement is quite surprising, and we will explore it in more depth using a theoretical approach which we will validate with measurements of plumage taken from published studies.

Taking a theoretical approach to demonstrate that structural barbule and structural barb coloration do not differ in presence or magnitude of iridescence, we modeled structural barbules as multilayer structures and structural barbs as photonic glasses, since this approximates the optics of the real structures well (Kinoshita et al., 2008, Stavenga et al., 2017, Prum, 2006). There are well-known relationships for how multilayers and photonic glasses scatter light with varying angle of incidence, which we adapted here to model iridescence (Kinoshita et al., 2008, Magkiriadou et al., 2014). Since multiple measurement geometries are possible to quantify iridescence, we chose the geometry that captures the maximum peak spectral wavelength shift of a multilayer ("constant angle bisector" *sensu* Gruson et al., 2019a), where the reflectance is measured at the mirror angle of light incidence (i.e. a specular configuration). We searched a parameter space that is relevant to bird structures, using known structure ranges. Our model estimates are simplifications, since structural barbules are not perfect multilayers and structural barbs can often display higher nanostructural ordering than a photonic glass. Note, however, that our simplifying assumptions bias our estimates towards more strongly angle-dependent barbule structural colors and less angle-dependent structural barb colors—i.e. it is a conservative estimate because we might expect barbule structural colors to be more angle-dependent than structural barb colors.

Optical modeling and plumage data

The iridescence of multilayer structures is estimated using the relationship:

$$2(n_a d_a \cos\theta_a + n_b d_b \cos\theta_b) = m\lambda, \tag{3.1}$$

where n_a and n_b are the refractive indices of the two materials in the multilayer, d_a and d_b are the thicknesses of the layers, and $\cos\theta_a$ and $\cos\theta_b$ are the angles of refraction in the materials (see Kinoshita et al., 2008 for a review of multilayer optics). We used refractive indices of 1.75 and 1.58 for melanin and keratin, respectively (Stavenga et al., 2015). The thicknesses of the layers were taken from a database of all known multilayer structures in feathers (Nordén et al., 2021), which was filtered to include only structures with melanin and keratin.

The iridescence of photonic glasses is approximated by the relationship

$$\lambda = \frac{4\pi n_{\text{eff}} d}{x_{\text{o}}} \sin\left(\tfrac{1}{2}\theta_{\text{sca}}\right), \tag{3.2}$$

where λ is the peak spectral wavelength, n_{eff} is the effective refractive index, d is the diameter of particles, and θ_{sca} is the scattering angle (Magkiriadou et al., 2014). Further, x_{o} is the magnitude of the dimensionless wavevector at the peak in the structure factor, defined as $x_{\text{o}} = (2\pi d)/(d_{\text{avg}})$, where d_{avg} is the average center-to-center spacing between coordination shells of particles (Magkiriadou et al., 2014). In the disordered porous packing in bird feathers, coordination shells are the arrangements of pores surrounding an arbitrary central pore. The first coordination shell refers to the pores directly in contact with the central pore. The second coordination shell refers to pores in contact with those in the second coordination shell, and so on. We estimate d_{avg} to be 0.9d, slightly larger than the distance between FCC (111) planes, which is the plane that scatters most strongly in a face-centered cubic lattice. Since the FCC packing fraction is 0.74, and these disordered structures have a lower packing fraction, we expect the distance between coordination shells to be larger than the distance between FCC (111) planes. We used the Bruggeman approximation to calculate the effective refractive index of structural barbs, using a range of air volume fraction from 50-66%. This range was based on a survey of structural barb structures in 320 species by Saranathan et al. (2012). We varied the diameter of particles over the 160-250nm, based on values in the literature (Urquia et al., 2020, Prum et al., 2009). We note that our approximation of lambda (the peak spectral wavelength) is agnostic to the precise packing of the structures. That is, our calculation assumes that the

structures are isotropic and have long-range disorder; we do not require a specific structure factor, such as the Percus-Yevick structure factor normally used to describe glasses. However, we still refer to the structures as photonic glasses because Equation (3.2) captures the peak spectral wavelengths of glasses (as well as other similar structures), and these porous keratin structures in birds are often referred to as photonic glasses in the literature. A summary of all model parameters can be found in Table 3.1.

Multilayer		Photonic glass	
Parameter	Value(s)	Parameter	Value(s)
n_a	1.58	n_{matrix}	1.58
n_b	1.75	n_{pores}	1
d_a	10-165 nm	d	160-250 nm
d_b	45-202 nm	d_{avg}	$0.9d$
		vf_{pores}	0.5-0.66

Table 3.1: Parameters used for optical modeling.

To validate the theoretical model, we obtained peak spectral wavelength information from published studies on structural coloration in plumage, where a similar measurement geometry had been used as in our theoretical modeling (specular configuration). Authors of nine different studies generously shared their data with us, resulting in a data set including 12 species (7 with structural barbule coloration and 5 with structural barb coloration).

Results

The results of our theoretical modeling show that structural barbs are capable of producing greater iridescence than structural barbules—though both types of structures generally overlap (Figure 3.4A). This result is supported by the plumage measurements we collected from the literature, which show that structural barb and structural barbule colors are broadly overlapping in iridescence (Figure 3.4B). Moreover, the wavelength shifts observed in our modeling simulations are of a similar magnitude to those measured in the plumage, validating our theoretical approach. This result does not change if we instead model plumage spectra in a

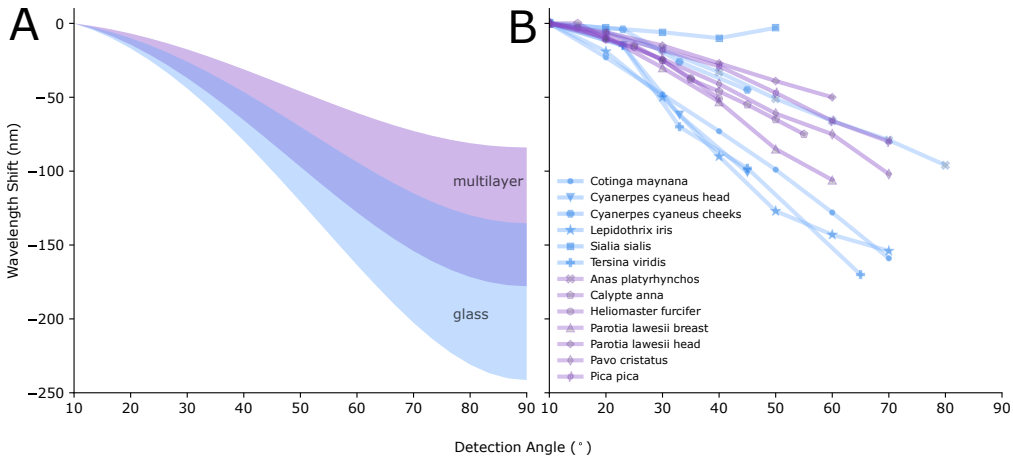

Figure 3.4: Structural barb and barbule colors do not differ in iridescence as measured by changing the angle between illumination and detection. Cumulative change in peak spectral wavelength with viewing angle for structural barbules and barbs using A) optical modeling, and B) data from plumage measurements. Data in B from Stavenga et al. (2017), Doucet (2006), Meadows et al. (2011), Freyer Pascal et al. (2019), Gruson et al. (2019a), Urquia et al. (2020), Skigin et al. (2019), Noh et al. (2010b), Wilts et al. (2014).

bird visual model and measure hue shift as the angular change on the (2-dimensional) hue sphere (see Appendix Figure B.1).

In summary, our results suggest that there is no difference in either the presence or degree of iridescence between "iridescent" and "non-iridescent" plumage coloration as measured by changing the angle between illumination and detection. However, it is important to point out that photonic glasses are expected to show little to no iridescence when the angle between illumination and detection are kept constant (which is theoretically equivalent to perfectly diffuse lighting)(Noh et al., 2010b, Osorio & Ham, 2002). This is because photonic glasses are rotationally symmetric, while multilayers are not. However, we would argue that this does not explain the general difference in visual appearance between structural barbule and barb coloration, which is clear under both directional and diffuse light.

3.4 All that glitters is not gold

Why do some objects in nature appear metallic? The natural starting point to answer this question is to explore whether metals have unique reflection properties that distinguish them from other natural objects. Most natural objects reflect light both specularly and diffusely (Figure 3.5A–B). The diffuse reflection arises from light that has been scattered many times

within the material just beneath the surface and exits at a random angle. It can therefore be seen in any direction at equal intensity. The specular reflection arises from the surface, has only been scattered once, and can therefore only be viewed at the mirror angle. On smooth objects, the specular reflection appears as highlights with sharp edges and is perceived as gloss (Figure 3.5A). On rough objects, unevenness of the surface will cause specular reflections to spread in multiple directions, mimicking the appearance of a diffuse reflection (Figure 3.5B). For most natural objects, the diffuse reflection gives rise to the color, while the specular reflection has the same spectral distribution as the illuminant, and is therefore typically white. In contrast, metals do not follow this typical reflection pattern: they exhibit only specular reflection, which is colored independently of the illuminant (Figure 3.5C–D). Thus, gold has a yellow specular reflection even if the illuminant is white. This unusual reflection property clearly set metals apart from other natural objects.

In contrast to man-made metallic paints, which simply contain metal particles coupled with a pigment (Rump et al., 2008), structural colors in nature that appear metallic do not contain any metals—they are built with organic materials such as keratin, chitin, and melanin. Why do they also appear metallic? If we contrast the reflection properties of structures that appear metallic (structural barbule coloration, Figure 3.2A), to those that do not (structural barb coloration, Figure 3.2B), it becomes clear that the structures that appear metallic mimic the reflection pattern of metals. We previously explained that the nanostructures in structural barbules can be approximated by a multilayer structure, while those in structural barbs can be approximated by a photonic glass. Multilayers function as a stack of mirrors, where the specular reflection from each mirror interferes to form a saturated color. Thus, multilayers produce colored specular reflections, just like metals. Moreover, the multilayers are built with highly absorbing melanin pigment (melanosomes, 3.2A), which nearly eliminates diffuse reflectance. Thus, structural barbule colors incorporate both of the key reflectance properties of metals—a colored specular reflection and very low diffuse reflection. Photonic glasses also produce color from interference effects, but, in contrast to multilayers, they reflect both specular and diffuse light. The specular reflection (in our terminology) is equivalent to what has previously been

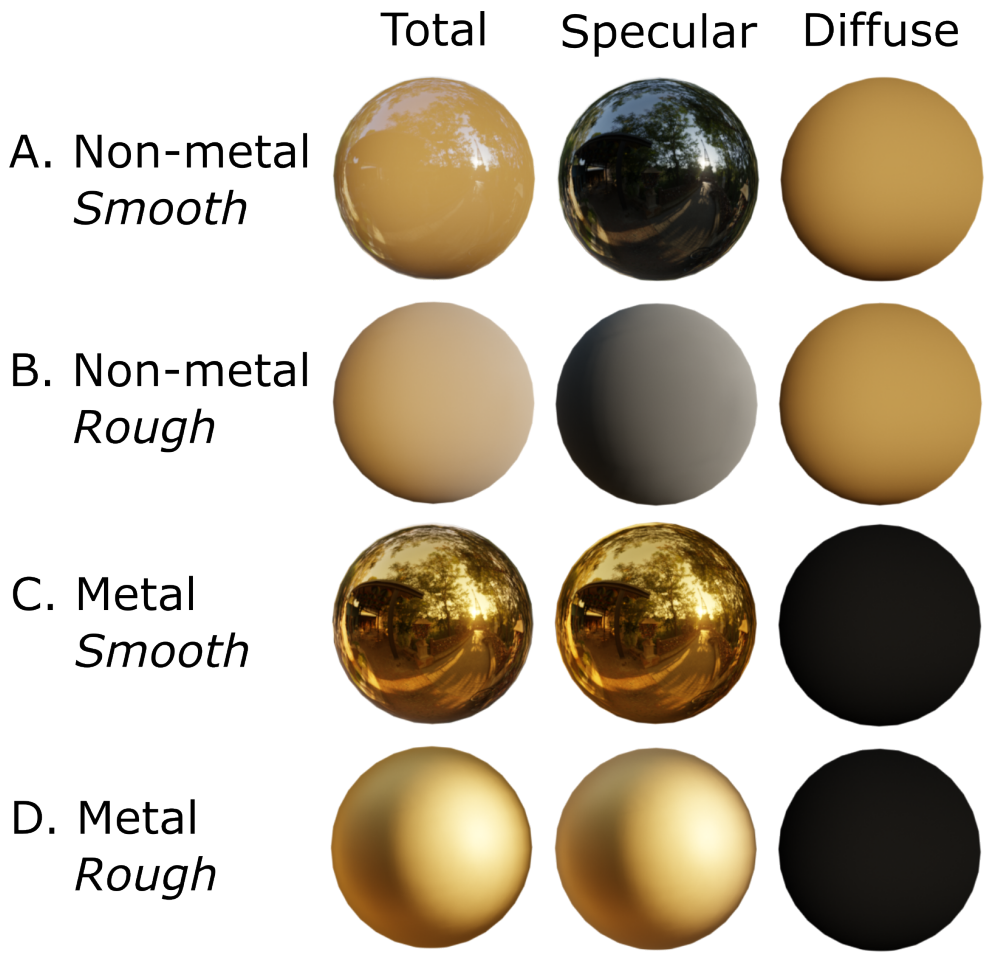

Figure 3.5: Metals have unique reflection properties: they reflect colored specular light. Rendered objects of different materials shown with total reflection, specular reflection only and diffuse reflection only (from left to right). A non-metal object reflects both diffusely and specularly, where the diffuse part confers the color while the specular part has the same spectral distribution as the illumination (A-B). The specular reflection of smooth non-metal objects appear as gloss (A), while on rough objects it appears similar to the diffuse reflection (B). Note, however, that the specular reflection has the same spectral distribution as the illuminant (here a 3D map of a daylight scene in Paris, with blue/white sky and darker ground/vegetation), while the diffuse reflection is colored. Metal objects reflect only specularly (C-D). A rough metal object (C) appears less glossy than a smooth metal object (D). Rendered objects created in Blender v. 3.4.1 (Community, 2022).

described as the single-scattered peak (Noh et al., 2010b,c,a, Hwang et al., 2020, 2021) and is colored. However, because photonic glasses also reflect diffusely (multiple-scattered peak), structural barb colors do not meet the dual criteria for metallic appearance (colored specular reflectance *and* low diffuse reflectance).

We are not the first to suggest that metallic luster can be characterized by some combination of reflection properties. In fact, a similar argument was made by Bancroft & Allen (1924) in a paper dedicated to the exploration of metallic luster. They mention two key aspects that are important for the perception of metallic luster: a strong surface reflection and high opacity of the object. Rephrased, this could be understood as equivalent to our condition of a high specular and low diffuse reflection, since "surface reflection" in this context has a similar meaning to our definition of specular reflection, and an opaque body per our definition lacks diffuse reflection (as it does not transmit light and thus no sub-surface scattering can occur). Bancroft & Allen (1924) also suggest that "selective reflection at the surface" gives rise to metallic luster—which is the equivalent of what we have described as a colored specular reflection. We have adopted the term "metallic luster" in this paper to highlight the link to these ideas, albeit having arrived upon them independently.

We suspect that part of the reason that metallic luster has not received more attention in the animal coloration literature is because there is no easy way to quantify it. We therefore propose cross-polarization photography as a method to measure the two key aspects of metallic luster that we have identified (colored specular reflectance and low diffuse reflectance), and we demonstrate this method on a sample of plumage patches with various color mechanisms.

3.5 Measuring metallic luster

With cross-polarization photography, it is possible to separate the specular and diffuse reflection of an object. We therefore used this method to quantify the two key aspects of metallic luster that we have identified above: 1) a colored specular reflection; and 2) a very low diffuse reflection. We measured the first aspect as the saturation of the specular reflection, and the second as the relative specular reflectance (out of the total reflectance, which is the sum of

specular and diffuse reflection).

3.5.1 Plumage selection

We photographed 103 plumage patches from bird specimens at the Princeton Bird Collection (Princeton, New Jersey, USA). We selected species with color mechanisms in the following categories: pigmentary (total of 15 patches, including carotenoid, turacoverdin, psittacofulvin, and melanin), structural barb (total of 11 patches), white (which can be considered as a type of structural coloration (Igic et al., 2018); total of 3 patches), and structural barbule ($n = 74$).The categorization was based on published sources ($n = 94$), and in some cases visual assessment by K. Nordén ($n = 9$, see Appendix B.3).

3.5.2 Cross-polarization photography

To measure the specular and diffuse reflection from bird plumage, we used cross-polarization photography. This technique takes advantage of the fact that light retains its original polarization when it is single-scattered, but not when it is multiple-scattered. By illuminating the plumage with polarized light, the single-scattered and multiple-scatted part of the reflection can therefore be separated with a second, rotatable polarization filter in front of the camera. Since specular reflections arise from single-scattered light, and diffuse reflections arise from multiple-scattered light, this separates specular and diffuse reflections. Polarization measurements using spectrophotometry have been used previously to study the reflectance properties of photonic structures, including structural barb and barbule coloration (Hwang et al., 2020, Noh et al., 2010b,a,c, Wilts et al., 2014).

Our set-up (Figure 3.6) consisted of two LED photography lamps which were covered with a polarizing film with a vertical polarization axis. The lamps were set at an approximately 45° angle. We used a Nikon D7000 camera, which we mounted on a copy stand and equipped with a rotatable linear polarizer. For each specimen, we took images in the following configurations: 1) with the polarization axis of the camera filter oriented vertically and therefore aligned with the lamps (plane-polarized, PPL, Figure 3.6A), and 2) with the polariza-

tion axis of the camera filter oriented horizontally and therefore perpendicular to the lamps (cross-polarized, XPL, Figure 3.6B). Using these two sets of images, the specular and diffuse reflectance components of the image can be calculated (see §3.5.4, *Analysis*). We repeated this process for each patch for a total of three times; each time, we moved the specimen slightly to image a different part of the same patch. The three samples (two images per sample) per patch were collected to get a more representative average of each patch. In each image, we included a color calibration chart (Colorchecker Classic Nano, Calibrate), which allowed us to calibrate camera measurements to known XYZ values (CIE 1931 color-matching functions). All images were captured in RAW format.

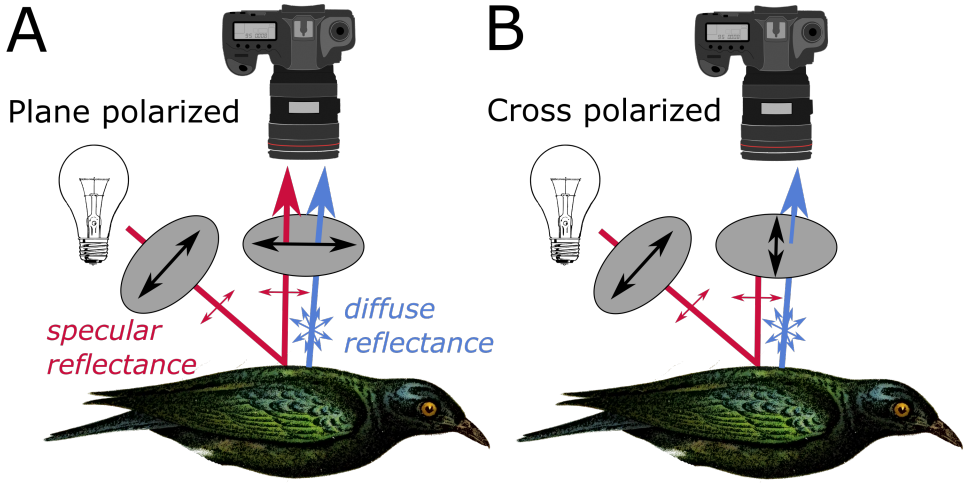

Figure 3.6: Set-up for cross-polarization photography of bird plumage. The camera was fixed on a copy stand above the specimen, and the lights were fixed at approximately 45°. Both camera and light were equipped with linear polarizing sheets. In the plane polarized condition (A), the camera polarizer was set at the same polarizing axis as the lamp, and hence both specular and diffuse reflectance were captured. In the cross-polarized condition (B), the camera polarizer was perpendicular to the axis of the polarizing axis of the lamp, thus only letting through diffuse reflectance.

3.5.3 Image processing and color calibration

We used a custom-written MATLAB script to process our RAW images, following Akkaynak et al. (2014) and Sumner (2014). First, images were linearized and demosaiced using bilinear interpolation. We aligned PPL and XPL images using the MATLAB function "imregcorr" to correct for slight shifts between images.

To color calibrate the images, we first combined the plane-polarized image (I_{ppl}) and the cross-polarized image (I_{xpl}) for each specimen to produce an image representing the total re-

flection (I_{total}). This was necessary because the values of the color standard are based on the total reflection, not the diffuse and specular reflection separately.

We then calculated the linear transformation to map color chart values in I_{total} to the known standard XYZ values (CIE 1931 color-matching functions, published for Calibrite Classic Color Checker Nano). This is solved as a linear regression problem of the form:

$$X_i = \beta_1 R_i + \beta_2 G_i + \beta_3 B_i, \tag{3.3}$$

where R_i, G_i and B_i denote the R, G, and B values respectively of the i-th color checker chip in the image I_{total}, and X_i denotes the standard X, Y, or Z value for the i-th color checker chip. The transformation was applied to the images I_{ppl} and I_{xpl} separately to achieve a color calibrated result. We checked final calibrated values in the image against standard XYZ values to ensure a good fit (see Appendix Figure B.1).

Finally, we converted our XYZ images to RGB space to ease further analysis and interpretation. We converted images to Wide Gamut RGB space, to avoid extensive clipping of values.

3.5.4 Analysis

We selected a patch (700×700 px) in each image which represented the patch we wanted to capture, for which all calculations were performed. We calculated the mean intensity values in each color channel for I_{ppl} and I_{xpl}, which we will call M_{xpl} and M_{ppl}, respectively. We chose this approach instead of performing calculations pixel by pixel on the whole patch because it produced more reproducible results. Shiny dark objects are notoriously hard to photograph because correctly exposed highlights will clip values in dark areas of the image and vice versa. Thus, darker areas in our images were more likely to be noisy and out of the calibrated range. Moreover, small shifts in absolute values can significantly shift calculations of ratios (i.e. relative amount of specular reflection and saturation). By averaging intensity over all pixels, we stabilized estimates of dark patches.

Measuring diffuse reflection

The PPL and XPL images can be related to the specular and diffuse reflection as follows:

$$I_{\text{specular}} = I_{\text{ppl}} - I_{\text{xpl}}, \tag{3.4}$$

$$I_{\text{diffuse}} = 2I_{\text{xpl}}. \tag{3.5}$$

The diffuse reflectance equals twice I_{xpl}, since a polarization filter will filter out half the intensity of unpolarized light, according to Malus' law. Thus, from the average intensity values we extracted the mean total intensity ($M_{\text{total}} = M_{\text{xpl}} + M_{\text{ppl}}$), mean specular reflection ($M_{\text{specular}} = M_{\text{ppl}} - M_{\text{xpl}}$) and mean diffuse reflection ($M_{\text{diffuse}} = 2 \times M_{\text{xpl}}$) for each color channel. Relative specular reflection (S) was calculated for the color channel of greatest mean total intensity as follows:

$$S = \frac{M_{\text{specular}}}{M_{\text{total}}}. \tag{3.6}$$

We selected the color channel of greatest mean total intensity, since this would best reflect the plumage color of interest. Thus, we calculated relative specular reflection in the blue color channel for a blue patch, but in the red channel for a red patch.

Measuring colored specular reflection

To measure saturation of the specular reflection, we represented samples in a trigonal RGB color space, i.e. a point $(R, B, G) \in \mathbb{R}_{\geq 0}$ gets mapped to

$$\boldsymbol{P} = \widetilde{R} \cdot \boldsymbol{v}_R + \widetilde{B} \cdot \boldsymbol{v}_B + \widetilde{G} \cdot \boldsymbol{v}_G, \tag{3.7}$$

where $\widetilde{R} = R/(R + B + G)$, $\widetilde{B} = B/(R + B + G)$, and $\widetilde{G} = G/(R + B + G)$ are the brightness normalized values and $\boldsymbol{v}_R$, $\boldsymbol{v}_B$, and $\boldsymbol{v}_G$ are the vertices of an equilateral triangle. We assume the triangle to be centered at the origin, i.e. $\boldsymbol{v}_R + \boldsymbol{v}_B + \boldsymbol{v}_G = \boldsymbol{0}$, such that the unsaturated color (white) is mapped to the origin $\boldsymbol{0}$. Saturation, in this space, is then represented as the ratio of the distance of the point $\boldsymbol{P}$ from the origin and the length of the line segment

of a ray from the origin through the point $\boldsymbol{P}$ contained within the triangle. Saturation therefore represents the relative imbalance of the values R, B, G (see (3.8)). Explicitly, saturation $\mathrm{Sat}(\boldsymbol{P})$ of the point $\boldsymbol{P}$, given by (3.7), is given by

$$\mathrm{Sat}(\boldsymbol{P}) = 1 - 3\min\{\widetilde{R}, \widetilde{B}, \widetilde{G}\} = \frac{R + B + G - 3\min\{R, B, G\}}{R + B + G}. \tag{3.8}$$

This may be seen as follows. For $\boldsymbol{P} = \boldsymbol{0}$, we have $\mathrm{Sat}(\boldsymbol{0}) = 0$ and $\widetilde{R} = \widetilde{B} = \widetilde{G} = \frac{1}{3}$. For $\boldsymbol{P} \neq \boldsymbol{0}$, we may suppose without loss of generality that $\widetilde{G} = \min\{\widetilde{R}, \widetilde{B}, \widetilde{G}\} < \frac{1}{3}$. Then, $\mathrm{Sat}(\boldsymbol{P})^{-1}$ is equal to the scalar t such that $t \cdot \boldsymbol{P}$ lies on the edge E_{RB} between $\boldsymbol{v}_R$ and $\boldsymbol{v}_B$. We have

$$\begin{aligned} t \cdot \boldsymbol{P} \in E_{RB} &\Leftrightarrow t\left((\widetilde{R} - \widetilde{G})\boldsymbol{v}_R + (\widetilde{B} - \widetilde{G})\boldsymbol{v}_B\right) \in E_{RB} \\ &\Leftrightarrow t\left((\widetilde{R} - \widetilde{G}) + (\widetilde{B} - \widetilde{G})\right) = t(1 - 3\widetilde{G}) = 1, \end{aligned} \tag{3.9}$$

where we have used $\boldsymbol{v}_R + \boldsymbol{v}_B + \boldsymbol{v}_G = \boldsymbol{0}$ and $\alpha\boldsymbol{v}_R + \beta\boldsymbol{v}_B \in E_{RB} \Leftrightarrow \alpha + \beta = 1$ and $\alpha, \beta \geq 0$.

3.5.5 Results

In Figure 3.7A, the results of the cross-polarization photography are visualized in terms of each patch's specular saturation and relative specular reflection. Of the plumage color types we tested, structural barbule colors standout as the only type that has a high relative specular reflection that is saturated (Figure 3.7A–B). They vary in the magnitude of specular saturation, which is likely tied to the number of melanosome layers in the nanostructure (Figure 3.2A). As the number of layers increase in a multilayer, spectral peak height increases while spectral peak width decreases (Kinoshita et al., 2008). Patches that record high specular saturation will therefore appear very bright and saturated (e.g. Resplendent quetzal (*Pharomachrus mocinno*), Figure 3.2Aa) while patches that record low specular saturation will appear less bright and saturated (e.g. Common raven (*Corvus corax*), Figure 3.2Ab). Thus, cross-polarization photography successfully captures the unique reflectance properties of plumage with metallic luster—proving that this could be used as a proxy to quantify it.

Plumage produced with other color mechanisms than structural barbules occupy different areas of the graph (Figure 3.7A). Structural barb colors cluster in the middle of the graph, suggesting that they reflect both diffuse light and colored specular light—in line with our expectations (Figure 3.7A, C). Structural white, on the other hand, exhibits low relative specular reflection, due to its very high diffuse reflectance (Figure 3.7A). Similarly, pigmentary patches primarily record low relative specular reflection and saturation (Figure 3.7A, D). However, there are two interesting variations to this trend.

Firstly, some pigmentary patches show high relative specular reflection and therefore plot close to patches with structural barbule coloration. This high specular component is present for pigmentary patches that are very dark (melanin based) yet glossy (e.g. Junglefowl (*Gallus gallus*), Figure 3.7Ac). The difference between dark glossy patches and patches with structural barbule coloration is that the gloss is unsaturated (white) for the former and colored for the latter. However, the difference between a colored and uncolored gloss is gradual rather than categorical, which is captured by our spectral saturation measurement. Patches with structural barbule coloration vary in their specular saturation, and towards the lower end they overlap with dark pigmentary and glossy patches. This gradual transition is mirrored on the nanostructural level in the feather—structural barbules and melanin pigmented barbules both consist of keratin and melanin, only differing in the extent to which the melanosomes are ordered (Figure 3.2A, C). In general, higher order of the melanosomes increases the saturation of the specular reflection. Some patches classified as structural barbule coloration with low specular saturation exist in this transition zone between glossy pigmentary plumage and metallic luster (e.g. Downy woodpecker (*Picoides pubescens*), Figure 3.7Ad).

Secondly, some pigmentary patches record a saturated specular reflection in combination with a diffuse reflection (e.g. Scarlet tanager (*Piranga olivacea*), Figure 3.7Ae and American goldfinch (*Carduelis tristis*), Figure 3.7Af). This is surprising, because pigments typically produce color through the diffuse reflection, and we would expect the specular part to be white (Figure 3.5A). Intriguingly, the patch which records the most saturated specular reflectance is the yellow back of the American goldfinch (*Carduelis tristis*, Figure 3.7Af)—a species which

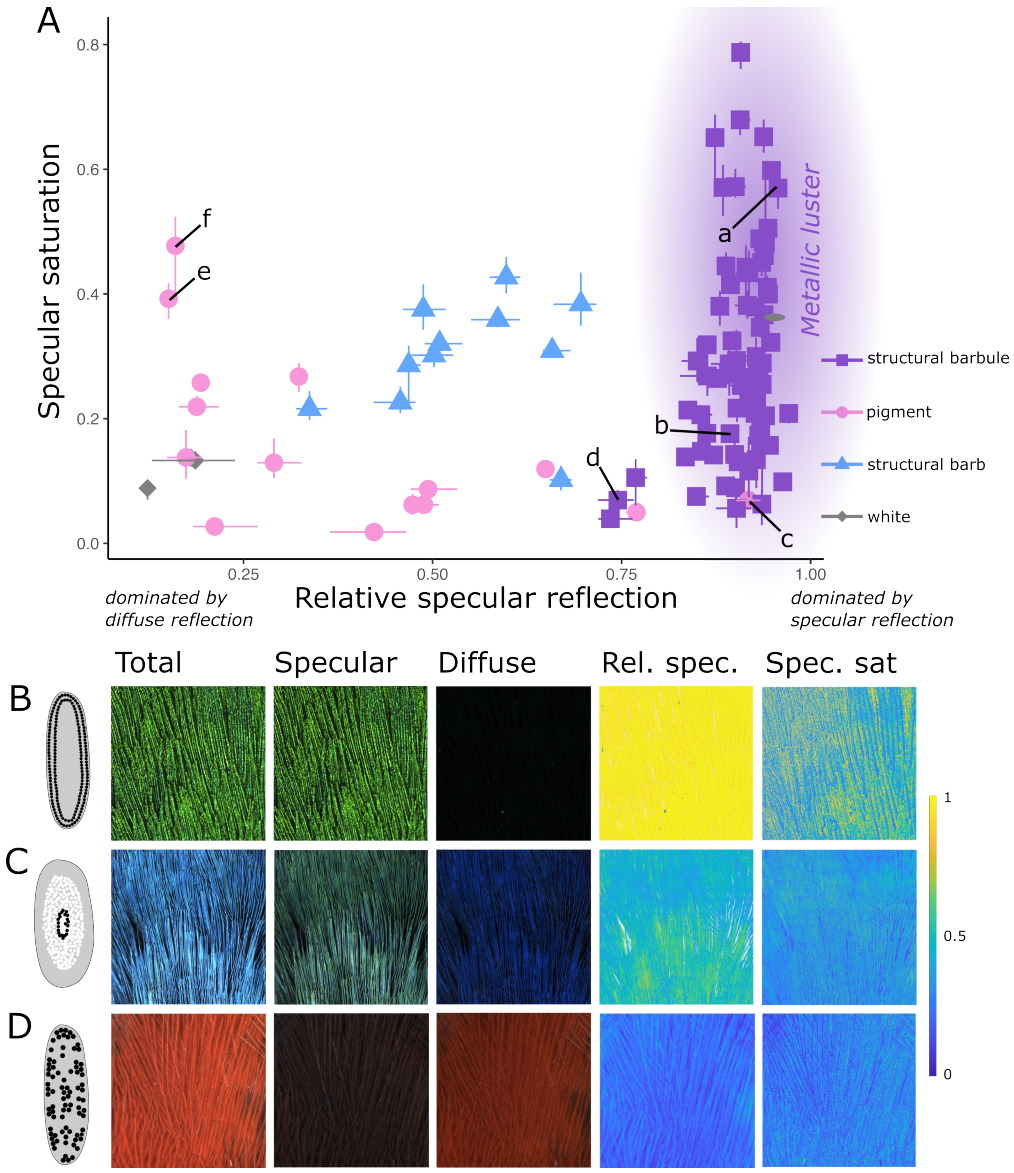

Figure 3.7: Cross-polarization photography effectively separates plumage patches with metallic luster (structural barbules) from other types of plumage. A, Relative specular reflection and specular saturation of plumage patches with different color mechanisms. Data points represent the average measurement of three samples (per patch), the lines represent the range of the samples. Lower case letters in A mark specific patches discussed in the result: a, *Pharomachrus mocinno*; b, *Corvus corax*; c, *Gallus gallus*; d, *Picoides pubescens*; e, *Piranga olivacea*; f, *Carduelis tristis*. B-D, example patches of each type of plumage shown as a total intensity image, specular image, diffuse image, and false-color images of relative specular reflection and specular saturation. B, structural barbule (Resplendent quetzal, (*Pharomachrus mocinno*)); C, structural barb (Swallow tanager, (*Tersina viridis*)); D, pigmentary (Northern cardinal, (*Cardinalis cardinalis*)).

has previously been shown to amplify pigmentary color using feather nanostructures (Shawkey & Hill, 2005). Air-filled vacuoles in the barbs function as mirrors reflecting light behind a carotenoid pigmented keratin layer. Thus, the specular colored light recorded for some pigmentary patches may in fact signal a structural amplification of the pigmentary color. This would need to be confirmed with additional studies of feather nanostructures—but if our inference is correct our results suggests structural amplification of carotenoid colors may be widespread in birds.

In summary, our results show that cross-polarization can be used to quantify a proxy of metallic luster, by measuring characteristics of the specular reflection.

3.6 Discussion

We have argued that the term "iridescence" is often used in animal coloration literature to describe metallic luster, and that this is a separate property from iridescence as commonly defined (a change in peak spectral wavelength with viewing or illumination angle). We quantify metallic luster using two reflection characteristics (specular saturation and relative specular reflectance), and show using bird plumage that while "iridescent" (structural barbule) and "non-iridescent" (structural barb) plumage do not differ in iridescence when changing the angle between illumination and observation (Figure 3.4), the latter lacks metallic luster (Figure 3.7). By separating iridescence and metallic luster, we clarify the terminology surrounding structural colors and construct a framework that can be applied to any structural coloration in nature, not only bird coloration.

In this section, we would like to explore two general critiques that may be raised in response to introducing metallic luster as a property of animal coloration. Firstly, while we might be able to measure this property, does it have any biological significance? For example, does the presence or absence of metallic luster in a signal matter to the receiver? Secondly, even if metallic luster has biological significance, how good is the measure we have proposed at capturing metallic luster, which in reality is a perceptual rather than an objective quality?

3.6.1 Biological significance of metallic luster

Objects with metallic luster appear to stand out to human observers—it is no coincidence that beetles and butterflies with metallic luster are favourite objects of collection (Finet, 2023), and bird feathers with metallic luster have been used to adorn clothing ranging from Aztec headdresses (McMahon, 2017) to ladies hats in the 1800s (Eluwawalage, 2015). But is there any reason to assume that metallic luster is a salient feature to other animals? If not, one might argue that even though it is a measurable property that matters to humans, it has little biological significance, and no role to play in the evolution of these colors.

There are not yet any studies investigating directly whether animals pay attention to objects with metallic luster—however, we can make a plausible argument that they do, based on the shared evolutionary role of vision in animals. For humans, the metallic luster of an object immediately tells us something about its material properties. It is therefore part of what has been termed our material perception, or our ability to estimate complex material properties from visual cues (e.g. surface texture, density, and viscosity (Fleming, 2017)). Material perception is critical for our ability to interact appropriately with objects in our environment—for example it allows us to predict the weight of an object, or whether a surface is wet or dry. Gloss in particular has been found to be of great importance for material perception (Fleming, 2017, Schmid et al., 2023, Ged et al., 2010). By adjusting specular strength, specular saturation, and the smoothness of computer-rendered objects shown on a screen, Schmid et al. (2023) found that people categorized objects into distinct categories such as "porcelain", "wax", "metal", and "plastic".

Classifying materials such as "plastic" or "porcelain" may not be relevant to most animals—but predicting the material properties of an object certainly is. Just like object detection probably has deep evolutionary roots (Soto & Wasserman, 2014, Jitsumori & Delius, 2001, Schumacher et al., 2016), material perception is likely widespread among other animals. For animals that rely on vision, cues derived from specular reflections are likely to be important for this task, since the appearance of the specular reflection is tightly linked to material properties. Moreover, there is limited direct evidence for gloss perception in non-human animals—

Okazawa et al. (2012) recorded specific neural responses to viewing glossy surfaces in macaques.

Thus, based on the key role of gloss perception for object and material recognition in humans, it is likely that many animals (that rely on vision) also perceive it (Franklin & Ospina-Rozo, 2021). Since an important feature of metallic luster is colored gloss, it is likely that many animals would also perceive metallic luster. This could be tested using behavioral trials.

However, there is a difference between being able to detect metallic luster, and being attracted to it. Humans tend to prefer shiny or glossy objects, including objects with metallic luster, over matte objects (Silvia et al., 2018, Meert et al., 2014, Silvia et al., 2021). The reason for this preference is still unknown (Fleming, 2017). Coss (1990) suggested that the attraction to glossy surfaces is an evolved adaptation to find water in terrestrial environments. He supported his argument by an experiment in which people rated papers with glossier surfaces as "wetter" than papers with matte surfaces (Coss, 1990). Coss et al. (2003) also conducted an experiment which showed that toddlers tended to lick glossy or metallic plates significantly more than matte plates—a behavior they interpreted as an indication that the toddlers perceived the glossy surfaces as wet. Alternatively, glossy or lustrous surfaces may capture our attention because they register as a movement (Braun & Braun, 1995). Visual perception of motion is critical to a variety of tasks, including judging the shape, depth, movement, and speed of objects, as well as identifying other animals in our environment (Sekuler et al., 2002). Since movement of objects catches our attention (Franconeri & Simons, 2005, 2003, Abrams & Christ, 2003), it is possible that glossy or lustrous surfaces do the same by mimicking or amplifying movement cues. Surfaces with metallic luster may additionally be attractive because they have unusual reflective properties—while many objects are glossy, only a few have a colored shine.

Little is known about animal preference or attention to glossy objects (Franklin & Ospina-Rozo, 2021). A few studies have explored preference for shiny objects in corvids, who according to widely held beliefs in European folklore collect shiny objects. Behavioral trials do not support this—only that corvids have a preference for exploring novel objects (Shephard et al., 2015, Heinrich, 1995, Jacobs et al., 2014). In addition, a couple of studies have investigated how

glossiness affects the detectability of prey. Specifically, these studies compared the attack rates (by bird predators) in the wild on replica beetles with either glossy or matte elytra. In one study, survival rates between glossy and matte beetles of a similar green hue placed in natural environments did not differ (Franklin et al., 2022), while a more recent study found that glossy beetles of three different hues were consistently easier to detect for bird predators than matte replicas (Thomas et al., 2014). Thus, while there is not yet much direct evidence to suggest that animals pay attention to glossy objects, it has not been tested in many species or contexts. The attention or preference for metallic luster specifically has to our knowledge never been investigated in animals .

Despite the scarcity of evidence there is reason to believe that metallic luster may have wider biological significance, since the two proposed hypotheses for the human preference for glossy surfaces—ability to identify water and to perceive motion—are likely to be important to a wide range of animals beyond humans. This hypothesis is particularly intriguing in birds, which have good vision and are known to use plumage with metallic luster in patches used for display. Previous studies have focused on how brightness, hue, saturation, and in some instances iridescence of such plumage patches influence mate choice or are tied to animal condition (Bitton et al., 2007, Loyau et al., 2007, Dakin & Montgomerie, 2013, Simpson & McGraw, 2019, Hill et al., 2005). For example, brighter plumage has been linked with increased mating success in Peafowl (*Pavo cristatus*, (Loyau et al., 2007)) and Tree swallow (*Tachycineta bicolor*, (Bitton et al., 2007)). Introducing metallic luster as a property of coloration allows us to ask whether it is the brightness in general that is important (which could arise from either diffuse or specular reflections), or the presence of metallic luster (bright and colored *specular* reflections only). On a macroevolutionary level, we could investigate what kind of environments or signal types may favor the evolution of metallic luster (as opposed to diffuse coloration such as pigmentary traits).

Thus, we would argue that there are many interesting biological questions that could be asked using the concept of metallic luster. Of course, to test these hypotheses we need a way to quantify it—which leads us to the second general critique. Can our measure of metallic

luster really capture this property, which as we have seen likely involves higher level visual processing?

3.6.2 Metallic luster as a Gestalt-like property

Our measure of metallic luster focuses on particular reflective properties of surfaces. Yet it is clear that metallic luster must be a perceptual rather than objective property of objects, because it is known that individuals can sometimes differ in their judgment of whether an object has metallic luster (Bancroft & Allen, 1924, Todd & Norman, 2018). This is why we have called our measure a proxy, just like a shift in peak spectral wavelength can be considered a proxy of the perceptual experience of iridescence. Proxies are useful since they allow us to quantify a property that is hard to measure directly—but by virtue of being proxies they can also be misleading in some contexts. Bancroft & Allen (1924) point out that variations in light intensity on a surface either in space or time is critical to the perception of metallic luster. A perfectly smooth mirror does not look metallic—it is only when some unevenness in the surface is introduced that it appears metallic. Our definition and measurement of metallic luster cannot distinguish between these two situations. Neither can our measure distinguish between a surface that is silvery and one that is dark and glossy (both have high specular reflectance but lack specular saturation). In fact, even human judgments of whether an objects is black and glossy or silvery can in some situations be highly variable (Todd & Norman, 2018).

Evidence emerging from studies of material perception and gloss is supporting the idea that the perception of gloss and metallic luster is dependent on a variety of cues, including the location and shape of specular highlights, their movement across the object, the contrast in highlights and low-lights, the surface texture of an object as well as the illumination characteristics (Chadwick & Kentridge, 2015, Schmid et al., 2023, Todd & Norman, 2018, Norman et al., 2020). Moreover, the expectation of an object being of a particular material affects how we perceive it. Matsumoto et al. (2015) found that objects that had a similar hue to gold were perceived as more glossy and metallic than objects that did not, despite having the same reflective properties. In another experiment, it was found that objects that feel smooth to the touch

are perceived as more glossy than rough objects (Adams et al., 2016). Our prior knowledge and expectation of an object or material can thus also directly influence how we perceive it (Alley et al., 2020).

These insights from studies of human perception of gloss and metallic luster suggest it can probably be best understood as a gestalt-like property (Schmid et al., 2023). Gestalt psychology originated in the early 1900s (Wagemans et al., 2012), but it has recently received renewed attention in visual perception research (Jäkel et al., 2016). A core concept of Gestalt theory is that the whole can be more than the sum of its parts (superadditivity) (Jäkel et al., 2016, Wagemans et al., 2012). To state this a bit more concretely in relation to metallic luster, we can see that there is no single point, or combination of points, in a color space, that can be called "gold". Rather, it is the particular distribution of colors and highlights of an object (the Gestalt) that together create the appearance of gold (Figure 3.8, cf. Komatsu et al., 2013).

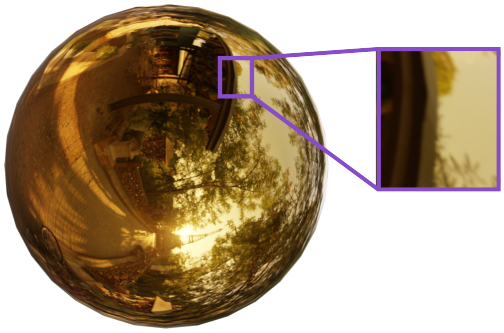

Figure 3.8: Metallic luster is probably a gestalt-like property that arises from the combination of many different cues, including the interaction between highlights and object shape. The cut-out of the sphere does not look golden on its own—it is only as part of the sphere as a whole that it appears golden. Figure based on Komatsu et al., 2013.

Gestalt psychology is not new to the field of animal coloration—but it has hitherto been limited to the study of animal camouflage, which was a favorite example of early Gestalt theorists (Osorio & Cuthill, 2015). However, a major problem with Gestalt psychology is that it is often hard to precisely quantify the concepts (Wagemans et al., 2012). We do not offer here any solution to this problem, but we argue that the Gestalt is a useful way of thinking of properties like metallic luster, gloss, and iridescence—even if we cannot yet quantify it as a Gestalt. That is to say, even though measurements of metallic luster or iridescence using proxies based on separate cues are useful, we need not assume that the perception itself operates in

a similar way. For example, if we view iridescence as the combination of many different hues, each seen at a specific angle of light and observation, it appears to be a very complicated signal to remember (Stuart-Fox et al., 2020, Thomas et al., 2023). If we instead consider iridescence as a holistic Gestalt, we need not assume that this signal is more complicated, or harder to remember, than any other.

In summary, the measure of metallic luster—a colored specular reflection in combination with low diffuse reflectance—we have proposed in this paper should be viewed as a proxy, rather than the equivalent, of metallic luster. This measure could be improved by adding additional features (e.g. contrast and coverage of high- and low-lights in the image)—although this is perhaps best done in step with increasing knowledge of different animals' perception of luster. Fundamentally, metallic luster is probably a gestalt-like quality rather than a single metric. Nevertheless, in the absence of a way to measure metallic luster directly, a simple proxy can still be a useful starting point to explore basic questions—or at the very least to make us aware of a different dimension of animal coloration.

3.7 Conclusion

That some objects in nature appear metallic has probably been appreciated by humans for as long as they have encountered animals and minerals with structural colors. Therefore, our goal in this paper is not to present the radical new idea that some natural objects have metallic-like reflections–but to highlight and develop a concept that has long existed, albeit in disparate literatures and with little direct examination. In particular, we argue that iridescence and metallic luster have become blurred in the literature, and we show using examples and data that they are in fact two distinct properties that may or may not occur together.

We developed a measure of metallic luster which is based on the unique reflection properties of metals, which successfully quantifies metallic luster in bird plumage. While this method of measuring metallic luster is quite simple, it is a useful starting point for exploring hypothesis about the importance of metallic luster to animals signals.

The parts of the Feathers of this glorious Bird appear, through the Microscope, no less gaudy then do the whole Feathers.

Robert Hooke, Micrographia

4

The role of historical contingency on feather barbule nanostructures in cuckoos

Notes

This work was developed with co-authors Christopher R. Cooney, Frane Babrović and Mary Caswell Stoddard.

Abstract

Plumage with metallic luster (e.g. the colored sheen of a peacock's tail) exists in many bird species—but its frequency in different clades varies. Frequent transitions to and from this structural color is intriguing, since producing bright and saturated metallic luster requires the evolution of both specialized melanosome shapes from an ancestral thick rod and their nanostructural arrangement in the barbule. We investigated whether historical contingency could play a role in the repeated evolution of metallic luster in Cuculidae by exploring feather nanostructures in species with and without the trait. Interestingly, species with gray and brown plumage, which lack metallic luster, retained specialized melanosome shapes (hollow and thin rods) but had lost nanostructural order. We suggest that this provides a mechanism for the repeated evolution of metallic luster in some clades, since only melanosome nanostructural arrangement but not melanosome shape has to re-evolve. This finding supports the idea that historical contingency plays a key role in shaping the evolution of plumage color diversity.

4.1 Introduction

The naturalist Alfred Russell Wallace noted in his landmark paper "The Colors of Animals and Plants" (Wallace, 1877) that clades of animals often share a similar color palette: "We [...] find that color is constant in whole genera and other groups of species. The Genistas are all yellow, the Erythrinas all red; many genera of Carabidae are entirely black; whole families of birds—as the Dendrocolaptidae—are brown; while among butterflies the numerous species of Lycaena [Lycaenidae] are all more or less blue, those of Pontia white, and those of Callidryas yellow." (Wallace, 1877). Birds, who display an astonishing variety of plumage colors (Stoddard & Prum, 2011), have been a favorite group to study color in nature. Following Wallace

and other foundational work (e.g. Endler, 1992), the focus has chiefly been on exploring the adaptive functions of plumage colors. For example, plumage color has been shown to evolve in response to sexual selection (Cooney et al., 2019, Dale et al., 2015), environmental lighting conditions (Gomez & Théry, 2004, Marcondes & Brumfield, 2019), background color (crypsis, Troscianko et al., 2016, Mason et al., 2023) and climate (thermoregulation, Romano et al., 2019, Rogalla et al., 2021). A large body of research shows that natural and sexual selection are key forces in shaping animal colors (Cuthill et al., 2017, Hill & McGraw, 2006a).

However, there is a second (not mutually exclusive) general explanation for color variation in animals which has been much less explored—historical contingency. By historical contingency we mean the path-dependency of biological processes (Desjardins, 2011, Blount et al., 2018), i.e. that evolutionary outcomes are biased by the developmental and genetic background of a lineage (Nordén & Price, 2018, Stryjewski & Sorenson, 2017, Price et al., 2000). Historical contingency is particularly relevant to explain large-scale patterns in plumage color diversity, such as the reoccurring color themes in families noted by Wallace (1877). This is because birds use many different mechanisms to produce color, and each mechanisms is associated with a particular genetic and developmental framework that takes time to evolve (Hill & McGraw, 2006b, Price-Waldman & Stoddard, 2021). Once a color mechanism has evolved in a clade, it is likely that it will repeatedly be used in response to selection, as opposed to individual species evolving entirely new mechanisms (Nordén & Price, 2018). Conserved genetic and developmental frameworks have been implicated in the repeated evolution of red carotenoid plumage pigmentation in some clades (Thomas et al., 2014, Nordén & Price, 2018, Twyman et al., 2018, Price et al., 2007, Prager & Andersson, 2010).

Here, we investigate whether historical contingency could explain the repeated evolution of a structural color—metallic luster—in some bird clades. Structural color produce colors from the interaction of light with a nanostructure (in contrast to pigmentary colors like carotenoids that produce colors from selective absorbance). Structural coloration in birds can be divided into two main types: 1) structural barbule coloration (Figure 4.1J), which is produced by arrays of melanin-filled organelles (melanosomes) in the barbules, and 2) structural barb coloration

(Figure 4.1K), which is produced by nanostructured "spongy" keratin in the barbs (Prum, 2006). Though the former are often called "iridescent structural colors" and the latter "non-iridescent structural colors", both types of structural colors do in fact display iridescence (a change in hue with viewing or observation angle, see Chapter 3). However, only structural barbule coloration produce colors with metallic luster—the metallic sheen of the peacock's plumage for example. We have previously shown that metallic luster is characterized by a colored specular reflectance and a low diffuse reflectance, which is present in structural barbule but not structural barb coloration (Chapter 3). Therefore, we will use metallic luster, and not iridescence, to describe structural barbule colors here.

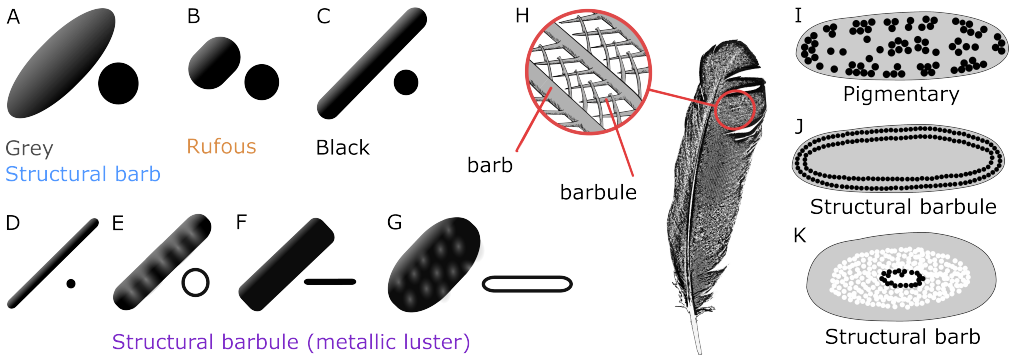

Figure 4.1: Known melanosome diversity and their structural arrangement in feather filaments. Three main types of melanosomes have been described from pigmentary feathers: large, ellipsoids in gray feathers (A), short rods in rufous feathers (B), and thick rods ($\geq$ 190nm in diameter) in black feathers (C). Thick rods can also produce faint (but not intense) metallic luster in some species (Nordén et al., 2021). Four derived melanosome types have been described from feathers with metallic luster: thin rods ($<$ 190nm in diameter, D), hollow rods (E), platelets (F), and hollow platelets (G). Melanosomes are also organized differently in the feather (H) depending on color mechanism. Cross-sections of I) a barbule from a pigmentary feather with disorganized thick rods, J) a barbule from a feather with metallic luster with thin rods organized in multiple layers, K) a barb with nanostructured "spongy" keratin and melanosomes in the interior. Figure adapted from Figure 2 in Nordén et al., 2021, and Figure 2 in Chapter 3.

The frequency of metallic luster varies greatly in different bird families, as was noted by the Austrian ornithologist Ludwig Auber over fifty years ago (Auber, 1957). In some families, like Anatidae, Phasianidae, Cuculidae and Columbidae, metallic luster is very frequent and often bright—but in others it is absent from most species, like Psittacidae and Cotingidae. Psittacidae and Cotingidae instead use other color mechanisms to produce bright colors, e.g. pigments and structural barb coloration (Prum et al., 2012, Tinbergen et al., 2013). To produce

bright and saturated metallic luster, it is necessary to evolve derived melanosome shapes (thin rods, hollow rods, solid platelets or hollow platelets) that differ from the ancestral thick rods found in pigmentary black or gray plumage (Figure 4.1A–G, see Nordén et al., 2021). During feather development, these melanosomes must be arranged into precisely spaced layers within the feather barbule to produce interference colors (Durrer, 1977, Maia et al., 2012). Moreover, feathers with metallic luster often display modified barbules, which are flattened and twisted to allow maximal reflection with the incoming light (Durrer, 1977). Thus, producing bright and saturated metallic luster requires several modifications to melanosome and feather development that are likely difficult to evolve. We therefore hypothesize that historical contingency is an important factor in explaining the large-scale presence and absence of metallic luster in bird clades.

Intriguing evidence from hummingbirds (family Trochilidae) and tree swifts (family Hemiprocnidae) provides a possible mechanism for the evolution of metallic luster as a historically contingent process. Until recently, derived melanosomes (thin rods, hollow rods, solid platelets or hollow platelets, Figure 4.1D–G) were thought to be uniquely found in plumage with metallic luster. Melanosomes are also present in black, gray, and brown/rufous feathers—but in this case they do not form nanostructures and therefore only function as a pigment (Figure 4.1I). Melanosomes are typically shaped as thick rods in black and gray plumage (Figure 4.1A, C), and as short rods in rufous plumage (Figure 4.1B)(Li et al., 2010). Thus, it has been assumed that melanosome shape is tied to plumage color production (Nordén et al., 2021, Li et al., 2012, 2010, Vinther, 2020, Nordén et al., 2019). This relationship between melanosome shape and color has been used to reconstruct colors of extinct animals, whose integumentary melanosomes sometimes fossilize (Nordén et al., 2019, Li et al., 2010, 2012, Babarović et al., 2019, Hu et al., 2018, Vinther et al., 2008, 2010). However, Smithwick (2019) described hollow platelets extracted from the gray and black plumage of several hummingbird species, and solid platelets from the gray plumage of tree swifts. These families are known to produce hollow platelets and solid platelets respectively in plumage with metallic luster (Durrer, 1977). Hummingbirds and tree swifts are unusual in that not a single species completely lacks metal-

lic luster. This led Smithwick (2019) to suggest that derived melanosomes may be retained in the entire body plumage if a species has metallic luster in at least one patch. Here, we take this hypothesis one step further and ask whether derived melanosomes may be retained in species that have lost metallic luster altogether. We hypothesize that while there is selective pressure to gain derived melanosomes when evolving metallic luster, there is no selective pressure to lose derived melanosomes when transitioning back to pigmentary colors. This is because the derived melanosomes would function much like a thick rod—simply as an absorbing pigment—if the nanostructural order in the barbule was lost. The shape of the melanosome is critical for the production of metallic luster (a structural color), but it is irrelevant for the absorbance properties of the pigment melanin. We speculate that the retention of derived melanosomes could provide a mechanism for the repeated gains and losses of metallic luster seen in some bird families, which gives rise to the biased distribution of this structural color in bird families noted by Auber (1957).

We test our hypothesis by exploring the diversity of feather nanostructures in the cuckoos (family Cuculidae), a family with widespread occurrence of metallic luster in the plumage. Previous studies have described three types of derived melanosomes in this clade from species with metallic luster: thin rods (in *Chrysococcyx cupreus*, described by Durrer, 1977), hollow rods (in *Centropus sinensis*, *Centropus violaceus* and *Centropus ateralbus*, described by Nordén et al., 2019) and solid platelets (in *Phaenicophaeus diardi* and *Phaenicophaeus curvirostris*, described by Nordén et al., 2019). We first phylogenetically mapped the presence of metallic luster in 126 cuckoo species (excluding 21 species lacking genetic data for the phylogenetic reconstruction) using a three-point scale based on visual assessment of their plumage. We then selected 21 representative species across the tree with and without metallic luster, and measured their plumage colors with cross-polarization photography to validate our visual scoring and quantify differences in metallic luster. From these representative species, we imaged cross-sections of feather samples using transmission electron microscopy to compare melanosome shape and feather nanostructure in species with and without metallic luster in five main clades. Finally, we compared the diversity of melanosome shape in plumage with and without metallic luster

in cuckoos to the melanosome shape diversity which has previously been described across all birds, to answer whether melanosome shape and plumage color is decoupled in cuckoos.

4.2 Results

4.2.1 Evolution of metallic luster in Cuculidae

We assigned scores to 10 plumage patches (crown, nape, mantle, rump, dorsal tail, wing covert, wing primaries/secondaries, throat, breast, and belly) to quantify the presence of metallic luster in cuckoos. Since metallic luster can vary in intensity (brightness and saturation), we scored it on a three-point scale: 0: absence, 1: faint-moderate, 2: intense (see §4.4.1, *Methods*, for more details). We validated our scores on a subset of samples using cross-polarization imaging , a technique that can measure the strength and saturation of the specular reflection, which we use as a proxy for metallic luster (see Chapter 3). A high relative specular reflection that is saturated indicates presence of metallic luster, while low relative specular reflection that is unsaturated indicates absence of metallic luster. The sampled patches did indeed vary in metallic luster, with patches scored as "0" measuring low relative specular reflectance and saturation and patches scored as "1" or "2" with higher specular reflection and saturation (Figure 4.2). While there is some overlap in "1" and "2", in general "2" has the highest specular reflection and specular saturation.

Metallic luster is widespread in Cuculidae, with over three fifths of species (62%) exhibiting the trait in at least one plumage patch (Figure 4.3A). Faint-moderate metallic luster is most common, while intense metallic luster is limited to a single genus (*Chrysococcyx*, Figure 4.3A, E). In terms of distribution on the body, metallic luster is more frequent in the dorsal than the ventral part of the plumage (Figure 4.4). Since the nanostructures giving rise to metallic luster are built with melanin, this pattern may be linked to the general bias for a melanized dark ventral and light dorsal body seen in many animals (for which the evolutionary reason is still debated, Rowland, 2008). Alternatively, or additionally, ventral plumage may tend to lack metallic luster because flattened barbules—which is a common barbule modification in plumage with metallic luster (Durrer, 1977)–may decrease waterproofing of feathers (Eliason

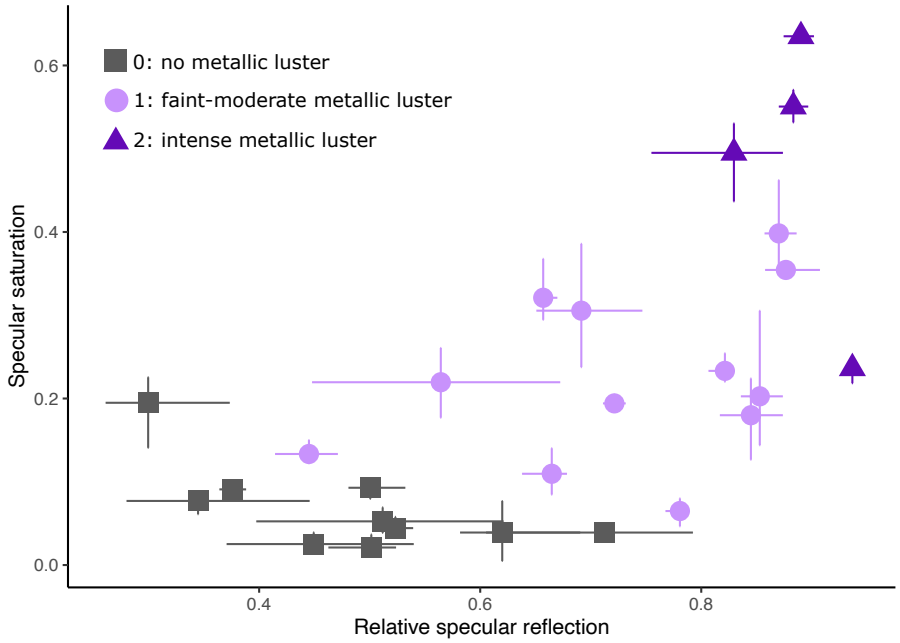

Figure 4.2: Plumage patches sampled from Cuculidae species vary in the intensity of metallic luster, as measured by the relative specular reflection and specular saturation. Colors and shapes indicate the score for the plumage patch based on visual assessment. Patches scored as "0" tended to have low relative specular reflection and saturation, indicative of absence of metallic luster, while patches scored as "1" and "2" recorded higher relative specular reflection and saturation, indicative of faint-intense metallic luster. "1" and "2" show overlapping distributions, but in general "2" measures the highest relative specular reflection and saturation. Lines represent the range of three repeated measurements of the same patch.

& Shawkey, 2011).

Nine genera lack metallic luster completely (*Guira*, *Tapera*, *Dromococcyx*, *Rhinortha*, *Pachycoccyx*, *Coccycua*, *Urodynamus*, *Cerococcyx* and *Hierococcyx*), but most genera contain species both with and without metallic luster. In some cases, species lacking metallic luster appear nested within a clade exhibiting the trait—e.g. *Coua cursor* and *Coua coquereli* within the *Coua* clade, and *Centropus celebensis* (Figure 4.3C) and *Centropus unirufus* within the *Centropus* clade. Similarly, *Chrysococcyx flavigularis* (Figure 4.3D) exhibit moderate metallic luster but is nested in a clade with intense metallic luster (Figure 4.3A, E). In other cases,the situation is reverse: species with metallic luster appear nested within clades otherwise lacking the trait—e.g. *Coccyzus pluvialis* within the *Coccyzus* clade, and *Cacomantis flabelliformis* within the *Cacomantis* clade (Figure 4.3A). We cannot make definitive inferences from these patterns, but based on phylogenetic bracketing, these are potential cases of losses and gains of metallic luster, respectively. While we did attempt to model rates of character transitions and recon-

struct ancestral states using Bayesian inference and continuous-time Markov models, our results were highly variable. This suggests that gains and losses of metallic luster are not well represented by a Markov process, and/or are difficult to reconstruct with existing approaches, and we therefore chose to not include the results here (see Appendix C.1 for further discussion).

Based on this overview of the distribution of metallic luster in Cuculidae, we can start to explore the nanostructural diversity. If derived melanosomes are retained when metallic luster is lost, we should observe this in species lacking metallic luster nested within clades that have metallic luster. We turn to this topic in the next section (§4.2.2, *Nanostructural diversity*).

4.2.2 Nanostructural diversity

To characterize feather nanostructural diversity, feather samples were collected from museum specimens representing 21 species across the Cuculidae. We plucked all feathers from the mantle patch to facilitate direct comparisons between species (with the exception of *Phaenicophaeus diardi*, which was sampled from the belly patch, and *Chrysococcyx xanthorhynchus* from which a loose feather of unknown patch was opportunistically sampled). All patches sampled were part of the set photographed with cross-polarization to validate differences in metallic luster (Figure 4.2).

Plumage with metallic luster

We first describe the melanosome shape and organization found in species with metallic luster (scored as "1" or "2").

Melanosome shape. Plumage with metallic luster was found to be produced with either solid rods (in *Chrysococcyx*, *Surniculus* and *Cuculus*, Figure 4.5A–G, Figure 4.3A) or hollow rods (in *Neomorphus*, *Geococcyx* and *Coua*, Figure 4.6A–D, Figure 4.3A). Using image analysis, we measured the diameter of solid rods in imaged barbule cross-sections to determine whether they could be considered thick rods ($\geq$ 190nm in diameter) or derived thin rods ($<$

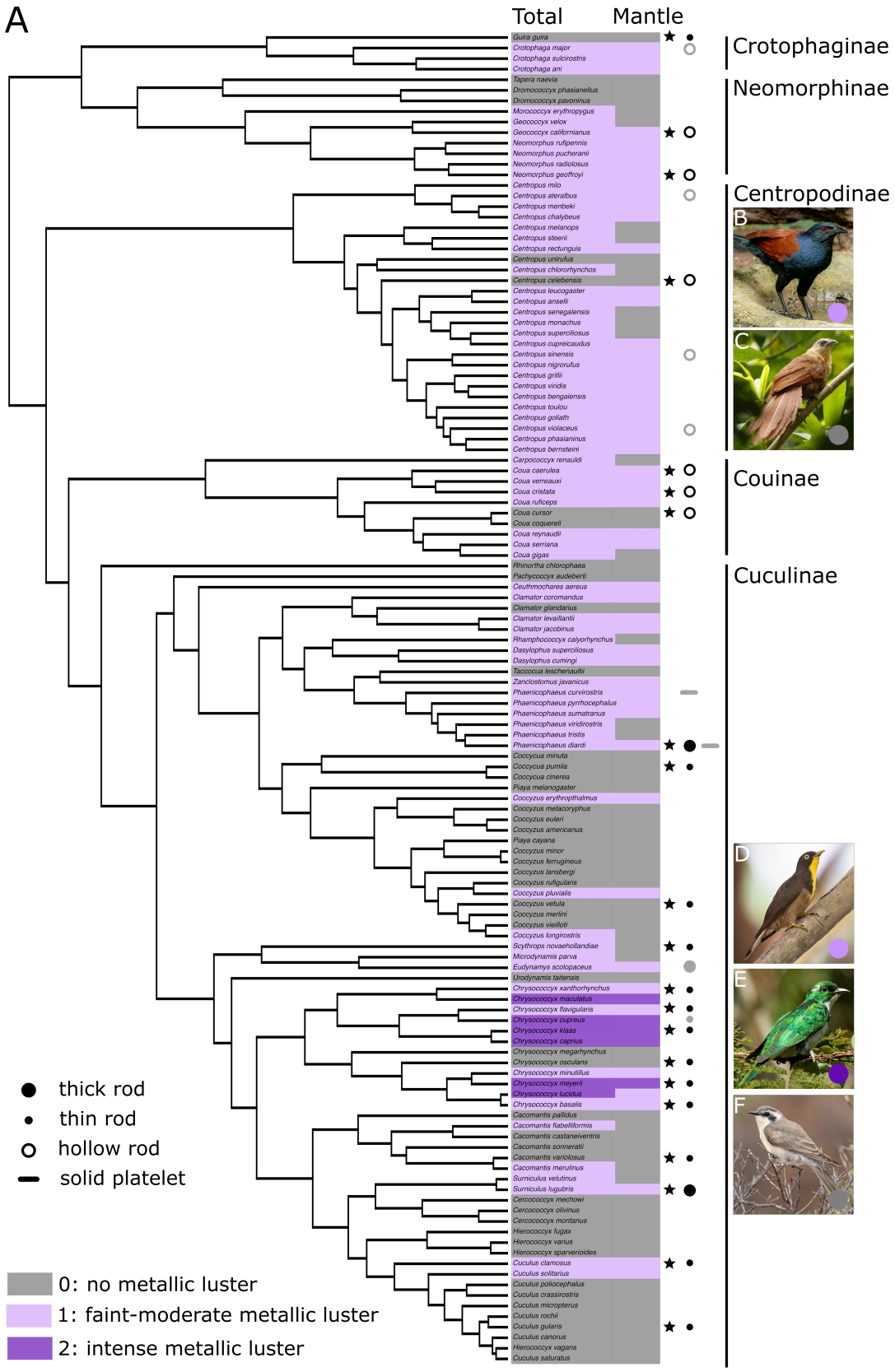
A
Total
Mantle
Crotophaginae
Neomorphinae
Centropodinae
Couinae
Cuculinae
B
C
D
E
F
thick rod
thin rod
hollow rod
solid platelet
0: no metallic luster
1: faint-moderate metallic luster
2: intense metallic luster

Figure 4.3: (Previous page) Plumage with metallic luster is widespread in Cuculidae. Each species was scored for the presence of metallic luster on a three-point scale (0: absent; 1: faint-moderate; 2: intense) across body patches (see §4.4.1, *Methods*). The result of this analysis is color coded on the tree (A), with gray, light and dark purple representing 0, 1 and 2 scores, respectively. "Total" describes the highest score received by each species anywhere on the body, "mantle" describes the score for the mantle patch. Species that were sampled for microscopy are marked by a star. Melanosome shape in the plumage is represented by symbols (large dot, thick rods; small dot, thin rods; open circle, hollow rod; platelet, solid platelet)—black symbols represent melanosome shapes described in this study, and gray symbols represent shapes described in previous studies (*Chrysococcyx cupreus* described in Durrer & Villiger, 1970a, all others from Nordén et al., 2019). The photographs showcase the variation in metallic luster of the cuckoos we sampled: B) *Centropus sinensis* (all rights reserved by copyright holder Sakkarin Sansuk, reproduced here with permission) C) *Centropus celebensis* (all rights reserved by copyright holder Marc Thibault, reproduced here with permission), D) *Chrysococcyx flavigularis* (all rights reserved by copyright holder Dubi Shapiro, reproduced here with permission), E) *Chrysococcyx klaas* (all rights reserved by copyright holder Luke Seitz, reproduced here with permission), F) *Chrysococcyx osculans* (all rights reserved by copyright holder David Ongley, reproduced here with permission).

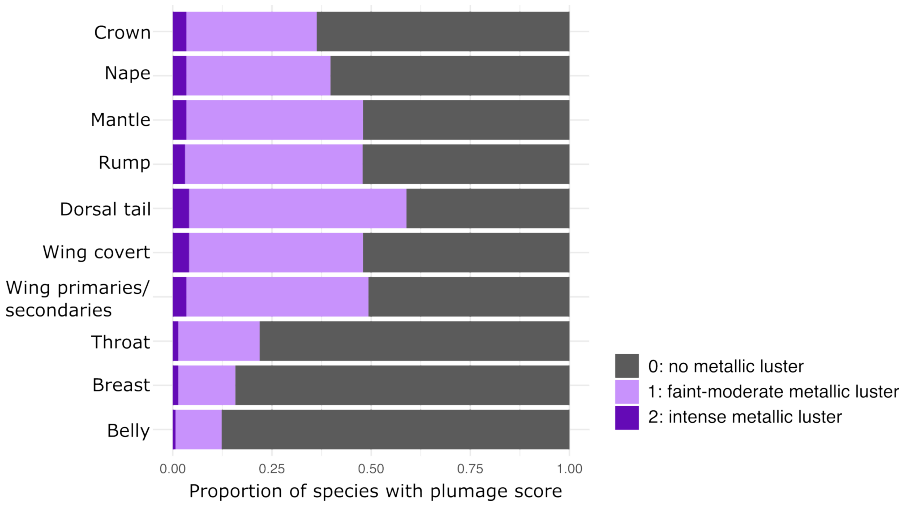

Figure 4.4: Metallic luster is more common in the dorsal (crown, nape, mantle, rump, dorsal tail, wing coverts, and wing primaries/secondaries) compared to the ventral plumage (throat, breast, and belly) in the Cuculidae. Bars show the proportion of species scored as "0", "1" or "2" (gray, light purple and dark purple respectively) for each plumage patch.

190nm in diameter, see Nordén et al., 2021). We found that melanosomes in all species sampled could be considered to be thin rods, except *Surniculus lugubris*, which had melanosomes with an average diameter of 203nm (Figure 4.7A, Figure 4.5F). From a previous study (Nordén et al., 2019), we also know that hollow rods are present in the plumage with metallic luster in *Crotophaga major*, *Centropus sinensis*, *Centropus violaceus* and *Centropus ateralbus* , while platelets are present in *Phaenicophaeus diardi* (Figure 4.5H) and *Phaenicophaeus curvirostris*. Since melanosome type in plumage with metallic luster is often conserved within a genus (Nordén et al., 2021, Durrer, 1977), together this suggests that metallic luster is produced with hollow rods in the clades Crotophaginae, Neomorphinae, Centropodinae and Couinae, while Cuculinae produces metallic luster with thin rods (with the exception of *Phaenicophaeus*). A summary

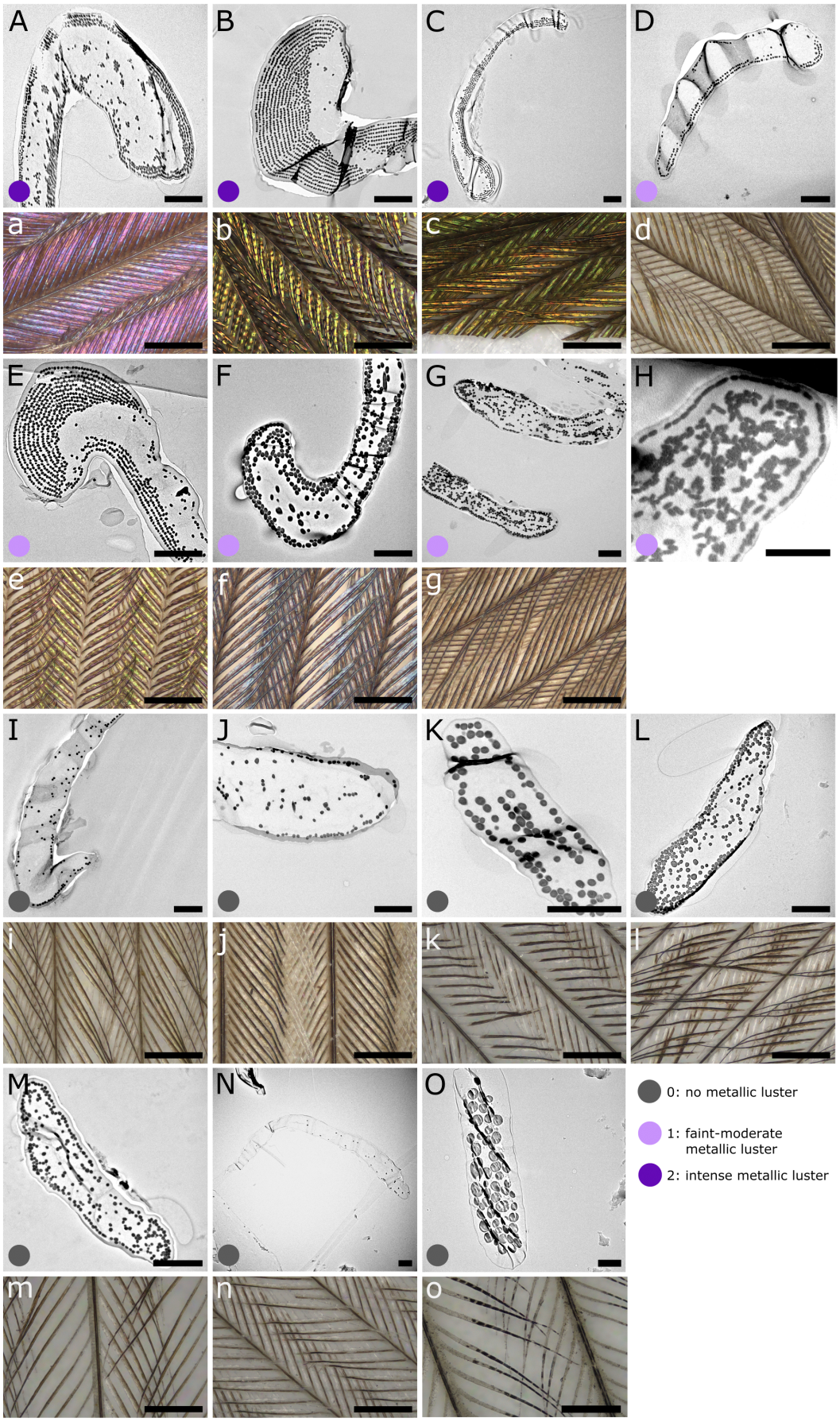
A
B
C
D
a
b
c
d
E
F
G
H
e
f
g
I
J
K
L
i
j
k
l
M
N
O
m
n
o
0: no metallic luster
1: faint-moderate metallic luster
2: intense metallic luster

Figure 4.5: (Previous page) Feather nanostructures in plumage with and without metallic luster in the Cuculinae clade. Dark and light purple dots indicate intense and moderate metallic luster, respectively. Gray dots indicate absence of metallic luster. Capital letters denote transmission electron microscope images of barbule cross-sections, lower case letters denote confocal microscope images of each feather sample. A-a) *Chrysococcyx xanthorhynchus*, B-b) *Chrysococcyx klaas*, C-c) *Chrysococcyx meyeri*, D-d) *Chrysococcyx basalis*, E-e) *Chrysococcyx flavigularis*, F-f) *Surniculus lugubris*, G-g) *Cuculus clamosus*, H) *Phaenicophaeus diardi* (from Nordén et al., 2019), I-i) *Chrysococcyx osculans*, J-j) *Scythrops novaehollandiae*, K-k) *Cuculus gularis*, L-l) *Cacomantis variolosus*, M-m) *Coccyzus vetula*, N-n) *Coccycua pumila*, O-o) *Phaenicophaeus diardi*. All scale bars in TEM and confocal images equal 2μm and 200μm, respectively.

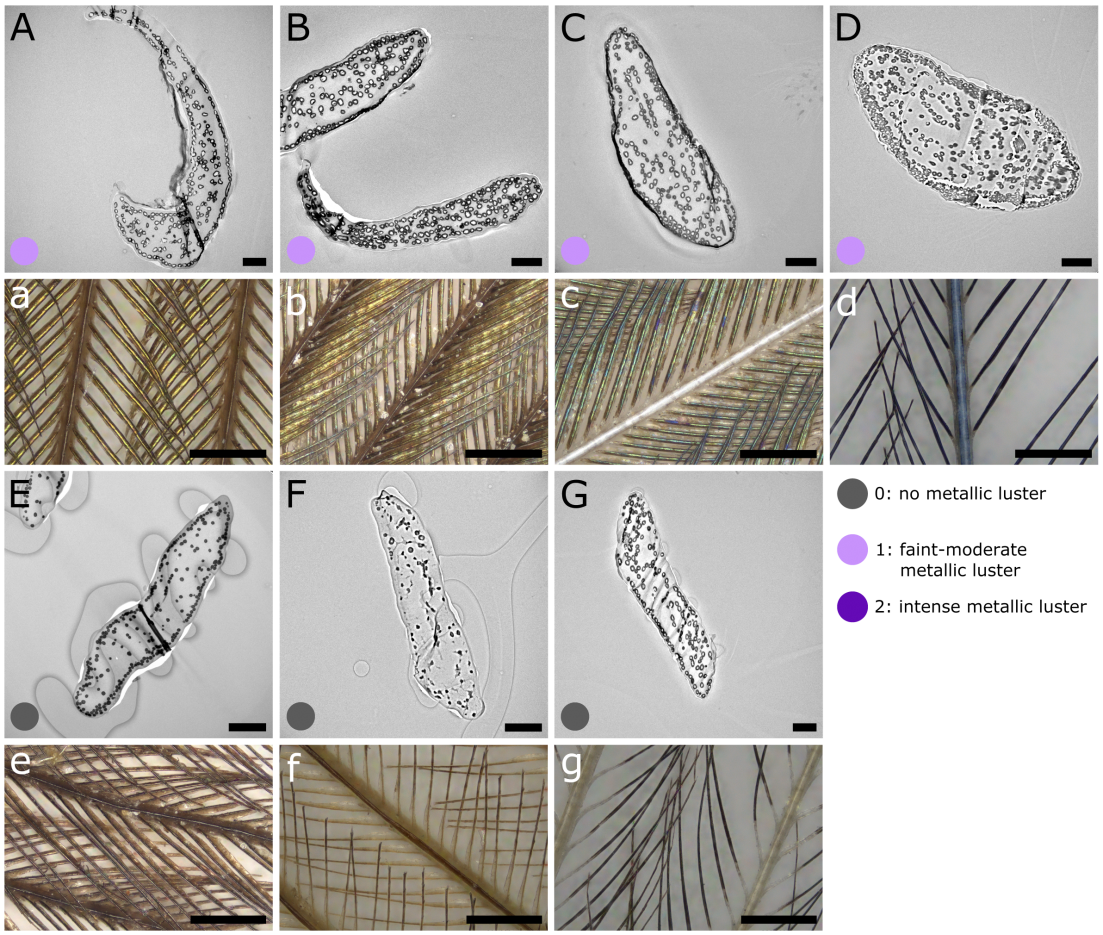

Figure 4.6: Feather nanostructures in plumage with and without metallic luster in the Crotophaginae, Neomorphinae, Centropodinae and Couinae clades. Dark and light purple dots indicate intense and moderate metallic luster, respectively. Gray dots indicate absence of metallic luster. Capital letters denote transmission electron microscope images of barbule cross-sections, lower case letters denote confocal microscope images of each feather sample. A-a) *Neomorphus geoffroyi*, B-b) *Geococcyx californianus*, C-c) *Coua cristata*, D-d) *Coua caerualela*, E-e) *Guira guira*, F-f) *Centropus celebensis*, G-g) *Coua cursor*. All scale bars in TEM and confocal images equal 2μm and 200μm, respectively.

of the known melanosome shapes in the cuckoos is shown in Figure 4.3A.

Melanosome organization. In all feathers with metallic luster, melanosomes were found to form a single or multiple ordered layers towards the outer border of the barbule (Figure 4.5A–H; Figure 4.6A–D). Most structures had only a single outer layer, while species in the genus *Chrysococcyx* exhibited up to 10 layers of melanosomes (Figure 4.5A–E). A greater number of layers increases the total reflection of the structure, resulting in brighter and more saturated colors (Kinoshita et al., 2008). Interestingly, *Chrysococcyx flavigularis* (Figure 4.5E), a species with moderate metallic luster, had as many melanosome layers as its sister species *Chysococcyx klaas* (Figure 4.5B) with intense metallic luster. However, closer inspection reveals that the melanosome layers in *C. flavigularis* are uneven and show a higher degree of disorder than in *C. klaas*. This demonstrates that even a slight decrease in nanostructural order—while retaining melanosome shape—can cause a stark change in plumage color.

Plumage without metallic luster

Having surveyed melanosome diversity in cuckoo species with metallic luster, we can now contrast this with the melanosome shape and organization in species lacking metallic luster.

Melanosome shape. Derived melanosome shapes were found in all but one of the plumage samples lacking metallic luster that we studied (the exception being the gray belly of *Phaenicophaeus diardi*). Moreover, the species lacking metallic luster had retained the same derived melanosome shape that was present in the sister species of that clade that had metallic luster. In *Crotophaga* and *Centropus*—two genera where species with metallic plumage have hollow rods—hollow rods were also present in the gray plumage of *Coua cursor* (Figure 4.6G) and the rufous plumage of *Centropus celebensis* (Figure 4.6F). In *Centroupus celebensis*, hollow rods are interspersed with irregularly shaped melanosomes, which may indicate a disruption of melanosome formation (see Li et al., 2019)(Figure 4.6F). In *Chrysococcyx*—a genus where species with metallic plumage have thin rods—thin rods were also found in the gray plumage of *Chrysococcyx osculans*. Even species in genera that mostly lack metallic luster were found to

have thin rods in their plumage: *Coccycua pumila*, *Coccyzus vetula*, *Cuculus gularis*, *Cacomantis variolosus*, *Scythrops novaehollandiae* (Figure 4.5J–N) and *Guira guira* (Figure 4.6E). The exception was the gray belly of *Phaenicophaeus diardi*, which had large melanosomes (approximately 1μm in diameter) that were likely ellipsoid in shape, based on the varied diameter seen in the cross-sections (Figure 4.5O). Thus, they were markedly different from the solid platelet melanosomes previously described in the mantle of *Phaenicophaeus diardi* with metallic luster (Figure 4.5H), and more similar to melanosomes that have previously been described in gray plumage of other birds (Figure 4.1A).

Melanosome organization. Melanosomes in samples without metallic luster tended to form a layer at the outer border of the barbule (Figure 4.5I–N, Figure 4.6E, G), similar to the melanosome organization seen in samples with metallic luster. However, this layer had multiple gaps (Figure 4.5I–N, Figure 4.6E, G). In general, we observed that the number of melanosomes in barbules appeared to have decreased compared to barbules from plumage with metallic luster. This was sometimes seen directly in individual cross-sections (e.g. Figure 4.5I, J and N), and in other cases seen from the distribution of melanin in the feather as a whole. Melanin was not deposited in the full length of the barbule but only in the end, middle or first part (Figure 4.5i–n, Figure 4.6f–g). Though difference in melanin content would have to be confirmed with a chemical test, we note that the plumage we sampled was gray in color, while plumage with metallic luster is much darker (in transmitted light). Thus, we speculate that the decreased amount of melanosomes may be a key factor disrupting the production of metallic luster, since not enough melanosomes are available to form continuous nanostructures in the entire barbule.

An exception in melanosome organization was seen in the sample from the gray belly of *Phaenicophaeus diardi*, which was also the only sample with large, ellipsoidal melanosomes (Figure 4.5O). Here, instead of forming a layer at the outer border of the barbule, the melanosomes grouped together at the center of the barbule.

Summary

Derived melanosomes are widespread in Cuculidae irrespective of plumage color (metallic luster versus gray or brown, Figure 4.3A). In particular, we found three instances in which species lacking metallic luster nested in clades with metallic luster had the same derived melanosome shapes as the parent clade (*Coua cursor* (Figure 4.6G), *Centropus celebensis* (Figure 4.6F), and *Chrysococcyx osculans* (Figure 4.5I)). This suggests that the derived melanosome shapes in these groups have been retained even as metallic luster was lost.

Derived melanosomes in plumage without metallic luster still formed partial layers in the outer border of the barbule, in a similar manner to melanosomes in plumage with metallic luster (Figure 4.5, Figure 4.6). However, the concentration of melanosomes appeared to have been reduced, resulting in partial melanization of the barbules. Thus, metallic luster may be lost by changing the concentration of melanosomes in the feather barbule, rather than reverting melanosome shape back to an ancestral thick rod.

Phaenicophaeus diardi differed from the pattern described above. It had large, ellipsoidal melanosomes in its gray plumage and solid platelets in the mantle patch with metallic luster (Figure 4.5H, O). Without also sampling the belly patch of other species, it is hard to say if *Phaenicophaeus diardi* is an exception to other cuckoos in terms of how it produces gray color, or an indication that melanosome shape varies with body patch.

Decoupling between melanosome shape and plumage color

The melanosome diversity in plumage with and without metallic luster that we have described in the section above (§4.2.2, *Nanostructural diversity*) suggest a decoupling between melanosome shape and plumage color. This is in contrast to previous studies, which have shown a relationship between melanosome shape and plumage color based on melanosome shape parameters collected from plumage samples of over 400 species (Li et al., 2010, 2012, Nordén et al., 2019, Babarović et al., 2019). To visualize this decoupling more clearly, we can compare the diameter of solid rods from different plumage colors recorded across birds to that of solid rods in Cuculidae (Figure 4.7B). It is clear that the variation of melanosome diameter in Cucul-

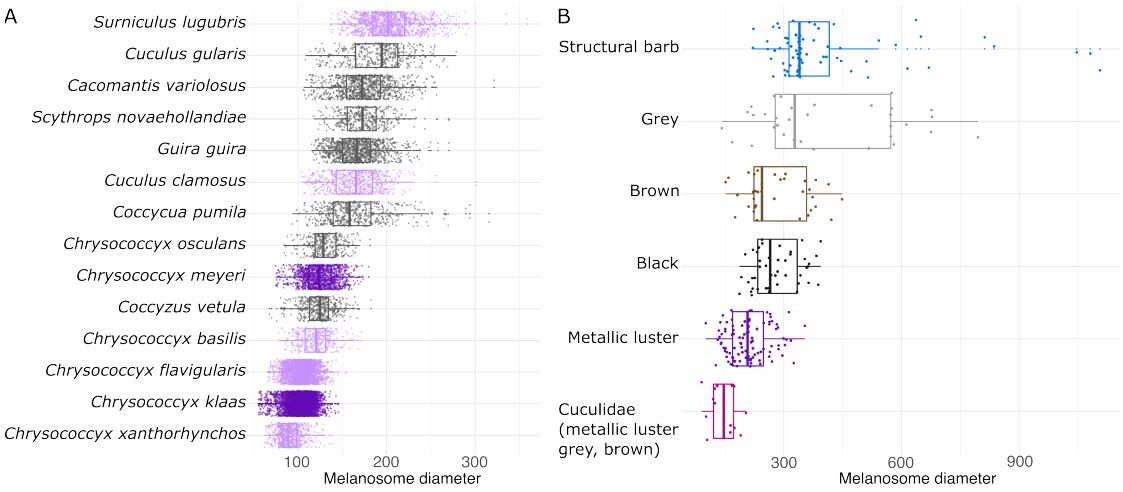

Figure 4.7: The diameter of solid rods in the Cuculidae is small irrespective of plumage color (A), which contrasts with the diversity seen across plumage colors in a broader sample of birds (B). Data in B (except for Cuculidae) from the following studies: Li et al. (2012), Babarović et al. (2019), Nordén et al. (2019).

idae is considerably smaller than what we would expect given their color variability (including metallic luster and gray color, Figure 4.7B). The diameter of the solid rods in Cuculidae differs significantly from all other color categories except metallic luster (ANOVA one-way test: $df = 5$, $F = 33.23$, $p < 0.001$; Tukey's post-hoc test, all comparisons $p < 0.005$ except for metallic luster, $p = 0.41$).

4.3 Discussion

We have described the evolution of metallic luster and its relationship to nanostructural barbule variation in the Cuculidae family. A key finding is that derived melanosome shapes can be retained in species lacking plumage with metallic luster. This is interesting because it suggests that derived melanosomes, once evolved, can be retained over long evolutionary timescales, potentially providing a mechanism for re-emergence of the trait. The widespread occurrence of derived melanosomes across Cuculidae—even in clades where the majority of species lack metallic luster (e.g. *Cuculus*, *Coccycua* and *Coccyzus*, Figure 4.7A)—supports this idea. Rather than switching melanosome type, species that lost metallic luster likely did so by reducing the amount of melanosomes in the feather barbule (Figure 4.6, 4.5). This might explain why many of the species in Cuculidae lacking metallic luster have gray, as opposed to black, plumage. Thus, we speculate that the retention of derived melanosomes in plumage lacking metallic

luster provides a mechanism for the frequent evolution of metallic luster in Cuculidae.

The finding that derived melanosome shape can be retained in plumage lacking metallic luster decouples the direct relationship between plumage color and melanosome shape that has been shown previously (Figure 4.1)(Li et al., 2010, 2012, Vinther, 2020, Nordén et al., 2019, Babarović et al., 2019). However, it also validates some of the ideas behind it. Thin rods and hollow rods were seen to form partial layers at the outer border of the barbule even in plumage lacking metallic luster (Figure 4.5I–N, Figure 4.6E, G). In contrast, the large, ellipsoidal melanosomes in the gray plumage of *Phaenicophaeus diardi* formed clusters towards the middle of the barbule (Figure 4.5O)—a phenomenon previously described in gray feathers by Babarović et al. (2019). These observations support earlier suggestions that melanosome shape plays a key role in the nanostructural arrangement of melanosomes in the barbule during feather development (Maia et al., 2012, Babarović et al., 2019). However, because there are other parameters that can be adjusted to mute the production of metallic luster—such as the number of melanosomes deposited— evolving a particular melanosome type is not necessary to produce gray plumage color. The great range of melanosome diameters recorded from gray plumage across birds indicates that gray color indeed is produced in various ways in different species (Figure 4.7B). Thus, historical contingency may shape melanosome diversity in many bird clades, not just Cuculidae. This would on the one hand complicate direct inferences of plumage color from melanosome shape in fossils, but on the other hand give insight into the plumage evolution of a clade. If derived melanosome shapes only evolve to produce metallic luster, the finding of such melanosomes in a species would signal the presence of metallic luster in the lineage, albeit not necessarily predicting metallic luster in a particular species.

Evidence that retention of derived melanosomes in plumage lacking metallic luster is more widespread is found in studies of plumage colors in starlings (family Sturnidae). Starlings, like cuckoos, frequently exhibit metallic luster in the plumage and are know to have evolved derived melanosomes (Durrer & Villiger, 1970a, Maia et al., 2013b, Craig & Hartley, 1985). Though derived melanosomes have not yet been described from starling species that completely lack metallic luster, they have been described from gray and rufous patches in species

which also have patches with metallic luster. In the Superb starling (*Lamprotornis superbus*), the non-metallic rufous plumage on the belly contains hollow platelets—the same melanosome type also produced in the species' metallic dorsal plumage (Rubenstein et al., 2021). Interestingly, many of the melanosomes in the rufous plumage appear irregularly shaped, just like in the rufous plumage of *Centropus celebensis* described in this paper (Figure 4.6F). These irregularly shaped melanosomes may signal a different melanosome chemistry (greater amount of pheomelanin) and/or a disruption of melanosome shape formation, as indicated by a similar phenomena in chicken (*Gallus gallus*, see Li et al., 2019). Two other species in the same genus, *Lamprotornis fischeri* and *Lamprotornis unicolor*, have hollow rods in their metallic plumage (Maia et al., 2013b) and also exhibit disorganized hollow rods in the gray body plumage (Craig & Hartley, 1985). Intriguingly, losses of metallic luster seem to coincide with tranistions to gray or rufous (as opposed to black) melanin coloration in Sturnidae, much like in Cuculidae. This might indicate shared developmental processes involved in the loss of metallic plumage in the two clades.

Our findings add to growing empirical evidence that historical contingency is important for plumage color evolution. A widely documented phenomenon in plumage coloration is color masking (Price-Waldman & Stoddard, 2021), where one color mechanism masks the effect of a co-occurring mechanism. This can arise if a broadly absorbing pigment (e.g. melanin) masks the effect of another pigment (e.g. carotenoid) or structural barb coloration (Nero, 1954, Moreau, 1958, Hudon et al., 2015, M. Hofmann et al., 2007, Aguillon et al., 2021, D'Alba et al., 2012, Fan et al., 2019, Driskell et al., 2010, Justyn & Weaver, 2023). Though this phenomenon could have adaptive explanations (for example if the pigment deposition provides other physiological or functional advantages), historical contingency often seems more likely as an explanation. For example, Driskell et al. (2010) found that some species of fairy-wrens (family *Maluridae*) had spongy, nanostructured keratin in the barbs of black feathers. Spongy keratin in the barbs (Figure 4.1K) typically gives rise to blue structural coloration (Prum, 2006)—but in the fairy-wrens, the blue color was masked by melanin deposition (Driskell et al., 2010). Since not all species with black plumage exhibited spongy keratin in the barbs, and structural

blue coloration is very common in this family, Driskell et al. (2010) concluded that the spongy keratin in black feathers was likely inherited from an ancestral species with blue structural coloration in this patch. Similarly, the red chest and belly of the painted bunting (*Passerina ciris*) is produced by carotenoid pigmentation, yet the same feathers also contain spongy, nanostructured keratin in the barbs (Justyn & Weaver, 2023). Suggestively, the ancestors of the painted bunting likely had full structural blue body coloration (Martínez–Meyer et al., 2004). These studies, and the phenomenon of color masking more generally, suggest that historical contingency is an important force in shaping the diversity of plumage colors.

While our study underlines the importance of historical contingency in shaping plumage color evolution, there are also interesting exceptions to this pattern. In *Phaenicophaeus diardi*, solid platelet melanosomes were not retained in the gray belly patch, despite being present in the mantle patch with metallic luster (Figure 4.5H, O). Why did this species differ from all other cuckoos we sampled? One possibility is that melanosome shape in the belly patch generally differs from that of the mantle patch in cuckoos—perhaps linked to different feather structures found in these two patches. Another possibility is that transitions from solid platelets to thick rods is easier than transitions from other types of derived melanosomes (thin rods and hollow rods) to thick rods. To resolve this question, and to get a deeper understanding of how metallic luster evolves in birds, studies of the genetics regulating melanosome shape and structuring is key. This might reveal whether the genetic underpinnings of metallic luster in *Phaenicophaeus diardi* differs from that of other cuckoos species. The literature on the genetic basis of structural coloration is small but rapidly growing (Price-Waldman & Stoddard, 2021, Saranathan & Finet, 2021), and offers a promising path forward for future research. The varied feather nanostructures we have described in Cuculidae, which represents a continuum from no metallic luster to intense metallic luster, provides an interesting test case for candidate genes previously linked to melanosome shape and structuring (Rubenstein et al., 2021, Gao et al., 2018, Hellström et al., 2011, Li et al., 2019).

4.4 Methods

4.4.1 Distribution of iridescence in Cuculidae

Metallic luster in plumage varies from a faint sheen to bright and saturated colors. We scored this continuous variation on a 0-2 scale to uncover large-scale patterns in the evolution of structural colors in Cuculidae. Scoring was based on illustrations and photographs from Birds of the World (Billerman et al., 2022). Since a single photograph may be misinterpreted due to for example unusual lighting conditions or inaccurate white balance, we always ensured metallic luster was visible in at least two separate photographs before assigning a score. We also used the verbal description of the species to support our interpretation. For example, descriptions such as "glossed green" or "metallic" would suggest metallic luster. The scale we used is a coarser version of a similar qualitative scale developed by Durrer (1977) and Auber (1957), where our score 1 spans "schwach schiller/faint iridescence" to "mässiger schiller/moderate iridescence", and 2 spans "intensiver schiller/intense iridescence" to "brillianter schiller/luxuriant iridescence". A score of 0 means no metallic luster was observed in the plumage. All scores were assigned by K. K. N., based on their visual assessment. We define our categories as follows:

0: Plumage lacking metallic luster, including plumage with uncolored (white) gloss. Examples: *Cuculus canorus, Centropus celebensis*.

1: Plumage with metallic luster, defined as a colored (of some saturation, not white) gloss. The gloss is weak-moderate in brightness/saturation. Examples: *Crotophaga major, Chrysococcyx basalis*.

2: Plumage with metallic luster that is high in brightness/saturation. Examples: *Chrycococcyx cupreus, Chrysococcyx meyeri*.

We scored the male of each species for 10 separate patches: crown, nape, mantle, rump, dorsal tail, wing covert, wing primaries/secondaries, throat, breast, and belly. We assessed the male because in cases where sexes vary in plumage coloration, the female is typically the sex lacking metallic luster. We then mapped the maximum score and mantle score for each

species onto a phylogenetic tree of Cuculidae. The tree was generated by downloading 1000 trees from birdtree.org, which is based on the Jetz et al. (2012) phylogeny. We only included species that had genetic data, which was 126 species in total (88% of the total). From our distribution of 1000 trees, we generated a maximum clade credibility tree using TreeAnnotator (Drummond et al., 2012). Branch lengths were summarized by taking the mean branch lengths from across the distribution of time trees.

4.4.2 Feather sampling and microscopy

We sampled feathers from museum bird skin specimens (in total 21 specimens: 13 from The Academy of Natural Sciences of Drexel University and 8 from The American Museum of Natural History, details in the Appendix, §C.2). For each specimen, a single feather was plucked from the mantle using forceps. One species, *Phaenicophaeus diardi*, was instead sampled from the belly patch using the same technique. In addition, the sample from *Chrysococcyx xanthorhynchus* came from an unknown patch with metallic luster, since we opportunistically sampled a feather that fell off the specimen during handling. To visualize the barbule microstructure, we imaged each feather using a confocal microscope (Keyence VK-X3050 Confocal).

The embedding protocol to prepare samples for transmission electron microscopy (TEM) imaging was based on methods described in Shawkey et al. (2003) with modifications based on discussions with Nicholas M. Justyn (Swansea University) and Paul Shao (Princeton University).

We cut a few barbs from each feather using a razor blade and placed the barbs in eppendorf tubes. We washed the samples by adding 100% ethanol and leaving them on a bench-top shaker for 20 minutes. This procedure was repeated once. We then mixed the embedding resin following the instructions on our kit (EMbed 812 kit, Electron Microscopy Sciences, Fort Washington, PA, USA) for a hard resin (20ml EMBed-812, 9ml DDSA, 12ml NMA, 0.72ml DMP-30). We infiltrated the feather samples with resin over four days, using solutions of the following proportions: day 1: 85% acetone and 15% resin, day 2: 50% acetone and 50% resin, day 3: 30% acetone and 70% resin, day 4: 100% resin. For each step, samples where covered

with the resin solution and left for 24h at room temperature. On day five, samples where transferred to a flat embedding mould filled with resin, and the samples were then cured at 60° for 16-20 hours. The samples were first trimmed by hand with a razor blade and then with a microtome trimming knife (DiATOME trim 45°, DiATOME, Nidau, Switzerland) to prepare the block for sectioning. We sectioned the block into 72nm ultrathin sections using a Leica Ultracut UCT Ultramicrotome equipped with a diamond knife (DiATOME ultra Diamond Knife, 3mm, 45°, DiATOME, Nidau, Switzerland). Samples were transferred to 200 mesh copper grids (covered with Formvar and carbon support film) using a perfect loop (Electron Microscopy Sciences, Fort Washington, PA, USA). We stained each sample first with with UranyLess (Electron Microscopy Sciences, Fort Washington, PA, USA) and then with lead citrate (Airless bottle, Electron Microscopy Sciences, Fort Washington, PA, USA) staining solutions. A droplet of the stain was placed on Parafilm and the grid placed on top of the droplet for one minute. For the lead citrate stain, the parfilm with a droplet of stain was put in a petri dish and surrounded with NaOH pellets, to limit CO_2 reactions. Each grid was then washed by dipping the grid 20 times in each of 3 beakers filled with CO_2-free water, and left to dry on filter paper.

Finally, the grids were imaged using a Talos F200X Transmission Electron Microscope at an operating voltage of 200kV.

4.4.3 Measuring melanosome diameter in TEM images

We measured the diameter of melanosomes (solid rods) in TEM images using a semi-automated image analysis approach based on the MATLAB function "imfindcircles". This would allow us to classify them as either thin rods ($<$190nm in diameter) or thick rods ($\geq$190nm in diameter, Nordén et al., 2021). In detail, we first measured a large and a small melanosome in the image to set the search range for the function. We then used morphological image closing to smooth out irregularities and holes in the image, while preserving the shape and size of objects (melanosomes). The image was then transformed to a binary image using a manually adjusted threshold. Finally, circles in this processed image was detected using the "imfindcir-

cles" function, from which diameters could be extracted. We plotted detected circles onto the original image and checked for errors by visual inspection. We also validated our method by comparing it with the results of manually measuring melanosomes using ImageJ (Abràmoff et al., 2004) for 3 random images (Appendix §C.3).

The melanosome diameters we recorded in Cuculidae was compared with melanosome diameters measured from samples of various plumage colors across birds . This data was compiled from previously published studies (Li et al., 2010, 2012, Nordén et al., 2019, Babarović et al., 2019). We included only samples with solid rods. Melanosome diameters were compared using a one-way ANOVA between the following categories: Cuculidae (all solid rods, both plumage with and without metallic luster), gray, black, brown, metallic luster and structural barbule. Note that metallic luster would have been described as "iridescent" in Nordén et al. (2019) and Li et al. (2012), and structural barbules as "non-iridescent" in Babarović et al. (2019).

4.4.4 Quantifying metallic luster

All species sampled for microscopy plus an additional five species where photographed using cross-polarization photography (see Appendix C.2 for specimen and sample information). This technique allows specular and diffuse reflections from a sample to be separated using polarization filters in front of camera and light source. Since plumage with metallic luster is uniquely characterized by a strong specular reflection that is colored, we used relative specular reflection and specular saturation as a proxy for the presence of metallic luster (see Chapter 3). We followed the methods outlined in Chapter 3 to capture and process polarization images. Briefly, our set-up consisted of a Nikon D7000 camera equipped with a rotatable linear polarization filter and two light sources covered by linear polarization film. We captured images of the mantle patch of each specimen in a cross-polarized and plane-polarized configuration, with two repeats, including a Calibrite Nano ColorChecker Classic Chart in each image. Images were captured in RAW format and color calibrated using custom MATLAB code based on code and methods in Akkaynak et al. (2014) and Sumner (2014). They were then analyzed

in MATLAB to calculate the relative specular reflection (specular reflection/total reflection) and the saturation of the specular reflection. The saturation was calculated as the distance to the center in a trigonal color space (RGB).

A

Appendix for Chapter 2

A.1 Additional figures

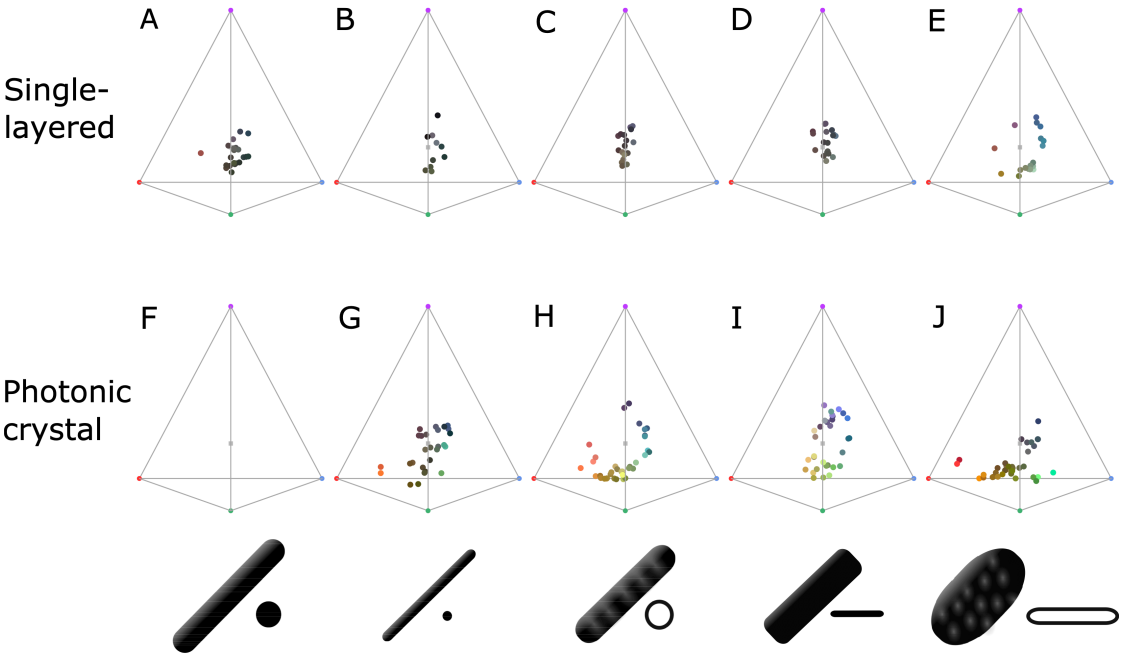

Figure A.1: Plumage color data (represented in avian color space) subdivided by type of structure; single-layered (A–E) and photonic crystal (F–J). Melanosome schematics in bottom row indicate the type of melanosome in the structures: thick solid rod (A, F), thin solid rod (B, G), hollow rod (C, H), solid platelet (D, I), and hollow platelet (E, J). Note that saturation is low for all single-layered structures, with the exception of hollow platelets (E). Data for (E) are mainly collected from African starlings; thus, it is not clear whether this is a general trend or specific to this group. Either way, it demonstrates that single-layered structures behave differently from photonic crystals and deserve further study.

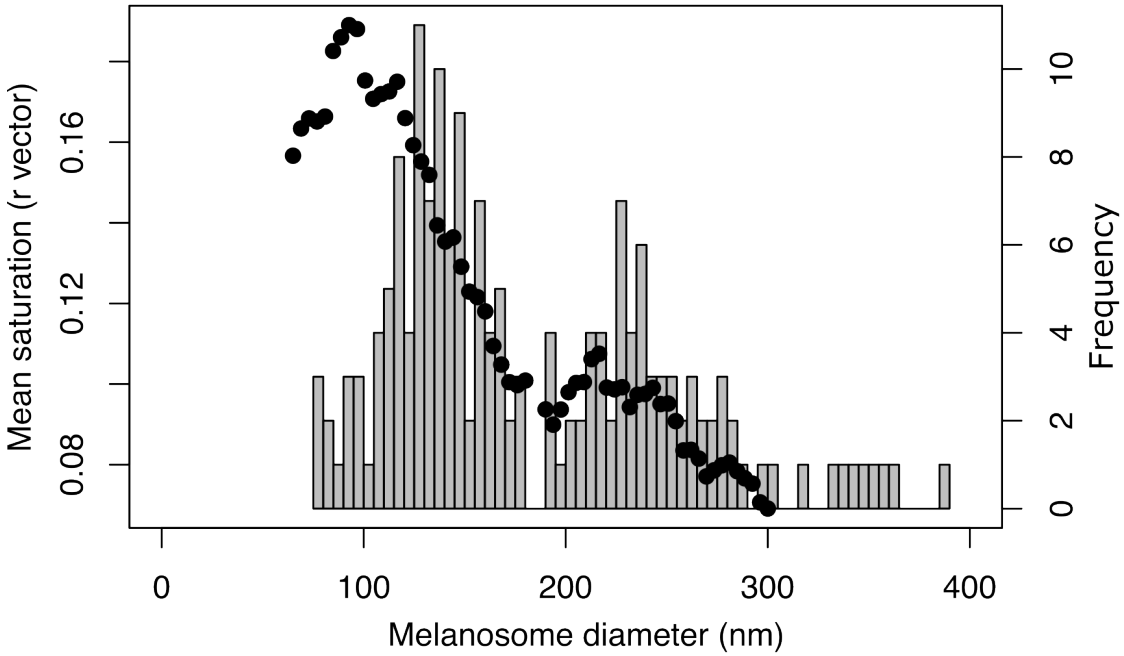

Figure A.2: Color saturation increases for structures with solid rods of diameter $<$190nm. Black dots show the mean saturation of simulated structures with solid rods of varying diameters, as estimated by the optical model. Histogram in the background shows the size distribution of solid rods in iridescent feather structures (data from feather iridescence database). Both the results of the optical model and the distribution of melanosome size in solid rods suggest that there is a shift at approximately 190nm, which we have defined as the dividing line between thin and thick melanin layers. Saturation reaches a maximum for melanin layer thickness of around 100nm, where the optical thickness approximates $\lambda/4$.

A.2 Additional tables

Table A.1: Result of phylogenetic pairwise t-test for difference in melanin layer thickness. P values corrected for multiple comparisons.

	thick solid rod	thin solid rod	hollow rod	solid platelet	hollow platelet	solid rod black feather
thick solid rod	1	0.0015	0.0015	0.0015	0.0015	0.0455
thin solid rod	0.0015	1	0.0015	0.2319	0.0048	0.0015
hollow rod	0.0015	0.0015	1	0.3862	0.5318	0.0015
solid platelet	0.0015	0.2319	0.3862	1	0.1608	0.0015
hollow platelet	0.0015	0.0048	0.5318	0.1608	1	0.0015
solid rod black feather	0.0455	0.0015	0.0015	0.0015	0.0015	1

Table A.2: Phylogenetic signal for traits used in phylogenetic t-tests and ANOVA.

Trait	Pagel's lambda	p
Melanin layer	0.96	$<$0.001
Air (diameter)	0.56	0.001
Number of layers	0.81	$<$0.001

Table A.3: Summary statistics for brightness and saturation of optical model data, subdivided by melanosome type (used in linear models).

Melanosome type	Mean saturation (vs cone)	Mean brightness	Mean peak reflectance (%)
Thick solid rod	0.090	0.054	11.58
Thin solid rod	0.149	0.075	19.93
Hollow rod	0.143	0.097	26.71
Solid platelet	0.187	0.095	25.23
Hollow platelet	0.167	0.224	51.89

Table A.4: Summary statistics for brightness and saturation of plumage data, subdivided by melanosome type (used in Bayesian linear models).

Melanosome type	Mean saturation (vs cone)	Mean brightness	Mean peak reflectance (%)
Thick solid rod	0.093	0.072	9.68
Thin solid rod	0.142	0.119	20.63
Hollow rod	0.159	0.235	38.72
Solid platelet	0.144	0.237	43.23
Hollow platelet	0.194	0.215	35.20

Table A.5: Color diversity and saturation for optical model data using the UVS cone sensitivity function.

Melanosome type	Mean color span	Occupied voxels	Mean saturation
Thick solid rod	0.109	33	0.081
Thin solid rod	0.211	97	0.148
Hollow rod	0.207	100	0.145
Solid platelet	0.262	116	0.192
Hollow platelet	0.247	108	0.179

Table A.6: Color diversity and saturation for plumage data using the UVS cone sensitivity function.

Melanosome type	Mean color span	Occupied voxels	Mean saturation
Thick solid rod	0.154	13	0.132
Thin solid rod	0.225	22	0.163
Hollow rod	0.216	22	0.170
Solid platelet	0.204	25	0.151
Hollow platelet	0.237	24	0.201

Table A.7: Summary of results for linear model of saturation for optical model data. Model: Saturation (r.vec) $\sim$ hollow $+$ thin $+$ platelet $+$ hollow $\cdot$ platelet. Residual standard error: 0.072 on 4495 degrees of freedom. Multiple $R^2 = 0.170$, adjusted $R^2 = 0.169$.

Coefficient	Estimate	Std. Error	t-value
thin	0.059622	0.003392	17.575
hollow	-0.006571	0.003392	-1.937
platelet	0.037834	0.003392	11.152
hollow*platelet	-0.014041	0.004798	-2.927
Intercept	0.089683	0.002399	37.386

Table A.8: Summary of results for linear model of brightness (double cone quantum catch) for optical model data. Model: Log brightness (double cone quantum catch) $\sim$ hollow $+$ thin $+$ platelet $+$ hollow $\cdot$ platelet. Residual standard error: 0.502 on 4495 degrees of freedom. Multiple $R^2 = 0.459$, adjusted $R^2 = 0.459$.

Coefficient	Estimate	Std. Error	t-value
thin	0.22949	0.02368	9.693
hollow	0.28932	0.02368	12.22
platelet	0.20454	0.02368	8.639
hollow·platelet	0.6386	0.03348	19.073
Intercept	-2.97208	0.01674	-177.528

Table A.9: Summary of results for linear model of brightness (peak reflectance) for model data. Model: log brightness (peak reflectance) $\sim$ hollow $+$ thin $+$ platelet $+$ hollow $\cdot$ platelet. Residual standard error: 0.4629 on 4495 degrees of freedom. Multiple $R^2 = 0.540$, adjusted $R^2 = 0.540$.

Coefficient	Estimate	Std. Error	t-value
thin	0.46605	0.02182	21.36
hollow	0.34085	0.02182	15.62
platelet	0.22359	0.02182	10.25
hollow·platelet	0.5059	0.03086	16.39
Intercept	2.38295	0.01543	154.44

Table A.10: Summary of results for Bayesian linear model of saturation for plumage data. Model: saturation (r.vec) $\sim$ hollow $+$ thin $+$ platelet $+$ hollow $\cdot$ platelet $+$ PC.

	post.mean	lower 95% CI	upper 95% CI	pMCMC
(Intercept)	0.0802273	0.0132239	0.148827	0.023
PC	0.0853062	0.0456787	0.1259197	0.00012
hollow	0.0309548	-0.0158424	0.078923	0.19776
platelet	-0.0003642	-0.0571464	0.0548228	0.98715
thin	-0.0022319	-0.0602206	0.0539252	0.93445
hollow:platelet	0.020505	-0.0472965	0.0875612	0.5444

Random effects	post. mean	lower 95% CI	upper 95% CI
phylogeny	0.003508	0.001273	0.006187
patch	0.002388	0.001442	0.003419

	post. mean	lower 95% CI	upper 95% CI
Residual variance	0.001387	0.00104	0.001775

Table A.11: Summary of results for Bayesian linear model of brightness (double cone quantum catch) for plumage data. Model: Log brightness (double cone quantum catch) $\sim$ hollow $+$ thin $+$ platelet $+$ hollow $\cdot$ platelet $+$ PC.

	post.mean	lower 95% CI	upper 95% CI	pMCMC
(Intercept)	-2.76472	-3.36719	-2.15182	<0.00001
PC	0.54649	0.17361	0.90788	0.00613
hollow	0.99645	0.54505	1.44248	<0.00001
platelet	0.69742	0.18471	1.19531	0.00759
thin	-0.30147	-0.83223	0.24127	0.26653
hollow:platelet	-0.52306	-1.14786	0.08163	0.09451

Random effects	post. mean	lower 95% CI	upper 95% CI
phylogeny	0.2626	0.03862	0.5218
patch	0.2403	0.1441	0.3436

	post. mean	lower 95% CI	upper 95% CI
Residual variance	0.07479	0.05483	0.09613

Table A.12: Summary of results for Bayesian linear model of brightness (peak reflectance) for plumage data. Model: Log brightness (peak reflectance) $\sim$ hollow $+$ thin $+$ platelet $+$ hollow $\cdot$ platelet $+$ PC.

	post.mean	lower 95% CI	upper 95% CI	pMCMC
(Intercept)	1.9479	1.3087	2.5866	<0.00001
PC	0.759	0.4074	1.1127	0.00018
hollow	1.1177	0.6987	1.5452	<0.00001
platelet	0.7802	0.2841	1.2764	0.00226
thin	-0.1655	-0.649	0.3212	0.50032
hollow:platelet	-0.7032	-1.3124	-0.12	0.02178

Random effects	post. mean	lower 95% CI	upper 95% CI
phylogeny	0.3539	0.114	0.6246
patch	0.1433	0.07449	0.2185

	post. mean	lower 95% CI	upper 95% CI
Residual variance	0.08233	0.06068	0.1064

B

Appendix for Chapter 3

B.1 Significance of defining iridescence as a change in hue versus peak spectral wavelength with viewing/illumination angle

We have defined iridescence as a shift in peak spectral wavelength with viewing or illumination angle—not as a shift in hue with viewing or illumination angle. This is partly out of convenience, because the former is agnostic to the viewer's visual capabilities, and partly because it is how iridescence is typically measured in the literature.

Would our conclusions differ if we instead measured iridescence as a shift in hue with illumination angle?

Generally, the answer is no, since peak spectral wavelength is a rough approximation of hue if measured within the visual range of the viewer. However, there are two exceptions to this.

Firstly, spectra that have multiple peaks instead of a single main peak will be poorly described by the peak spectral wavelength. Moreover, if the relative heights of multiple peaks in a spectrum change over varying incidence angles, the peak spectral wavelength might not describe the gradual change of a single peak, but jump between different peaks for each angular measurement. In such a situation, we would not expect hue shift to roughly approximate the shift in peak spectral wavelength.

The second exception is spectra with very broad peaks. Multilayer structures that produce broad peaks (broadband reflectors) give rise to silvery or golden appearances, and can be found in for example some beetles (Seago et al., 2009). The broadband reflection arise from variations in the layer thicknesses in the stack, which results in constructive interference at multiple wavelengths (Seago et al., 2009, Parker et al., 1998). Just like any other multilayer reflector, the spectral peak will shift as the angle of light or observations is changed. However, this effect is hardly perceivable, since the reflectance peak is very broad. Thus, the golden Christmas beetle (*Anoplognathus aureus*) appears to a human observer golden just like the metal gold—despite exhibiting a measurable shift in spectral peak location (Ospina-Rozo et al., 2022). Therefore, such broadband reflectors might be considered iridescent if measured as a shift in peak spectral wavelength (or here spectral location, which captures the same property for broad peaks), but

not if measured as a shift in (human) hue.

In §3.3.2, *Iridescence*, we compare the iridescence of plumage with structural barbule and barb coloration by plotting their cumulative shift in peak spectral wavelength over increasing specular angles. Since the spectra we used had well defined, single peaks and were not very broad, we would expect a similar result if we instead had measured hue shift. However, to test this directly we also calculated hue shifts using a bird visual model. We included all species where we had access to the raw spectral data (12 species). Spectra were processed and modeled in a bird visual model using the R package *pavo* (Maia et al., 2013a), (cone sensitivities set as "avg.uv" for all species). Using the relative quantum cone catches from the visual model, we mapped each spectrum to coordinates in a tetrahedral color space, where each vertex represents one cone in the avian eye (Endler & Mielke, 2005, Stoddard & Prum, 2008). The hue shift was then calculated as the (cumulative) change in angle between these points (arising from spectra measured at varying specular angles).

The results (Figure B.1) are comparable to the earlier results for peak spectral wavelength (Figure 3.4B)—structural barbule and structural barb coloration broadly overlap in iridescence. Thus, interpreting iridescence as a hue shift with viewing or observation angle does not change our conclusion.

B.2 Validation of image color calibration

B.3 Specimens imaged with cross-polarization photography

Table B.1: Specimens imaged with cross-polarization photography (all from the Princeton Bird Collection). The reference for each species' plumage color mechanism is listed under "Source".

Species	Cat. no	Color mechanism	Source
Cardinalis cardinalis	16465	carotenoid	Hill & McGraw (2006b, Ch. 5)

Continued on next page

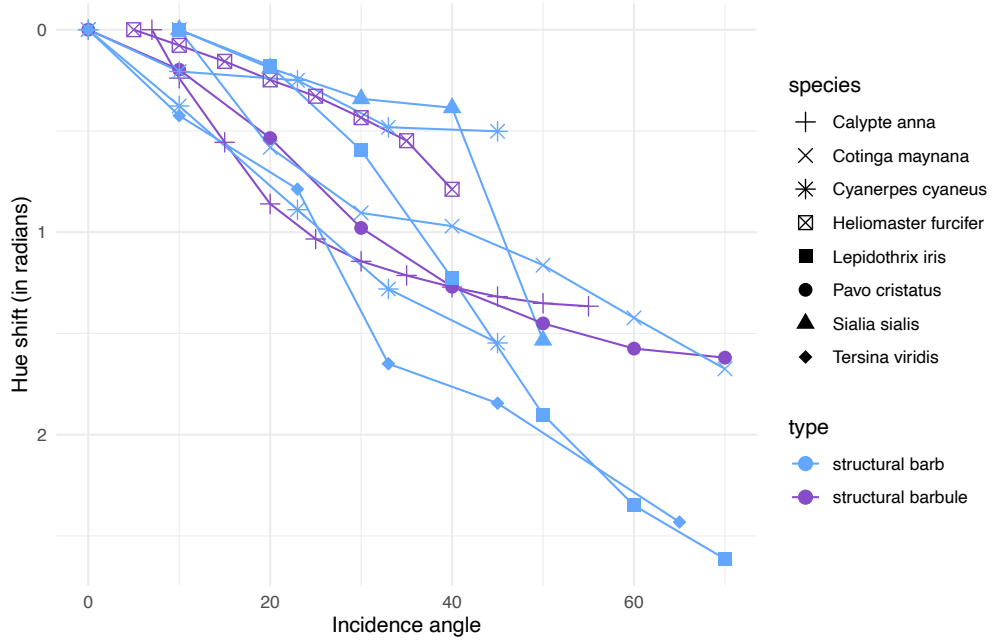

Figure B.1: Hue shift over varying angles (specular configuration) for species with structural barbule coloration (purple), and structural barb coloration (blue). Data from Meadows et al. (2011), Freyer Pascal et al. (2019), Gruson et al. (2019a), Urquia et al. (2020), Skigin et al. (2019), Noh et al. (2010b).

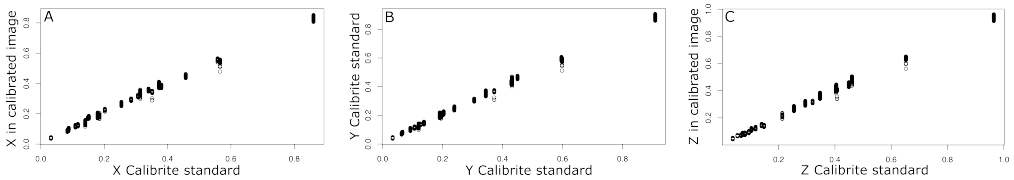

Figure B.1: Calibrated XYZ values for each calibrated image plotted against the published Calibrite XYZ standard values, for X (A), Y (B) and Z (C). All images show good convergence to the standard.

Table B.1: Specimens imaged with cross-polarization photography (all from the Princeton Bird Collection). The reference for each species' plumage color mechanism is listed under "Source". (continued)

Species	Cat. no	Color mechanism	Source
Carduelis tristis	17537	carotenoid	Hill & McGraw (2006b, Ch. 5)
Piranga olivacea	1548	carotenoid	Hill & McGraw (2006b, Ch. 5)
Ramphocelus dimidatus	113047	carotenoid	Hill & McGraw (2006b, Ch. 5)

Continued on next page

Table B.1: Specimens imaged with cross-polarization photography (all from the Princeton Bird Collection). The reference for each species' plumage color mechanism is listed under "Source". (continued)

Species	Cat. no	Color mechanism	Source
Sphyrapicus varius	17251	carotenoid	Hill & McGraw (2006b, Ch. 5)
Callipepla californica	na	melanin	Maia et al. (2011)
Cardelius tristis	17148	melanin	Hill & McGraw (2006b, Ch. 6)
Dolichonyx oryzivorus	15090	melanin	Shawkey et al. (2006)
Gallus gallus	20725	melanin	Hill & McGraw (2006b, Ch. 6)
Hirundo rutstica	1641	melanin	Hill & McGraw (2006b, Ch. 6)
Junco hyemalis	16950	melanin	Personal observation
Sialis sialis	17499	melanin	Hill & McGraw (2006b, Ch. 6)
Sturnella neglecta	3041	melanin	Shawkey et al. (2006)
Ara macao	16047	psittacofulvin	Hill & McGraw (2006b, Ch. 8)
Calyptomena viridis	12300	structural barb	Saranathan et al. (2012)
Chiroxiphia caudata	998	structural barb	Saranathan et al. (2012)
Coracias benghalensis	8499	structural barb	Saranathan et al. (2012)
Cotinga cayana	9972	structural barb	Saranathan et al. (2012)
Cyanocitta cristatus	3266	structural barb	Saranathan et al. (2012)

Continued on next page

Table B.1: Specimens imaged with cross-polarization photography (all from the Princeton Bird Collection). The reference for each species' plumage color mechanism is listed under "Source". (continued)

Species	Cat. no	Color mechanism	Source
Cyanocorax beecheii	13340	structural barb	Saranathan et al. (2012)
Irena puella	10354	structural barb	Saranathan et al. (2012)
Passerina ciris	17421	structural barb	Saranathan et al. (2012)
Sialis sialis	17499	structural barb	Saranathan et al. (2012)
Tersina viridis male	14285	structural barb	Saranathan et al. (2012)
Tersina viridis female	14286	structural barb	Saranathan et al. (2012)
Acridotheres cristatellus	na	structural barbule	Durrer & Villiger (1970a)
Agelaius phoeniceus	3109	structural barbule	Personal observation
Aix sponsa	5305	structural barbule	Eliason et al. (2015)
Anas acuta	9103	structural barbule	Eliason et al. (2015)
Anas americana	4624	structural barbule	Eliason et al. (2015)
Anas bahamensis	9095	structural barbule	Eliason et al. (2015)
Anas crecca	15362	structural barbule	Eliason et al. (2015)
Anas cyanoptera	8935	structural barbule	Eliason et al. (2015)
Anas discors	15368	structural barbule	Eliason et al. (2015)
Anas falcata	15367	structural barbule	Eliason et al. (2015)
Anas formosa	15363	structural barbule	Eliason et al. (2015)
Anas querquedula	9092	structural barbule	Eliason et al. (2015)
Aplonis panayensis	13094	structural barbule	Durrer & Villiger (1970a)

Continued on next page

Table B.1: Specimens imaged with cross-polarization photography (all from the Princeton Bird Collection). The reference for each species' plumage color mechanism is listed under "Source". (continued)

Species	Cat. no	Color mechanism	Source
Butorides virescens	9047	structural barbule	Durrer (1977)
Caloenas nicobarica	17237	structural barbule	Durrer (1977)
Chalcophaps indica	9477	structural barbule	Dyck (1976)
Chlorestes notata	na	structural barbule	Dyck (1976)
Chloroceryle americana	na	structural barbule	Durrer (1977)
Chrysococcyx cupreus	9538	structural barbule	Durrer & Villiger (1970b)
Cicinnurus magnificus	13491	structural barbule	Dorst et al. (1974)
Cicinnurus regius	13491	structural barbule	Durrer (1977)
Colibri coruscans	11881	structural barbule	Nordén et al. (2019)
Collocalia esculenta	na	structural barbule	Durrer (1977)
Columba livia	16994	structural barbule	Durrer (1977)
Coragyps atratus	5205	structural barbule	Personal observation
Corvus brachyrhynchos	4459	structural barbule	Personal observation
Corvus corax	na	structural barbule	Nordén et al. (2019)
Cosmopsaurus regius	13122	structural barbule	Durrer & Villiger (1970a)
Crotophaga major	16105	structural barbule	Nordén et al. (2019)
Epimachus fastuosus	13479	structural barbule	Durrer (1977)
Eugenes fulgens	na	structural barbule	Hu et al. (2018)
Galbula ruficauda	12270	structural barbule	Durrer (1977)

Continued on next page

Table B.1: Specimens imaged with cross-polarization photography (all from the Princeton Bird Collection). The reference for each species' plumage color mechanism is listed under "Source". (continued)

Species	Cat. no	Color mechanism	Source
Gallus gallus	20725	structural barbule	Nordén et al. (2019)
Gracula religiosa	13121	structural barbule	Durrer & Villiger (1970a)
Hemiprocne comata	201919	structural barbule	Durrer (1977)
Hirundo rutstica	1641	structural barbule	Personal observation
Hirundo smithii	101490	structural barbule	Nordén et al. (2019)
Lamprotornis caudatus	13389	structural barbule	Durrer & Villiger (1970a)
Lophorina superba	13468	structural barbule	Durrer (1977)
Lophura ignita	na	structural barbule	Durrer (1977)
Meleagris gallopavo	9237	structural barbule	Durrer (1977)
Mino dumontii	7004	structural barbule	Durrer & Villiger (1970a)
Molothrus aeneus	11169	structural barbule	Shawkey et al. (2006)
Molothrus ater	17953	structural barbule	Shawkey et al. (2006)
Molothrus bonariensis	1632	structural barbule	Shawkey et al. (2006)
Molothrus oryzivorus	16346	structural barbule	Shawkey et al. (2006)
Nectarinia sperata	13858	structural barbule	Durrer (1962)
Onychognathus salvadorii	13115	structural barbule	Durrer & Villiger (1970a)
Paradisaea rubra	13466	structural barbule	Durrer (1977)

Continued on next page

Table B.1: Specimens imaged with cross-polarization photography (all from the Princeton Bird Collection). The reference for each species' plumage color mechanism is listed under "Source". (continued)

Species	Cat. no	Color mechanism	Source
Parotia sefilata	13473	structural barbule	Durrer (1977)
Patagioenas fasciata	15996	structural barbule	Durrer (1977)
Phaenicophaeus curvirostris	na	structural barbule	Nordén et al. (2019)
Pharomachrus mocinno	na	structural barbule	Durrer & Villiger (1966)
Phasianus colchicus	15594	structural barbule	Durrer (1977)
Pica pica	na	structural barbule	Dyck (1976)
Picoides pubescens	3613	structural barbule	Personal observation
Prosthemadera novaeseelandiae	7144	structural barbule	Durrer (1977)
Pycnonotus atriceps	10341	structural barbule	Dyck (1976)
Quiscalus major	16709	structural barbule	Shawkey et al. (2006)
Quiscalus mexicanus	na	structural barbule	Shawkey et al. (2006)
Quiscalus quiscula	16932	structural barbule	Shawkey et al. (2006)
Rollulus rouloul	15865	structural barbule	Durrer (1977)
Sarcops calvus	13111	structural barbule	Durrer & Villiger (1970a)
Sturnus vulgaris	13058	structural barbule	Durrer & Villiger (1970a)
Tachycineta bicolor	17368	structural barbule	Nordén et al. (2019)
Tetrao tetrix	15494	structural barbule	Durrer (1977)

Continued on next page

Table B.1: Specimens imaged with cross-polarization photography (all from the Princeton Bird Collection). The reference for each species' plumage color mechanism is listed under "Source". (continued)

Species	Cat. no	Color mechanism	Source
Trogon collaris	11899	structural barbule	Quintero & Espinosa de los Monteros (2011)
Trogon elegans	23761	structural barbule	Quintero & Espinosa de los Monteros (2011)
Trogon massena	193	structural barbule	Quintero & Espinosa de los Monteros (2011)
Trogon melanocephalus	11896	structural barbule	Quintero & Espinosa de los Monteros (2011)
Trogon melanurus	46	structural barbule	Quintero & Espinosa de los Monteros (2011)
Trogon violaceus	12481	structural barbule	Durrer & Villiger (1966)
Vanellus vanellus	3342	structural barbule	Durrer (1977)
Volatinia jacarina	12493	structural barbule	Maia et al. (2009)
Tauraco hartlaubi	16120	turacoverdin	Hill & McGraw (2006b, Ch. 8)
Columba livia	16994	white	Personal observation
Cyanocitta cristatus	3266	white	Personal observation
Pica pica	na	white	Personal observation

C

Appendix for Chapter 4

C.1 Ancestral state reconstructions

We attempted to model the evolution of metallic luster in Cuculidae using Bayesian inference and continuous-time Markov models, as well as with a maximum likelihood approach. Specifically, we ran 4 different models using BayesTrait (Pagel et al., 2004, Pagel & Meade, 2006), using the mantle patch scores as input data:

1. Markov chain Monte Carlo analysis, all rates variable (MCMC variable), i.e. all character transitions were allowed and could have different rates.

2. Markov chain Monte Carlo analysis, restricted, where transitions had to be sequential (MCMC restricted), i.e. transitions rates $0 \rightarrow 2$ and $2 \rightarrow 0$ were set to 0.

3. Reverse jump Markov chain Monte Carlo (RJMCMC), where the number of parameters to include in the model is determined by the analysis (Pagel & Meade, 2006).

4. Maximum likelihood approach, all rates variable (ML variable).

In all MCMC analyses, priors were set to an exponential distribution with a mean of 10, and run for 1010000 iterations with the first 10000 iterations discarded as burn-in.

These analyses generated transition rates between character states (Table A.1), which we then used to reconstruct ancestral states using simulated stochastic character maps (Bollback, 2006) implemented in the "make.simmap" fucntion in phytools (Revell, 2012).

The results of our analyses were very variable, yet many estimates had similar likelihood values (Table C.1). While the MCMC variable analysis can be discounted due to the lower likelihood values and unrealistically high transition rates, the other analyses had similar likelihood values, yet resulted in drastically different ancestral state reconstructions (Table C.1, Figure C.1). For example, two different solutions in the RJMCMC analysis with similar likelihood suggest that Cuculidae was either state "2" at the root, and this state has subsequently been lost in every single clade (transitions to "2" is 0, Table C.1, Figure C.1C)—or state "2" was independently gained in every single species of *Chrysococcyx* (transitions to "2" is unrealistically high, Table C.1, Figure C.1D). The MCMC restricted and the ML analysis give somewhat

more evolutionary plausible results, but the likelihood of these analyses are very similar to that of the RJMCMC runs (note also that the higher number of free parameters in the ML analysis is expected to increase likelihood). Thus, it is not possible on the basis of these analysis to identify a single set of well-supported transition rates. Of course, we can use our knowledge of how metallic luster is likely to have evolved in Cuculidae (e.g. based on phylogenetic bracketing), and pick the transition rates that are most consistent with our reasoning—but this approach would not test the evolution of this trait in an unbiased way (which is our goal). With the number of parameters in these models, any evolutionary scenario could be reconstructed with enough modifications.

We conclude that the evolution of metallic luster in plumage is not well modeled by a Markov process (transition rates may not be equal across the tree, see similar issue documented by Wiens et al., 2007), and/or our data set is too small to achieve robust results.

Model	log Lh	$0 \rightarrow 1$	$0 \rightarrow 2$	$1 \rightarrow 0$	$1 \rightarrow 2$	$2 \rightarrow 0$	$2 \rightarrow 1$
MCMC var	-103.0	0.3078	0.1202	0.3781	1.851	2.771	21.06
	-103.1	11.04	1.878	15.20	1.714	10.63	32.83
MCMC res	-84.76	0.02396	0	0.03461	0.007663	0	0.1014
	-87.74	0.02416	0	0.03082	0.6918	0	7.307
RJMCMC	-85.90	0.02806	0	0.02806	0	0.02806	0.02806
	-86.13	0.01667	0	0.01667	0.01667	0.01667	0.01667
ML	-84.15	0.02147	0.001531	0.03199	0.001347	0.000	0.06087

Model	p (root 0)	p (root 1)	p (root 2)
MCMC var	0.3333	0.3333	0.3333
	0.3333	0.3333	0.3333
MCMC res	0.3017	0.3449	0.3534
	0.3489	0.3256	0.3255
RJMCMC	0.000105	0.000084	0.9998
	0.7823	0.1397	0.07799
ML	0.3544	0.3770	0.2686

Table C.1: Transition rates and root posterior probabilities for characters "0" (no metallic luster), "1" (faint-moderate metallic luster) and "2" (intense metallic luster) in Cuculidae (mantle patch), found using four different models. To demonstrate that the model runs did not find a single solution, we have included two solutions (iterations in the chain) for each MCMC model, which have similar likelihood but very different transition rates. log Lh denotes log likelihood. Model abbreviations: MCMC var, Markov chain Monte Carlo model with variable rates; MCMC res, Markov chain Monte Carlo model with rates $0 \rightarrow 2$ and $2 \rightarrow 0$ set to 0; RJMCMC, reverse jump Markov chain Monte Carlo model; ML, maximum likelihood. See text for further explanation of models.

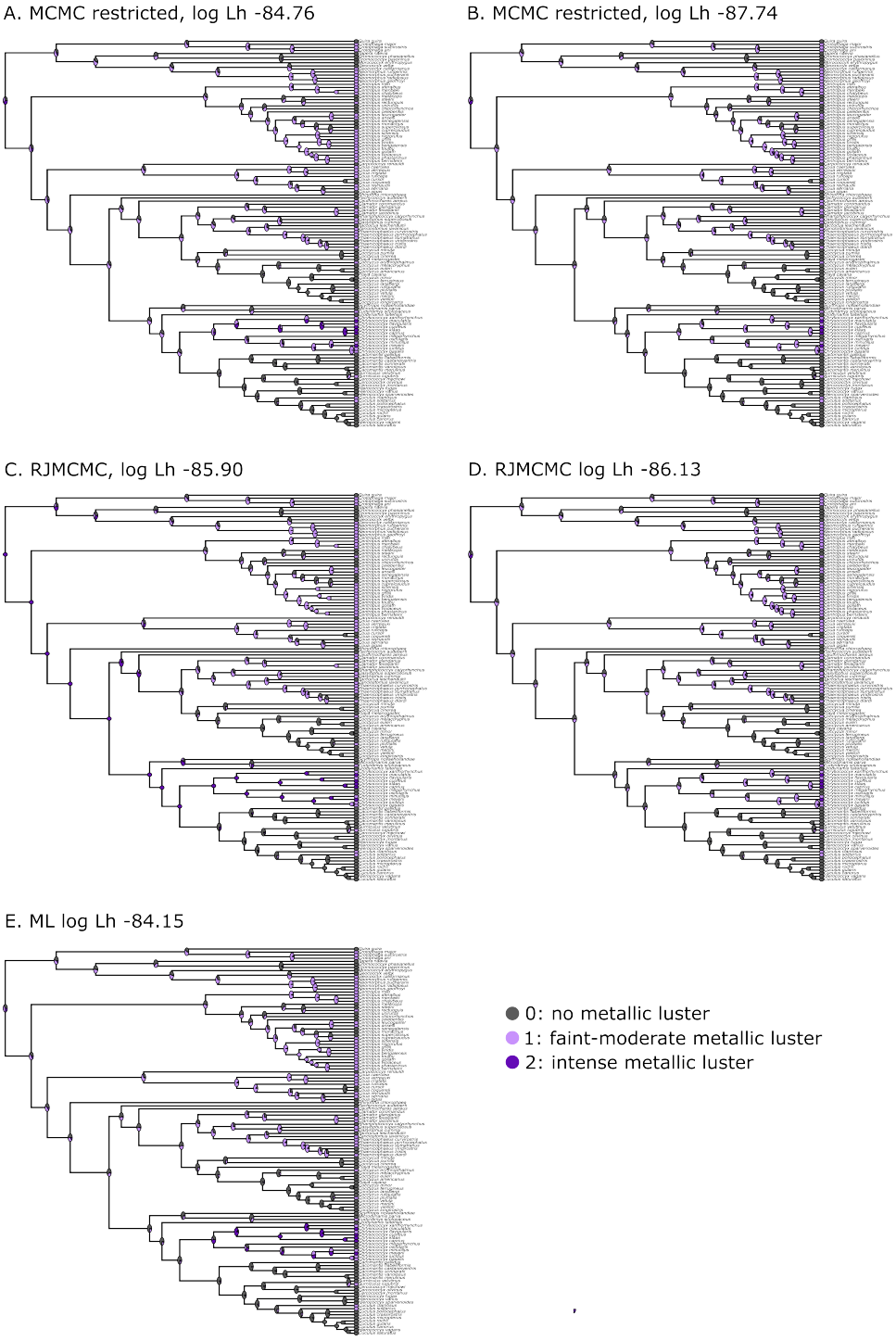

Figure C.1: Ancestral state reconstructions of metallic luster in Cuculidae (mantle patch) using different transition rates extracted from the models (Table C.1). The pie charts at the nodes represent the percentage of iterations that a node was reconstructed as a particular character state in the stochastic character mapping. Note that the RJMCMC model presents two extreme but quite unlikely scenarios, which nevertheless have a similar likelihood values to the ML and MCMC restricted analysis.

C.2 Specimens sampled and imaged with cross-polarization photography

Table C.2: Specimens sampled and/or photographed for the study.

Species	Cat. no	Institution[1]	Photography	Feather sample
Chrysococcyx meyeri	132128	ANSP	mantle	mantle
Chrysococcyx basilis	189621	ANSP	mantle	mantle
Chysococcyx klaas	108663	ANSP	mantle	mantle
Cuculus gularis	166403	ANSP	mantle	mantle
Cuculus clamosus	94471	ANSP	mantle	mantle
Scythrops novaehollandiae	140492	ANSP	mantle	mantle
Chrysococcyx osculans	190450	ANSP	mantle	mantle
Chrysococcyx caprius	50262	ANSP	mantle	na
Chrysococcyx lucidus	10905	ANSP	mantle	na
Chrysococcyx xanthorhynchus	39150	ANSP	mantle	unknown
Chrysococcyx maculatus	82777	ANSP	mantle	na
Guira guira	793721	AMNH	mantle	mantle
Coccycua pumila	75431	AMNH	mantle	mantle
Chrysococcyx flavigularis	159104	AMNH	mantle	mantle
Surniculus lugubris	782046	AMNH	mantle	mantle
Coua cursor	411666	AMNH	mantle	mantle
Centropus celebensis	628178	AMNH	mantle	mantle
Cacaomantis variolusus	625755	AMNH	mantle	mantle
Coccyzus vetula	475694	AMNH	mantle	mantle

Continued on next page

Table C.2: Specimens sampled and/or photographed for the study. (continued)

Species	Cat. no	Institution[1]	Photography	Feather sample
Geococcyx californianus	27286	ANSP	mantle	mantle
Coua cristata	50322	ANSP	mantle	mantle
Coua caeruela	50319	ANSP	mantle	mantle
Coua caeruela	50319	ANSP	tail	na
Neomorphus geoffroyi	103874	ANSP	mantle	mantle
Phaenicophaeus diardi	20256	ANSP	belly	belly
Phaenicophaeus diardi	20256	ANSP	mantle	na

[1] Institutional abbreviations: ANSP, The Academy of Natural Sciences of Drexel, Philadelphia, USA; AMNH, The American Museum of Natural History, New York City, USA.

C.3 Validation of image analysis method to estimate melanosome diameters

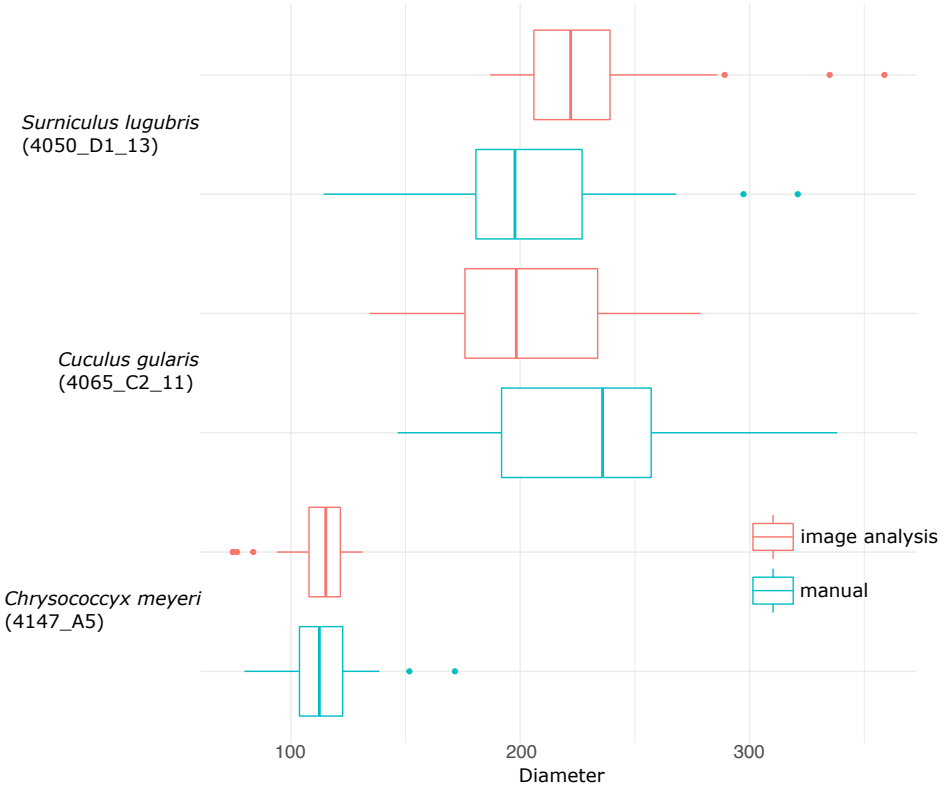

Figure C.2: Comparison of melanosome diameter measurements using the semi-automated image analysis method (red) and manual measuring by hand using ImageJ (blue), for three TEM images (each from a different species). The code under species names identifies the specific sample and image measured.

Bibliography

Abrams, R. A. & Christ, S. E. (2003). Motion onset captures attention. *Psychological science*, 14(5), 427–432.

Abràmoff, M. D., Magalhães, P. J., & Ram, S. J. (2004). Image processing with imageJ. *Biophotonics International*, 11(7), 36–41.

Adams, W. J., Kerrigan, I. S., & Graf, E. W. (2016). Touch influences perceived gloss. *Scientific Reports*, 6(1), 21866.

Aguillon, S. M., Walsh, J., & Lovette, I. J. (2021). Extensive hybridization reveals multiple coloration genes underlying a complex plumage phenotype. *Proceedings of the Royal Society B: Biological Sciences*, 288(1943), 20201805.

Akkaynak, D., Treibitz, T., Xiao, B., Gürkan, U. A., Allen, J. J., Demirci, U., & Hanlon, R. T. (2014). Use of commercial off-the-shelf digital cameras for scientific data acquisition and scene-specific color calibration. *JOSA A*, 31(2), 312–321.

Allaby, M., Ed. (2013). *A dictionary of geology and earth sciences*. Oxford paperback reference. Oxford: Oxford University Press, fourth edition edition.

Alley, L. M., Schmid, A. C., & Doerschner, K. (2020). Expectations affect the perception of material properties. *Journal of Vision*, 20(12), 1–1.

Ameijeiras-Alonso, J., Crujeiras, R. M., & Rodríguez-Casal, A. (2018). Multimode: An R Package for Mode Assessment. *Preprint: arXiv*, 1803.00472.

Andersson, S. & Prager, M. (2006). Quantifying colors. In G. E. Hill & K. J. McGraw (Eds.), *Bird Coloration Vol. I: Mechanisms and Measurements* (pp. 90–147). Cambridge, MA: Harvard University Press.

Auber, L. (1957). The distribution of structural colours and unusual pigments in the class Aves. *Ibis*, 99(3), 463–476.

Babarović, F., Puttick, M. N., Zaher, M., Learmonth, E., Gallimore, E.-J., Smithwick, F. M., Mayr, G., & Vinther, J. (2019). Characterization of melanosomes involved in the production of non-iridescent structural feather colours and their detection in the fossil record. *Journal of The Royal Society Interface*, 16(155), 20180921.

Bancroft, W. D. & Allen, R. (1924). Metallic luster. II. *The Journal of Physical Chemistry*, 29(5), 564–586.

Beltrán, D. F., Shultz, A. J., & Parra, J. L. (2021). Speciation rates are positively correlated with the rate of plumage color evolution in hummingbirds. *Evolution*, 75(7), 1665–1680.

Billerman, S. M., Keeney, B. K., Rodewald, P. G., & Schulenberg, T. S. (2022). *Birds of the World*. New York, USA: Cornell Lab of Ornithology.

Bitton, P.-P., O'Brien, E. L., & Dawson, R. D. (2007). Plumage brightness and age predict extrapair fertilization success of male tree swallows, Tachycineta bicolor. *Animal Behaviour*, 74(6), 1777–1784.

Blount, Z. D., Lenski, R. E., & Losos, J. B. (2018). Contingency and determinism in evolution: Replaying life's tape. *Science*, 362(6415), eaam5979.

Bollback, J. P. (2006). SIMMAP: Stochastic character mapping of discrete traits on phylogenies. *BMC Bioinformatics*, 7(1), 88.

Braun, J. H. & Braun, S. W. (1995). Speculations about the value of gloss. *Color Research & Application*, 20(6), 397–398.

Brink, D. J. & van der Berg, N. G. (2004). Structural colours from the feathers of the bird Bostrychia hagedash. *Journal of Physics D: Applied Physics*, 37(5), 813–818.

Brodie, J., Ingham, C. J., & Vignolini, S. (2021). Does Structural Color Exist in True Fungi? *Journal of Fungi*, 7(2), 141.

Burtt Jr., E. H. (1979). Tips on wings and other things. In E. H. Burtt Jr. (Ed.), *The behavioral significance of colour* (pp. 75–125). New York: Garland STPM Press.

Chadwick, A. C. & Kentridge, R. W. (2015). The perception of gloss: A review. *Vision Research*, 109, 221–235.

Community, B. O. (2022). Blender - a 3D modelling and rendering package.

Cooney, C. R., Varley, Z. K., Nouri, L. O., Moody, C. J. A., Jardine, M. D., & Thomas, G. H. (2019). Sexual selection predicts the rate and direction of colour divergence in a large avian radiation. *Nature Communications*, 10(1), 1773.

Coss, R. G. (1990). All that Glistens: Water Connotations in Surface Finishes. *Ecological Psychology*, 2(4), 367–380.

Coss, R. G., Ruff, S., & Simms, T. (2003). All That Glistens: II. The Effects of Reflective Surface Finishes on the Mouthing Activity of Infants and Toddlers. *Ecological Psychology*, 15(3), 197–213.

Craig, A. J. F. K. & Hartley, A. H. (1985). The Arrangement and Structure of Feather Melanin Granules as a Taxonomic Character in African Starlings (Sturnidae). *The Auk*, 102(3), 629–632.

Cuthill, I. C., Allen, W. L., Arbuckle, K., Caspers, B., Chaplin, G., Hauber, M. E., Hill, G. E., Jablonski, N. G., Jiggins, C. D., Kelber, A., Mappes, J., Marshall, J., Merrill, R., Osorio, D., Prum, R., Roberts, N. W., Roulin, A., Rowland, H. M., Sherratt, T. N., Skelhorn, J., Speed,

M. P., Stevens, M., Stoddard, M. C., Stuart-Fox, D., Talas, L., Tibbetts, E., & Caro, T. (2017). The biology of color. *Science*, 357(6350).

Dakin, R. & Montgomerie, R. (2013). Eye for an eyespot: how iridescent plumage ocelli influence peacock mating success. *Behavioral Ecology*, 24(5), 1048–1057.

Dale, J., Dey, C. J., Delhey, K., Kempenaers, B., & Valcu, M. (2015). The effects of life history and sexual selection on male and female plumage colouration. *Nature*, 527(7578), 367–370.

Delhey, K. (2015). The colour of an avifauna: A quantitative analysis of the colour of Australian birds. *Scientific Reports*, 5.

Desjardins, E. (2011). Historicity and experimental evolution. *Biology & Philosophy*, 26(3), 339–364.

Dorst, J., Gastaldi, G., Hagege, R., & Jacquemart, J. (1974). Différents aspects des barbules de quelques Paradisaeidés sur coupes en microscopie électronique. *Comptes Rendus de l'Academie des Sciences Paris*, 278, 285–290.

Doucet, S. M. (2006). Iridescent plumage in satin bowerbirds: structure, mechanisms and nanostructural predictors of individual variation in colour. *Journal of Experimental Biology*, 209(2), 380–390.

Doucet, S. M. & Meadows, M. G. (2009). Iridescence : a functional perspective. *Journal of The Royal Society Interface*, 6, S115–S132.

Driskell, A. C., Prum, R. O., & Pruett-Jones, S. (2010). The evolution of black plumage from blue in Australian fairy-wrens (Maluridae): Genetic and structural evidence. *Journal of Avian Biology*, 41(5), 505–514.

Drummond, A. J., Suchard, M. A., Xie, D., & Rambaut, A. (2012). Bayesian phylogenetics with BEAUti and the BEAST 1.7. *Molecular Biology and Evolution*, 29(8), 1969–1973.

Ducrest, A.-L., Keller, L., & Roulin, A. (2008). Pleiotropy in the melanocortin system, coloration and behavioural syndromes. *Trends in Ecology & Evolution*, 23(9), 502–510.

Durrer, H. (1962). Schillerfarben beim Pfau (Pavo cristatus L.). *Verhandlungen der Naturforschenden Gesellschaft in Basel*, 73(1), 204–224.

Durrer, H. (1977). *Schillerfarben der Vogelfeder als Evolutionsproblem*. PhD Thesis, University of Basel.

Durrer, H. & Villiger, W. (1966). Schillerfarben der Trogoniden. *Journal für Ornithologie*, 107(1), 1–26.

Durrer, H. & Villiger, W. (1970a). Schillerfarben der Stare (Sturnidae). *Journal für Ornithologie*, 111(2), 133–153.

Durrer, H. & Villiger, W. (1970b). Schillerradien des goldkuckucks (Chrysococcyx cupreus (Shaw)) im elektronenmikroskop. *Zeitschrift für Zellforschung und Mikroskopische Anatomie*, 109(3), 407–413.

Dyck, J. (1976). Structural colours. *Proceedings of the International Ornithological Congress*, 16, 426–437.

D'Alba, L., Kieffer, L., & Shawkey, M. D. (2012). Relative contributions of pigments and biophotonic nanostructures to natural color production: a case study in budgerigar (Melopsittacus undulatus) feathers. *Journal of Experimental Biology*, 215(8), 1272–1277.

D'Alba, L. & Shawkey, M. D. (2019). Melanosomes: Biogenesis, Properties, and Evolution of an Ancient Organelle. *Physiological Reviews*, 99(1), 1–19.

Eliason, C. M., Bitton, P.-P., & Shawkey, M. D. (2013). How hollow melanosomes affect iridescent colour production in birds. *Proceedings of the Royal Society B: Biological Sciences*, 280(1767), 20131505.

Eliason, C. M., Maia, R., Parra, J. L., & Shawkey, M. D. (2020). Signal evolution and morphological complexity in hummingbirds (Aves: Trochilidae). *Evolution*, 74(2), 447–458.

Eliason, C. M., Maia, R., & Shawkey, M. D. (2015). Modular color evolution facilitated by a complex nanostructure in birds. *Evolution*, 69(2), 357–367.

Eliason, C. M. & Shawkey, M. D. (2011). Decreased hydrophobicity of iridescent feathers: a potential cost of shiny plumage. *Journal of Experimental Biology*, 214(13), 2157–2163.

Eliason, C. M. & Shawkey, M. D. (2012). A photonic heterostructure produces diverse iridescent colours in duck wing patches. *Journal of The Royal Society Interface*, 9(74), 2279–2289.

Eluwawalage, D. (2015). Exotic fauna and flora: fashion trends in the nineteenth century. *International Journal of Fashion Design, Technology and Education*, 8(3), 243–250.

Endler, J. A. (1992). Signals, signal conditions, and the direction of evolution. *The American Naturalist*, 139, S125–S153.

Endler, J. A. & Mielke, P. W. (2005). Comparing entire colour patterns as birds see them. *Biological Journal of the Linnean Society*, 86(4), 405–431.

Fan, M., D'alba, L., Shawkey, M. D., Peters, A., & Delhey, K. (2019). Multiple components of feather microstructure contribute to structural plumage colour diversity in fairy-wrens. *Biological Journal of the Linnean Society*, 128(3), 550–568.

Finet, C. (2023). Light as matter: natural structural colour in art. *Humanities and Social Sciences Communications*, 10(1), 1–14.

Fisher, N. I. & Marron, J. S. (2001). Mode testing via the excess mass estimate. *Biometrika*, 88(2), 499–517.

Fleming, R. W. (2017). Material Perception. *Annual Review of Vision Science*, 3(1), 365–388.

Franconeri, S. L. & Simons, D. J. (2003). Moving and looming stimuli capture attention. *Perception & Psychophysics*, 65(7), 999–1010.

Franconeri, S. L. & Simons, D. J. (2005). The dynamic events that capture visual attention: A reply to Abrams and Christ (2005). *Perception & psychophysics*, 67(6), 962–966.

Franklin, A. M. & Ospina-Rozo, L. (2021). Gloss. *Current Biology*, 31(4), R172–R173.

Franklin, A. M., Rankin, K. J., Ospina Rozo, L., Medina, I., Garcia, J. E., Ng, L., Dong, C., Wang, L.-Y., Aulsebrook, A. E., & Stuart-Fox, D. (2022). Cracks in the mirror hypothesis: High specularity does not reduce detection or predation risk. *Functional Ecology*, 36(1), 239–248.

Freyer Pascal, Wilts Bodo D., & Stavenga Doekele G. (2019). Reflections on iridescent neck and breast feathers of the peacock, Pavo cristatus. *Interface Focus*, 9(1), 20180043.

Gadow, H. (1882). On the Colour of Feathers as affected by their Structure. *Proceedings of the Zoological Society of London.*, 50(3), 409 – 422.

Gammie, K. K. (2013). *The evolution of iridescent plumage in the Galliformes: Proximate mechanisms and ultimate functions*. PhD Thesis, University of Windsor.

Gao, G., Xu, M., Bai, C., Yang, Y., Li, G., Xu, J., Wei, Z., Min, J., Su, G., Zhou, X., Guo, J., Hao, Y., Zhang, G., Yang, X., Xu, X., Widelitz, R. B., Chuong, C.-M., Zhang, C., Yin, J., & Zuo, Y. (2018). Comparative genomics and transcriptomics of Chrysolophus provide insights into the evolution of complex plumage coloration. *GigaScience*, 7(10), giy113.

Garland, Jr., T., Dickerman, A. W., Janis, C. M., & Jones, J. A. (1993). Phylogenetic Analysis of Covariance by Computer Simulation. *Systematic Biology*, 42(3), 265–292.

Ged, G., Obein, G., Silvestri, Z., Le Rohellec, J., & Viénot, F. (2010). Recognizing real materials from their glossy appearance. *Journal of Vision*, 10(9), 18–18.

Ginneken, B. v., Stavridi, M., & Koenderink, J. J. (1998). Diffuse and Specular Reflectance from Rough Surfaces. *Appl. Opt.*, 37(1), 130–139.

Goldsmith, T. H. (1990). Optimization, Constraint, and History in the Evolution of Eyes. *The Quarterly Review of Biology*, 65(3), 281–322.

Goldstein, G., Flory, K. R., Browne, B. A., Majid, S., Ichida, J. M., & Burtt Jr., E. H. (2004). Bacterial Degradation of Black and White Feathers. *The Auk*, 121(3), 656–659.

Gomez, D. & Théry, M. (2004). Influence of ambient light on the evolution of colour signals: Comparative analysis of a Neotropical rainforest bird community. *Ecology Letters*, 7(4), 279–284.

Greenewalt, C. H., Brandt, W., & Friel, D. D. (1960). Iridescent Colors of Hummingbird Feathers. *Journal of the Optical Society of America*, 50(10), 1005–1013.

Gruson, H., Andraud, C., Daney de Marcillac, W., Berthier, S., Elias, M., & Gomez, D. (2019a). Quantitative characterization of iridescent colours in biological studies: a novel method using optical theory. *Interface Focus*, 9(1), 20180049.

Gruson, H., Elias, M., Andraud, C., Djediat, C., Berthier, S., Doutrelant, C., & Gomez, D. (2019b). Hummingbird iridescence: an unsuspected structural diversity influences colouration at multiple scales. *Preprint: bioRxiv*, 10.1101/699744.

Hackett, S. J., Kimball, R. T., Reddy, S., Bowie, R. C. K., Braun, E. L., Braun, M. J., Chojnowski, J. L., Cox, W. A., Han, K.-L., Harshman, J., Huddleston, C. J., Marks, B. D., Miglia, K. J., Moore, W. S., Sheldon, F. H., Steadman, D. W., Witt, C. C., & Yuri, T. (2008). A Phylogenomic Study of Birds Reveals Their Evolutionary History. *Science*, 320(5884), 1763–1768.

Hadfield, D. J. (2010). MCMC Methods for Multi-Response Generalized Linear Mixed Models: The MCMCglmm R Package. *Journal of Statistical Software*, 33(2), 1–22.

Haecker, V. (1890). Ueber die Farben der Vogelfedern. *Archiv für mikroskopische Anatomie*, 35, 68–87.

Hart, N. S. (2001). The Visual Ecology of Avian Photoreceptors. *Progress in Retinal and Eye Research*, 20(5), 675–703.

Harvey, T. A., Bostwick, K. S., & Marschner, S. (2013). Directional reflectance and milli-scale feather morphology of the African Emerald Cuckoo, Chrysococcyx cupreus. *Journal of The Royal Society Interface*, 10(86), 20130391.

Heinrich, B. (1995). Neophilia and exploration in juvenile common ravens, Corvus corax. *Animal Behaviour*, 50(3), 695–704.

Hellström, A. R., Watt, B., Fard, S. S., Tenza, D., Mannström, P., Narfström, K., Ekesten, B., Ito, S., Wakamatsu, K., Larsson, J., Ulfendahl, M., Kullander, K., Raposo, G., Kerje, S., Hallböök, F., Marks, M. S., & Andersson, L. (2011). Inactivation of Pmel Alters Melanosome Shape But Has Only a Subtle Effect on Visible Pigmentation. *PLOS Genetics*, 7(9), e1002285.

Hill, G. E., Doucet, S. M., & Buchholz, R. (2005). The effect of coccidial infection on iridescent plumage coloration in wild turkeys. *Animal Behaviour*, 69(2), 387–394.

Hill, G. E. & McGraw, K. J., Eds. (2006a). *Bird coloration*, volume II. Cambridge, Mass: Harvard University Press.

Hill, G. E. & McGraw, K. J., Eds. (2006b). *Bird coloration*, volume I. Cambridge, MA: Harvard University Press.

Hooke, R. (1665). *Micrographia and Some Physiological Descriptions of Minute Bodies Made by Magnifying Glasses with Observations and Inquiries thereupon*. New York: Dover.

Hu, D., Clarke, J. A., Eliason, C. M., Qiu, R., Li, Q., Shawkey, M. D., Zhao, C., D'Alba, L., Jiang, J., & Xu, X. (2018). A bony-crested Jurassic dinosaur with evidence of iridescent plumage highlights complexity in early paravian evolution. *Nature Communications*, 9(217).

Hudon, J., Wiebe, K. L., Pini, E., & Stradi, R. (2015). Plumage pigment differences underlying the yellow-red differentiation in the Northern Flicker (Colaptes auratus). *Comparative Biochemistry and Physiology Part B: Biochemistry and Molecular Biology*, 183, 1–10.

Hwang, V., Stephenson, A. B., Barkley, S., Brandt, S., Xiao, M., Aizenberg, J., & Manoharan, V. N. (2021). Designing angle-independent structural colors using Monte Carlo simulations of multiple scattering. *Proceedings of the National Academy of Sciences*, 118(4), e2015551118.

Hwang, V., Stephenson, A. B., Magkiriadou, S., Park, J.-G., & Manoharan, V. N. (2020). Effects of multiple scattering on angle-independent structural color in disordered colloidal materials. *Physical Review E*, 101(1), 012614.

Igic, B., D'Alba, L., & Shawkey, M. D. (2018). Fifty shades of white: how white feather brightness differs among species. *The Science of Nature*, 105(3), 18.

Iskandar, J.-P., Eliason, C. M., Astrop, T., Igic, B., Maia, R., & Shawkey, M. D. (2016). Morphological basis of glossy red plumage colours. *Biological Journal of the Linnean Society*, 119(2), 477–487.

Jacobs, I. F., Osvath, M., Osvath, H., Mioduszewska, B., von Bayern, A. M. P., & Kacelnik, A. (2014). Object caching in corvids: Incidence and significance. *Behavioural Processes*, 102, 25–32.

Jetz, W., Thomas, G. H., Joy, J. B., Hartmann, K., & Mooers, A. O. (2012). The global diversity of birds in space and time. *Nature*, 491(7424), 444–448.

Jitsumori, M. & Delius, J. D. (2001). Object Recognition and Object Categorization in Animals. In T. Matsuzawa (Ed.), *Primate Origins of Human Cognition and Behavior* (pp. 269–293). Tokyo: Springer Japan.

Joannopoulos, J. D., Johnson, S. G., Winn, J. N., & Meade, R. D. (2008). *Photonic Crystals: Molding the Flow of Light*. Singapore: Princeton University Press, 2 edition.

Jones, C. D. & Osorio, D. (2004). Discrimination of oriented visual textures by poultry chicks. *Vision Research*, 44(1), 83–89.

Justyn, N. M. & Weaver, R. J. (2023). Painting the Bunting: Carotenoids and structural elements combine to produce the feather coloration of the male Painted Bunting. *Ornithology*, 140(1), ukac052.

Jäkel, F., Singh, M., Wichmann, F. A., & Herzog, M. H. (2016). An overview of quantitative approaches in Gestalt perception. *Vision Research*, 126, 3–8.

Kinoshita, S. (2008). *Structural Colors in the Realm of Nature*. Singapore: World Scientific Publishing.

Kinoshita, S., Yoshioka, S., & Miyazaki, J. (2008). Physics of structural colors. *Reports on Progress in Physics*, 71(7), 076401.

Komatsu, H., Nishio, A., Okazawa, G., & Goda, N. (2013). Computational Color Imaging. In S. Tominaga, R. Schettini, & A. Trémeau (Eds.), *'Yellow' or 'Gold'?: Neural Processing of Gloss Information* (pp. 1–12). Berlin, Heidelberg: Springer.

Kritsky, G. (1991). Beetle Gods of Ancient Egypt. *American Entomologist*, 37(2), 85–89.

Land, M. F. (1972). The physics and biology of animal reflectors. *Progress in Biophysics and Molecular Biology*, 24, 75–106.

Lee, E., Miyazaki, J., Yoshioka, S., Lee, H., & Sugita, S. (2012). The weak iridescent feather color in the Jungle Crow (Corvus macrorhynchos). *Ornithological Science*, 11(1), 59–64.

Li, J., Bed'hom, B., Marthey, S., Valade, M., Dureux, A., Moroldo, M., Péchoux, C., Coville, J.-L., Gourichon, D., Vieaud, A., Dorshorst, B., Andersson, L., & Tixier-Boichard, M. (2019). A missense mutation in TYRP1 causes the chocolate plumage color in chicken and alters melanosome structure. *Pigment Cell & Melanoma Research*, 32(3), 381–390.

Li, Q., Clarke, J. A., Gao, K.-Q., Zhou, C.-F., Meng, Q., Li, D., D'Alba, L., & Shawkey, M. D. (2014). Melanosome evolution indicates a key physiological shift within feathered dinosaurs. *Nature*, 507(7492), 350–353.

Li, Q., Gao, K.-Q., Meng, Q., Clarke, J. A., Shawkey, M. D., D'Alba, L., Pei, R., Ellison, M., Norell, M. A., & Vinther, J. (2012). Reconstruction of Microraptor and the evolution of iridescent plumage. *Science*, 335(6073), 1215–1219.

Li, Q., Gao, K.-Q., Vinther, J., Shawkey, M. D., Clarke, J. A., D'Alba, L., Meng, Q., Briggs, D. E. G., & Prum, R. O. (2010). Plumage color patterns of an extinct dinosaur. *Science*, 327(5971), 1369–1372.

Ligon, R. A., Diaz, C. D., Morano, J. L., Troscianko, J., Stevens, M., Moskeland, A., Laman, T. G., & Iii, E. S. (2018). Evolution of correlated complexity in the radically different courtship signals of birds-of-paradise. *PLOS Biology*, 16(11), e2006962.

Loyau, A., Gomez, D., Moureau, B., Théry, M., Hart, N. S., Jalme, M. S., Bennett, A. T. D., & Sorci, G. (2007). Iridescent structurally based coloration of eyespots correlates with mating success in the peacock. *Behavioral Ecology*, 18(6), 1123–1131.

M. Hofmann, C., J. McGraw, K., W. Cronin, T., & E. Omland, K. (2007). Melanin coloration in New World orioles I: carotenoid masking and pigment dichromatism in the orchard oriole complex. *Journal of Avian Biology*, 38(2), 163–171.

Magkiriadou, S., Park, J.-G., Kim, Y.-S., & Manoharan, V. N. (2014). Absence of red structural color in photonic glasses, bird feathers, and certain beetles. *Phys. Rev. E*, 90(6), 062302.

Maia, R., Caetano, J. V. O., Bao, S. N., & Macedo, R. H. (2009). Iridescent structural colour production in male blue-black grassquit feather barbules: the role of keratin and melanin. *Journal of The Royal Society Interface*, 6, S203–S211.

Maia, R., D'Alba, L., & Shawkey, M. D. (2011). What makes a feather shine? A nanostructural basis for glossy black colours in feathers. *Proceedings of the Royal Society B: Biological Sciences*, 278(1714), 1973–1980.

Maia, R., Eliason, C. M., Bitton, P. P., Doucet, S. M., & Shawkey, M. D. (2013a). pavo: An R package for the analysis, visualization and organization of spectral data. *Methods in Ecology and Evolution*, 4(10), 906–913.

Maia, R., Macedo, R. H. F., & Shawkey, M. D. (2012). Nanostructural self-assembly of iridescent feather barbules through depletion attraction of melanosomes during keratinization. *Journal of The Royal Society Interface*, 9(69), 734–743.

Maia, R., Rubenstein, D. R., & Shawkey, M. D. (2013b). Key ornamental innovations facilitate diversification in an avian radiation. *Proceedings of the National Academy of Sciences*, 110(26), 10687–10692.

Marcondes, R. S. & Brumfield, R. T. (2019). Fifty shades of brown: Macroevolution of plumage brightness in the Furnariida, a large clade of drab Neotropical passerines. *Evolution*, 73(4), 704–719.

Martínez–Meyer, E., Townsend Peterson, A., & Navarro–Sigüenza, A. G. (2004). Evolution of seasonal ecological niches in the *Passerina* buntings (Aves: Cardinalidae). *Proceedings of the Royal Society of London. Series B: Biological Sciences*, 271(1544), 1151–1157.

Mason, N. A., Riddell, E. A., Romero, F. G., Cicero, C., & Bowie, R. C. K. (2023). Plumage Balances Camouflage and Thermoregulation in Horned Larks (Eremophila alpestris). *The American Naturalist*, 201(2), E23–E40.

Matsumoto, T., Fukuda, K., & Uchikawa, K. (2015). Appearance of 'gold' affects glossiness and metallicity of a surface. *Journal of Vision*, 15(12), 819–819.

McCoy, D. E., Shultz, A. J., Vidoudez, C., van der Heide, E., Dall, J. E., Trauger, S. A., & Haig, D. (2021). Microstructures amplify carotenoid plumage signals in tanagers. *Scientific Reports*, 11(1), 8582.

McMahon, B. C. (2017). *Iridescence, vision, and belief in the Early Modern Hispanic World*. PhD thesis, University of Southern California.

Meadows, M. G., Morehouse, N. I., Rutowski, R. L., Douglas, J. M., & McGraw, K. J. (2011). Quantifying iridescent coloration in animals: a method for improving repeatability. *Behavioral Ecology and Sociobiology*, 65(6), 1317–1327.

Meert, K., Pandelaere, M., & Patrick, V. M. (2014). Taking a shine to it: How the preference for glossy stems from an innate need for water. *Journal of Consumer Psychology*, 24(2), 195–206.

Michelson, A. (1911). On metallic colouring in birds and insects. *The London, Edinburgh, and Dublin Philosophical Magazine and Journal of Science*, 21(124), 554–567.

Montgomerie, R. (2006). Analyzing Colors. In K. J. Mcgraw & G. E. Hill (Eds.), *Bird Coloration Vol. I: Mechanisms and Measurements* (pp. 90–147). Cambridge, MA: Harvard University Press.

Moreau, R. E. (1958). Some aspects of the Musophagidae. *Ibis*, 100(2), 238–270.

Nero, R. W. (1954). Plumage Aberrations of the Redwing (Agelaius phoeniceus). *The Auk*, 71(2), 137–155.

Noh, H., Liew, S. F., Saranathan, V., Mochrie, S. G. J., Prum, R. O., Dufresne, E. R., & Cao, H. (2010a). How Noniridescent Colors Are Generated by Quasi-ordered Structures of Bird Feathers. *Advanced Materials*, 22(26-27), 2871–2880.

Noh, H., Liew, S. F., Saranathan, V., Prum, R. O., Mochrie, S. G. J., Dufresne, E. R., & Cao, H. (2010b). Contribution of double scattering to structural coloration in quasiordered nanostructures of bird feathers. *Physical Review E*, 81(5), 051923.

Noh, H., Liew, S. F., Saranathan, V., Prum, R. O., Mochrie, S. G. J., Dufresne, E. R., & Cao, H. (2010c). Double scattering of light from Biophotonic Nanostructures with short-range order. *Optics Express*, 18(11), 11942–11948.

Nordén, K. K., Eliason, C. M., & Stoddard, M. C. (2021). Evolution of brilliant iridescent feather nanostructures. *eLife*, 10, e71179.

Nordén, K. K., Faber, J. W., Babarović, F., Stubbs, T. L., Selly, T., Schiffbauer, J. D., Štefanić, P. P., Mayr, G., Smithwick, F. M., & Vinther, J. (2019). Melanosome diversity and convergence in the evolution of iridescent avian feathers—Implications for paleocolor reconstruction. *Evolution*, 73(1), 15–27.

Nordén, K. K. & Price, T. D. (2018). Historical contingency and developmental constraints in avian coloration. *Trends in Ecology and Evolution*, 3(8), 574–576.

Norman, J. F., Todd, J. T., & Phillips, F. (2020). Effects of illumination on the categorization of shiny materials. *Journal of Vision*, 20(5), 2.

Okazawa, G., Goda, N., & Komatsu, H. (2012). Selective responses to specular surfaces in the macaque visual cortex revealed by fMRI. *NeuroImage*, 63(3), 1321–1333.

Oskooi, A. F., Roundy, D., Ibanescu, M., Bermel, P., Joannopoulos, J. D., & Johnson, S. G. (2010). Meep: A flexible free-software package for electromagnetic simulations by the FDTD method. *Computer Physics Communications*, 181, 687–702.

Osorio, D. & Cuthill, I. C. (2015). Camouflage and perceptual organization in the animal kingdom. In J. Wagemans (Ed.), *The Oxford handbook of perceptual organisation*. Oxford University Press.

Osorio, D. & Ham, A. D. (2002). Spectral reflectance and directional properties of structural coloration in bird plumage. *Journal of Experimental Biology*, 205(14), 2017–2027.

Ospina-Rozo, L., Roberts, A., & Stuart-Fox, D. (2022). A generalized approach to characterize optical properties of natural objects. *Biological Journal of the Linnean Society*, 137(3), 534–555.

Ozaki, R., Kikumoto, K., Takagaki, M., Kadowaki, K., & Odawara, K. (2021). Structural colors of pearls. *Scientific Reports*, 11(1), 15224.

Pagel, M. & Meade, A. (2006). Bayesian Analysis of Correlated Evolution of Discrete Characters by Reversible-Jump Markov Chain Monte Carlo. *The American Naturalist*, 167(6), 808–825.

Pagel, M., Meade, A., & Barker, D. (2004). Bayesian Estimation of Ancestral Character States on Phylogenies. *Systematic Biology*, 53(5), 673–684.

Parker, A. R., Mckenzie, D. R., & Large, M. C. J. (1998). Multilayer Reflectors in Animals Using Green and Gold Beetles as Contrasting Examples. *Journal of Experimental Biology*, 201(9), 1307–1313.

Parra, J. L. (2010). Color Evolution in the Hummingbird Genus Coeligena. *Evolution*, 64(2), 324–335.

Prager, M. & Andersson, S. (2010). Convergent evolution of red carotenoid coloration in Widowbirds and Bishops (Euplectes spp.). *Evolution*, 64(12), 3609–3619.

Price, J. J., Friedman, N. R., & Omland, K. E. (2007). Song and plumage evolution in the New World Orioles (Icterus) show similar lability and convergence in patterns. *Evolution*, 61(4), 850–863.

Price, T. D., Lovette, I. J., Bermingham, E., Gibbs, H. L., & Richman, A. D. (2000). The Imprint of History on Communities of North American and Asian Warblers. *The American Naturalist*, 156(4), 354–367.

Price-Waldman, R. & Stoddard, M. C. (2021). Avian Coloration Genetics: Recent Advances and Emerging Questions. *Journal of Heredity*, 112(5), 395–416.

Prum, R. O. (2006). Anatomy, physics, and evolution of structural colors. In G. E. Hill & K. J. McGraw (Eds.), *Bird coloration* (pp. 295–353). Cambridge, MA: Harvard University Press.

Prum, R. O., Dufresne, E. R., Quinn, T., & Waters, K. (2009). Development of colour-producing β-keratin nanostructures in avian feather barbs. *Journal of The Royal Society Interface*, 6, S253–S265.

Prum, R. O., LaFountain, A. M., Berro, J., Stoddard, M. C., & Frank, H. A. (2012). Molecular diversity, metabolic transformation, and evolution of carotenoid feather pigments in cotingas (Aves: Cotingidae). *Journal of Comparative Physiology B*, 182(8), 1095–1116.

Quintero, E. & Espinosa de los Monteros, A. (2011). Microanatomy and evolution of the nanostructures responsible for iridescent coloration in Trogoniformes (Aves). *Organisms Diversity & Evolution*, 11(3), 237.

R Core team (2019). R: A language and environment for statistical computing. R foundation for statistical computing , Vienna, Austria. URL http://www.R-project.org/.

Reed, S., Simpson, R. K., & McGraw, K. J. (2020). Feather morphological predictors of angle-dependent color changes in parrot plumage. *Avian Biology Research*, 13(4), 108–117.

Revell, L. J. (2012). phytools: An R package for phylogenetic comparative biology (and other things). *Methods in Ecology and Evolution*, 3(2), 217–223.

Rogalla, S., Patil, A., Dhinojwala, A., Shawkey, M. D., & D'Alba, L. (2021). Enhanced photothermal absorption in iridescent feathers. *Journal of The Royal Society Interface*, 18(181), 20210252.

Romano, A., Séchaud, R., Hirzel, A. H., & Roulin, A. (2019). Climate-driven convergent evolution of plumage colour in a cosmopolitan bird. *Global Ecology and Biogeography*, 28(4), 496–507.

Rowland, H. M. (2008). From Abbott Thayer to the present day: what have we learned about the function of countershading? *Philosophical Transactions of the Royal Society B: Biological Sciences*, 364(1516), 519–527.

Rubenstein, D. R., Corvelo, A., MacManes, M. D., Maia, R., Narzisi, G., Rousaki, A., Vandenabeele, P., Shawkey, M. D., & Solomon, J. (2021). Feather Gene Expression Elucidates the Developmental Basis of Plumage Iridescence in African Starlings. *Journal of Heredity*, 112(5), 417–429.

Rump, M., Müller, G., Sarlette, R., Koch, D., & Klein, R. (2008). Photo-realistic Rendering of Metallic Car Paint from Image-Based Measurements. *Computer Graphics Forum*, 27(2), 527–536.

Saranathan, V. & Finet, C. (2021). Cellular and developmental basis of avian structural coloration. *Current Opinion in Genetics & Development*, 69, 56–64.

Saranathan, V., Forster, J. D., Noh, H., Liew, S.-F., Mochrie, S. G. J., Cao, H., Dufresne, E. R., & Prum, R. O. (2012). Structure and optical function of amorphous photonic nanostructures from avian feather barbs: a comparative small angle X-ray scattering (SAXS) analysis of 230 bird species. *Journal of The Royal Society Interface*, 9(75), 2563–2580.

Schmid, A. C., Barla, P., & Doerschner, K. (2023). Material category of visual objects computed from specular image structure. *Nature Human Behaviour*, 7(7), 1152–1169.

Schumacher, S., Burt de Perera, T., Thenert, J., & von der Emde, G. (2016). Cross-modal object recognition and dynamic weighting of sensory inputs in a fish. *Proceedings of the National Academy of Sciences*, 113(27), 7638–7643.

Seago, A. E., Brady, P., Vigneron, J.-P., & Schultz, T. D. (2009). Gold bugs and beyond: a review of iridescence and structural colour mechanisms in beetles (Coleoptera). *Journal of The Royal Society Interface*, 6, S165–S184.

Sekuler, R., Watamaniuk, S. N. J., & Blake, R. (2002). Perception of visual motion. In *Steven's handbook of experimental psychology: Sensation and perception, Vol. 1, 3rd ed* (pp. 121–176). Hoboken, NJ, US: John Wiley & Sons Inc.

Shawkey, M. D., Estes, A. M., Siefferman, L. M., & Hill, G. E. (2003). Nanostructure predicts intraspecific variation in ultraviolet-blue plumage colour. *Proceedings of the Royal Society B: Biological Sciences*, 270(1523), 1455–1460.

Shawkey, M. D., Hauber, M. E., Estep, L. K., & Hill, G. E. (2006). Evolutionary transitions and mechanisms of matte and iridescent plumage coloration in grackles and allies (Icteridae). *Journal of The Royal Society Interface*, 3(11), 777–786.

Shawkey, M. D. & Hill, G. E. (2005). Carotenoids need structural colours to shine. *Biology Letters*, 1(2), 121–124.

Shephard, T. V., Lea, S. E. G., & Hempel de Ibarra, N. (2015). 'The thieving magpie'? No evidence for attraction to shiny objects. *Animal Cognition*, 18(1), 393–397.

Silvia, P. J., Christensen, A. P., Cotter, K. N., Jackson, T. A., Galyean, C. B., McCroskey, T. J., & Rasheed, A. Z. (2018). Do people have a thing for bling? Examining aesthetic preferences for shiny objects. *Empirical Studies of the Arts*, 36, 101–113.

Silvia, P. J., Rodriguez, R. M., Cotter, K. N., & Christensen, A. P. (2021). Aesthetic Preference for Glossy Materials: An Attempted Replication and Extension. *Behavioral Sciences*, 11(4), 44.

Simpson, J. A., Weiner, E. S. C., & Press, O. U., Eds. (1989). *The Oxford English dictionary*. Oxford : Oxford ; New York: Clarendon Press ; Oxford University Press, 2nd ed edition.

Simpson, R. K. & McGraw, K. J. (2019). Interspecific Covariation in Courtship Displays, Iridescent Plumage, Solar Orientation, and Their Interactions in Hummingbirds. *The American Naturalist*, 194(4), 441–454.

Skigin, D. C., Inchaussandague, M. E., D'Ambrosio, C., Barreira, A., & Tubaro, P. (2019). How the observed color of the Swallow Tanager (Tersina viridis) changes with viewing geometry. *Optik*, 182, 639–646.

Smithwick, F. M. (2019). *A taphonomic and palaeoecological approach to the study of palaeocolour*. PhD thesis, University of Bristol.

Soto, F. A. & Wasserman, E. A. (2014). Mechanisms of object recognition: what we have learned from pigeons. *Frontiers in Neural Circuits*, 8.

Stavenga, D. G., Leertouwer, H. L., Marshall, N. J., & Osorio, D. (2011). Dramatic colour changes in a bird of paradise caused by uniquely structured breast feather barbules. *Proceedings of the Royal Society B: Biological Sciences*, 278(1715), 2098–2104.

Stavenga, D. G., Leertouwer, H. L., Osorio, D. C., & Wilts, B. D. (2015). High refractive index of melanin in shiny occipital feathers of a bird of paradise. *Light: Science and Applications*, 4(1), e243.

Stavenga, D. G., Leertouwer, H. L., & Wilts, B. D. (2018). Magnificent magpie colours by feathers with layers of hollow melanosomes. *Journal of Experimental Biology*, 221(4).

Stavenga, D. G., van der Kooi, C. J., & Wilts, B. D. (2017). Structural coloured feathers of mallards act by simple multilayer photonics. *Journal of The Royal Society Interface*, 14(133), 20170407.

Stoddard, M. C. & Prum, R. O. (2008). Evolution of Avian Plumage Color in a Tetrahedral Color Space: A Phylogenetic Analysis of New World Buntings. *The American Naturalist*, 171(6), 755–776.

Stoddard, M. C. & Prum, R. O. (2011). How colorful are birds? Evolution of the avian plumage color gamut. *Behavioral Ecology*, 22(5), 1042–1052.

Stryjewski, K. F. & Sorenson, M. D. (2017). Mosaic genome evolution in a recent and rapid avian radiation. *Nature Ecology & Evolution*, 1(12), 1912–1922.

Stuart-Fox, D., Ospina-Rozo, L., Ng, L., & Franklin, A. M. (2020). The Paradox of Iridescent Signals. *Trends in Ecology & Evolution*.

Sumner, R. (2014). Processing RAW images in MATLAB.

Sutton, P. & Snow, M. (2015). *Iridescence: The Play of Colours*. Thames & Hudson Australia.

Thomas, D. B., McGraw, K. J., Butler, M. W., Carrano, M. T., Madden, O., & James, H. F. (2014). Ancient origins and multiple appearances of carotenoid-pigmented feathers in birds. *Proceedings of the Royal Society B: Biological Sciences*, 281(1788), 20140806–20140806.

Thomas, D. H. N., Kjernsmo, K., Scott-Samuel, N. E., Whitney, H. M., & Cuthill, I. C. (2023). Interactions between color and gloss in iridescent camouflage. *Behavioral Ecology*, (pp. arad050).

Tinbergen, J., Wilts, B. D., & Stavenga, D. G. (2013). Spectral tuning of Amazon parrot feather coloration by psittacofulvin pigments and spongy structures. *Journal of Experimental Biology*, 216(23), 4358–4364.

Todd, J. T. & Norman, J. F. (2018). The visual perception of metal. *Journal of Vision*, 18(3), 9–9.

Troscianko, J., Wilson-Aggarwal, J., Stevens, M., & Spottiswoode, C. N. (2016). Camouflage predicts survival in ground-nesting birds. *Scientific Reports*, 6(1), 19966.

Twyman, H., Prager, M., Mundy, N. I., & Andersson, S. (2018). Expression of a carotenoid-modifying gene and evolution of red coloration in weaverbirds (Ploceidae). *Molecular Ecology*, 27(2), 449–458.

Urquia, G. M., Inchaussandague, M. E., Skigin, D. C., Lester, M., Barreira, A., & Tubaro, P. (2020). Theoretical approaches to study the optical response of the red-legged honeycreeper's plumage (Cyanerpes cyaneus). *Applied Optics*, 59(13), 3901–3909.

Vinther, J. (2020). Reconstructing Vertebrate Paleocolor. *Annual Review of Earth and Planetary Sciences*, 48(1), 345–375.

Vinther, J., Briggs, D. E., Prum, R. O., & Saranathan, V. (2008). The colour of fossil feathers. *Biology Letters*, 4(5), 522–525.

Vinther, J., Briggs, D. E. G., Clarke, J., Mayr, G., & Prum, R. O. (2010). Structural coloration in a fossil feather. *Biology Letters*, 6(1), 128–131.

Wagemans, J., Elder, J. H., Kubovy, M., Palmer, S. E., Peterson, M. A., Singh, M., & von der Heydt, R. (2012). A century of Gestalt psychology in visual perception: I. Perceptual grouping and figure–ground organization. *Psychological Bulletin*, 138, 1172–1217.

Wallace, A. R. (1877). The Colors of Animals and Plants. *The American Naturalist*, 11(11), 641–662.

Wiens, J. J., Kuczynski, C. A., Duellman, W. E., & Reeder, T. W. (2007). Loss and re-evolution of complex life cycles in marsupial frogs: does ancestral trait reconstructuin mislead? *Evolution*, 61(8), 1886–1899.

Wilts, B. D., Michielsen, K., Raedt, H. D., & Stavenga, D. G. (2014). Sparkling feather reflections of a bird-of-paradise explained by finite-difference time-domain modeling. *Proceedings of the National Academy of Sciences*, 111(12), 4363–4368.

Yin, H., Shi, L., Sha, J., Li, Y., Qin, Y., Dong, B., Meyer, S., Liu, X., Zhao, L., & Zi, J. (2006). Iridescence in the neck feathers of domestic pigeons. *Physical Review E*, 74(5).

Zi, J., Yu, X., Li, Y., Hu, X., Xu, C., Wang, X., Liu, X., & Fu, R. (2003). Coloration strategies in peacock feathers. *Proceedings of the National Academy of Sciences*, 100(22), 12576–12578.

Ödeen, A. & Håstad, O. (2003). Complex Distribution of Avian Color Vision Systems Revealed by Sequencing the SWS1 Opsin from Total DNA. *Molecular Biology and Evolution*, 20(6), 855–861.